ABSTRACT

MERTENS, BRITTANY SEDZIOL. New Colloidal Approaches for Human Norovirus Cleanup and Inactivation using Surfactants and Copper Ion-based Disinfectants. (Under the direction of Dr. Orlin D. Velev).

Understanding of the colloidal interactions of human norovirus particles in aqueous medium could provide insights on the origins of the notorious stability and infectivity of these widespread viral agents. Norovirus interactions were modified to enhance cleaning and disinfection using various classes of surfactants and aqueous copper. Surfactant adsorption onto human norovirus virus-like particles (VLPs) changed the behavior of the particles in solution and has implications for the efficacy of surfactant-based cleaners. Aqueous copper solutions caused permanent capsid damage that eliminated virus infectivity.

We characterized the effects of solution pH and surfactant type and concentration on the aggregation, dispersion, and disassembly of VLPs using dynamic light scattering, electrophoretic light scattering, and transmission electron microscopy. Owing to net negative surface charge of the VLPs at neutral pH, low concentrations of cationic surfactant showed tendency to aggregate the VLPs, whereas low concentrations of anionic surfactant tended to disperse the particles. Increasing the concentration of these surfactants beyond their critical micelle concentration led to virus capsid disassembly and breakdown of VLP aggregates. Non-ionic surfactants, however, had little effect on virus interactions and likely stabilized them additionally in suspension. We used zeta potential data to characterize virus surface charge and interpret the mechanisms behind these demonstrated surfactant-virus interactions based on the theory of colloidal stabilization. The fundamental understanding and control of these interactions will aid in practical formulations for virus inactivation and removal from contaminated surfaces.

We also characterized the effects that copper ions have on virus integrity to explain empirical data indicating virus inactivation by copper alloy surfaces, and as means of developing novel metal ion-based virucides. Cu(II) ions aggregated VLPs at low concentration but have little effect on the infectivity of human norovirus surrogates. The generation of low concentrations of monovalent copper ions (~0.1 mM) caused permanent capsid protein damage that prevented human norovirus capsids from binding to cell receptors and induced a greater than 4-log reduction in infectivity of Tulane virus, a human norovirus surrogate. The number of genetic copies of human norovirus-infected stool samples were reduced in titer by about 2-log as measured by RT-qPCR. SDS-PAGE data indicate substantial major capsid protein cleavage of both GI.7 and GII.4 norovirus capsid proteins, and TEM images show complete loss of capsid integrity of the GI.7 Norovirus strain. GII.4 virus-like particles (VLPs) were less susceptible to inactivation by copper ion treatments than GI.7 VLPs when comparing binding to histo-blood group antigen (HBGA) cell receptors and major capsid protein cleavage. The combined data demonstrate that pending further work such copper-based formulations can form the basis of efficient and safe antivirals.

While copper ion and ascorbate mixtures had high efficacy in human norovirus surrogate inactivation, the ascorbate readily oxidized during storage in aqueous solution and is therefore not suitable for use in practical formulations. As an alternative to ascorbate, we evaluated three polyphenolic materials, lignin nanoparticles, tannic acid, and (+)-catechin, for their ability to reduce Cu(II) to Cu(I) and inactivate Tulane virus after storage in aqueous solution. Lignin nanoparticles and tannic acid retained their ability to reduce copper ions after storage but were not effective in reducing Tulane virus infectivity even when prepared fresh. (+)-Catechin retained its ability to both reduce copper ions and inactivate Tulane virus in the

presence of copper ions after storage for months. We therefore propose (+)-catechin and copper ion mixtures as effective and practical formulations for human norovirus inactivation.

The surfactant and copper-based methods of virus modification presented in this thesis provide means of improving the cleaning and disinfection of human noroviruses that could limit their spread in the environment and help reduce their burden on society.

New Colloidal Approaches for Human Norovirus Cleanup and Inactivation using Surfactants and Copper Ion-based Disinfectants

by
Brittany Sedziol Mertens

A dissertation submitted to the Graduate Faculty of
North Carolina State University
in partial fulfillment of the
requirements for the degree of
Doctor of Philosophy

Chemical Engineering

Raleigh, North Carolina

2017

APPROVED BY:

_____	_____
Dr. Orlin D. Velev Chair of Advisory Committee	Dr. Lee-Ann Jaykus
_____	_____
Dr. Balaji Rao Minor Member	Dr. Saad Khan

DEDICATION

This dissertation is dedicated to my daughter, Skylar Elizabeth Mertens, whom inspires me to be the best version of myself. I love you!

BIOGRAPHY

Brittany Mertens was born in Cincinnati, Ohio to Kenn and Rita Sedziol. She has one older brother, Brian Sedziol. Brittany attended Indian Hill Schools from Kindergarten through 12th grade, and upon graduation moved to Clemson, South Carolina to begin college at Clemson University. She completed undergraduate research with Dr. Anthony Guiseppi-Elie on hydrogels towards the development of an implantable biosensor. Brittany also took part in campus life, including being a member of the University Singers, working as a tutor for the Academic Success Center, and being a member and acting as President of Gamma Sigma Sigma (a service sorority). Brittany graduated *magna cum laude* from the Chemical and Biomolecular Engineering Bachelor of Science program at Clemson University in 2012. She moved to Raleigh, North Carolina and began graduate studies in Chemical and Biomolecular Engineering at North Carolina State University in Fall 2012. Brittany's PhD research project, advised by Dr. Orlin D. Velev, is part of the multi-institutional NoroCORE, led by Dr. Lee-Ann Jaykus.

Brittany married Kevin Mertens in July 2013, and they have since purchased and renovated a house, adopted two cats, and adopted their Great Dane, Titan. Brittany gave birth to their daughter, Skylar Elizabeth Mertens, on February 19, 2016. After completion of her graduate studies, Brittany will begin an internship in technical development with Baebies, Inc. in Research Triangle Park, NC, where she will help develop newborn screening assays.

ACKNOWLEDGMENTS

I would first like to thank my research advisor, Dr. Orlin D. Velev, for his support and guidance throughout my graduate career. He has been a wonderful mentor and resource in all aspects of my development as a scientist. I am also grateful to Dr. Lee-Ann Jaykus for all her guidance with the biological aspects my work and for allowing me full access to her lab. I consider her my unofficial second advisor. I also greatly appreciate my other committee members, Dr. Saad Khan and Dr. Balaji Rao, for their insights and direction during my PhD work.

I would like to thank all the members of the Velev and Jaykus labs whom have shared both knowledge and laughs with me. From the Velev group, I give special thanks to Dr. Alexander Richter for introducing me to dynamic light scattering and to Dr. Stephanie Lam for passing down her general lab knowledge. From the Jaykus group, I give special thanks to Dr. Chip Manuel for teaching me mammalian cell culture; Dr. Matthew D. Moore for teaching me many lab techniques, collaborating on multiple projects, and engaging in many interesting conversations; and Dr. Blanca Escudero for her assistance in the lab. I am also grateful to the undergraduate students whom worked with me for varying lengths of time throughout my PhD, especially Ryan Fox and Tierra Knight.

I am grateful to my parents, Kenn and Rita Sedziol, for inspiring me to make an impact on the world and setting me up for success in life. I am also grateful for the support of my close friends at NC State, Drs. Erinn and Craig Needham, Deepti Srivastava, Joe Tilly, Ashton and Joe Lavoie, Jenna and Daniel Armstrong, Mariah and Dexter King, and Jenny Ovental, whom have been like a second family. Finally, I give the biggest thanks to my husband, Kevin, for carrying me through the most difficult times and giving me more love and support than I could

ever deserve. Thank you for joining me on so many adventures and for keeping me focused on what is truly important. I love you.

TABLE OF CONTENTS

LIST OF FIGURES

CHAPTER 1

Introduction and Overview

1.1 Introduction

The spread of pathogenic viruses is partially affected by their colloidal properties, which facilitate attachment to and detachment from produce, surfaces, and other viruses. Adsorption and aggregation influence virus persistence in the environment[1] and strongly impact the measures undertaken to remove or disinfect virus particles. This review chapter summarizes the current research related to the colloidal properties of non-enveloped human enteric ssRNA viruses with icosahedral geometry and the implications for virus persistence in the environment. These viruses are members of the *Picornaviridae*, *Astroviridae*, *Caliciviridae*, and *Reoviridae* families of viruses.[2] They are composed of a proteinaceous capsid surrounding a genome of single (*Picornaviridae*, *Astroviridae*, and *Caliciviridae*) or double-stranded (*Reoviridae*) RNA. Single-stranded RNA genomes bind to the inside of the capsid, while double-stranded genomes are relatively homogeneously distributed spatially.[3] Specific pathogenic viruses of interest include enterovirus,[4, 5] Hepatitis A (HAV),[6, 7] rotavirus,[8, 9] and human norovirus (HuNoV).[10-12]

The structural simplicity of these viruses contributes to their relative robustness. Viruses that infect the human gastrointestinal tract generally have high persistence in the environment and resistance to disinfection due to their stability in both the extreme acidity of the stomach and slightly basic conditions of the intestinal tract.[13] These viruses are transmitted via the oral-fecal route and spread through the environment in food and water, on contaminated

surfaces, through vomitus droplets in the air that are swallowed, and by direct person-to-person contact.[14] They are relatively stable in a wide range of temperature and relative humidity.[15] HAV, poliovirus, and rotavirus have been shown in various studies to persist for up to a year depending on storage conditions, with colder temperatures leading to longer periods of viability.[14] Even longer persistence of human norovirus in groundwater has also been reported.[16] The ability of very low quantities of such viruses to infect an individual[15,17] further contributes to their spreading.

Because of their structural similarities to food and water-borne enteric viruses, F-specific RNA bacteriophages are commonly used as surrogates to study the properties of the human pathogens.[18] Specifically, phages that infect enteric *E. coli* are used because they are indicative of the presence of enteric pathogens in the environment. MS2 is the most prevalent surrogate for enteric viruses based on its structure and size (about 28 nm)[19] and ssRNA genome.[20] While these phages are useful for studying the general colloidal properties and interactions of enteric viruses, surrogates specific to each viral pathogen are used to more effectively determine disinfection efficacy based on their relative resistance. Specific surrogates for human norovirus, including Tulane virus (TV), murine norovirus (MNV), and feline calicivirus (FCV),[21,22] are especially important in present research as cell culture models for human norovirus have only recently been developed[23-25] and are not yet widely available for disinfection studies.

1.2 Biocolloidal Interactions Overview

1.2.1 Biological Surface Forces

Interactions between biological surfaces have been described extensively as they relate to the intrinsic properties of proteins and lipid bilayer membranes.[26,27] They are summarized here for their relevance to virus interactions. DLVO theory describes interactions between particles that are governed by the combination of attractive van der Waals (VdW) forces and attractive or repulsive electrostatic forces. VdW forces are ubiquitous between all molecules, arising from interactions between the dipole moments of the molecules. These forces between biological molecules are always attractive, and their magnitude depends on the geometry, distance of separation, and dielectric and optical properties of the molecules. Electrostatic interactions are the other origin of omnipresent forces described in DLVO theory and comprise attractive or repulsive forces between the electrical double layers of two molecules or surfaces. Electrical double layers are composed of surface charges as well as the adsorbed and diffuse ion layers. The Debye length, defined as $1/\kappa$, describes the decay of the diffuse ion layers and is dependent on the ionic strength of the solution. The Debye length decreases with increasing ionic strength, shielding the effects of electrostatic interactions. At physiological conditions, the Debye length is small at about 0.8 nm, so close-range interactions are predominant even with highly charged molecules. These close-range interactions are governed by the osmotic pressure produced by the ions trapped in the double layer between the molecules. The surface charge and surface potential can be related by the Grahame equation,

$$\sigma^2 = 2\varepsilon_0 \varepsilon kT\left(\sum_i \rho_{0i} - \sum_i \rho_{\infty i}\right) \tag{1.1}$$

where σ is the surface charge density, ε_0 represents vacuum permittivity, ε represents the relative permittivity of water, k is the Boltzmann constant, T the temperature, and ρ_i represents the ion density.[28] The ion density is described by a Boltzmann distribution,

$$\rho_{0i} = \rho_{\infty i} e^{\frac{-z_i e \psi_0}{kT}} \tag{1.2}$$

where ρ_{0i} represents the density of ion i at the surface, $\rho_{\infty i}$ represents the density of ion i in the bulk liquid, z_i represents the valence of ion i, e represents the electron charge, and ψ_0 represents the surface potential.[28] When the Debye length is sufficiently small, the surface potential is often approximated using the zeta potential, which is calculated from a measured electrophoretic mobility. The zeta potential represents the potential drop at the slip plane, where fluid flow is zero.

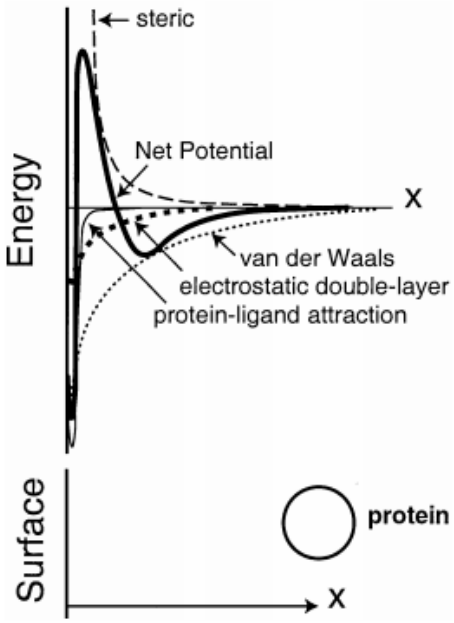

Figure 1.1 Representative profiles of the van der Waals, electrostatic, steric, and specific interactions and their contributions to the net potential energy of a biological molecule interacting with a surface.[26]

VdW and electrostatic interactions add together to form the net DLVO interaction profile. As shown in the net potential curve in Figure 1.1, at very short distances interactions are strongly attractive because of the predominance of VdW forces. At larger distances, electrostatics dominate, and at still larger distances interactions become weak. Surface and solution properties define the shape of the net interaction potential curve.

Also shown in Figure 1.1 is the effect of other, non-DLVO forces. Multiple types of interactions between biointerfaces exist outside of those described by DLVO theory, including solvation forces, steric forces, and (bio)specific interactions.[27] Solvation forces, which include hydrophobic interactions, are called hydration forces in aqueous solutions because water molecules form hydrating shells around suspended particles. The shells formed by the water molecules vary based on surface hydrophobicity and can cause attraction or repulsion, depending on the alignment between the hydrating shells. Highly hydrophobic molecules preferentially interact with each other in the absence of these hydrating shells (depletion), resulting in forces that can oscillate between attractive and repulsive for complex biological molecules. Hydration forces allow proteins to remain stable at the high ionic strength present under physiological conditions[29] and may contribute to protein folding.[30] Steric forces, including bridging and polymer depletion forces, involve polymer-covered surfaces and can be attractive or repulsive depending on the nature of the polymer and solvent. The length, density, hydrophilicity, and flexibility of the polymer layers impact their relative attraction to each other and to the solvent, which determines the particle's steric interactions. Steric forces are present for many biological surfaces, including ones of cells, which have attached flexible

groups such as polysaccharides or lipids. The protrusions within the capsid structure of most icosahedral viruses are not large or flexible enough to generate substantial steric forces, so these forces are largely ignored in this review. Some mention is given to steric forces related to MS2 bacteriophages, which have small (~1 nm protrusion) hydrophilic peptide loops that were speculated to be a source of certain steric repulsion.[31] Specific interactions involve a combination of all of the forces discussed thus far and enable the high selectivity of many biological processes such as ligand binding, enzyme catalysis, and antigen recognition. The geometries of molecules and the configurations of charges and hydrophobic regions on those molecules result in high affinity for specific complementary molecules in a "lock-and-key" match. Proteins also exhibit specific ion-dependent interactions that deviate from traditional colloidal theory.[32]

1.2.2 Colloidal Properties of Viruses

Classical DLVO theory has been developed for hard, spherical particles. More recently, theory has been developed and reviewed by Ohshima describing soft colloidal particles, specifically particles with a hard core and soft ion-penetrable polyelectrolyte layers.[33-35] Fluid flow through the polyelectrolyte layer is slowed by frictional forces, and zeta potential is no longer a concept that matches well with the system physics because charges are distributed throughout the volume of the surface layer. This theory takes into account Donnan effects, where soft particles act as semi-permeable membranes. Langlet *et al.* have extended this soft particle theory to viruses, describing them as soft colloidal particles with three layers of different charge density.[36]

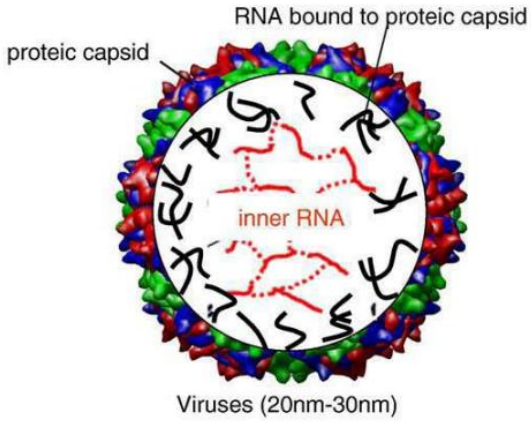

Figure 1.2 Schematics of the three layers of charge density within non-enveloped viruses, using MS2 as an example model. The protein capsid, RNA bound to the inside of the capsid, and unbound RNA inside the capsid are depicted.[37]

Figure 1.2 exemplifies the three layers of non-enveloped virus charge density, including the protein capsid, compact RNA bound to the inner surface of the capsid, and free RNA at the center of the virus. The presence or absence of nucleic acid and the three-dimensional charge distribution of the capsid, which is characteristic of each virus,[38] have significant impacts on electrostatic interactions between such particles.[39,40] Langlet *et al.* have modeled the bacteriophage MS2 in detail, using the capsid protein and RNA compositions to determine charge densities of each layer of the virus.[36] Duval *et al.* expanded soft particle and surface theory to include spatial heterogeneities and partial dissociation of ionic groups within soft layers.[37] This expanded theory has been applied to proteins and protein particles such as spider silk[41] and has been found relevant to metal ion uptake by microorganisms.[42] For simplicity, many researchers still use DLVO theory to describe the electrostatic component of

virus particle interactions, including most of the work presented in this review. Because non-enveloped viruses have a protein shell as their outermost layer, their interactions are largely governed by the same forces that govern individual protein interactions. However, viruses also have deviations from molecular protein behavior because of the stabilizing effects of adjacent capsid proteins, larger particle size with defined structural characteristics, and the incorporation of internal nucleic acid.

Viruses have electrostatically diverse capsids composed of proteins with charged residues of varying pKa, and their interactions are partially influenced by electrostatic forces. The zwitterionic nature of protein capsids allows viruses to possess a net positive charge at low pH and have negative charge at high pH. The size and symmetry of charged patches on particle surfaces greatly influence particle interactions and can even determine whether interaction forces are attractive or repulsive.[43] Additional considerations pertaining to double-layer dynamics must be taken into account even for symmetrical zwitterionic particles.[44] An equal number of positively and negatively charged residues exist on the capsid at the isoelectric point (pI), creating a net neutral charge that minimizes electrostatic repulsion.[45] The isoelectric points of many viruses, determined mostly by isoelectric focusing techniques, have been summarized by Michen and Graule.[45]

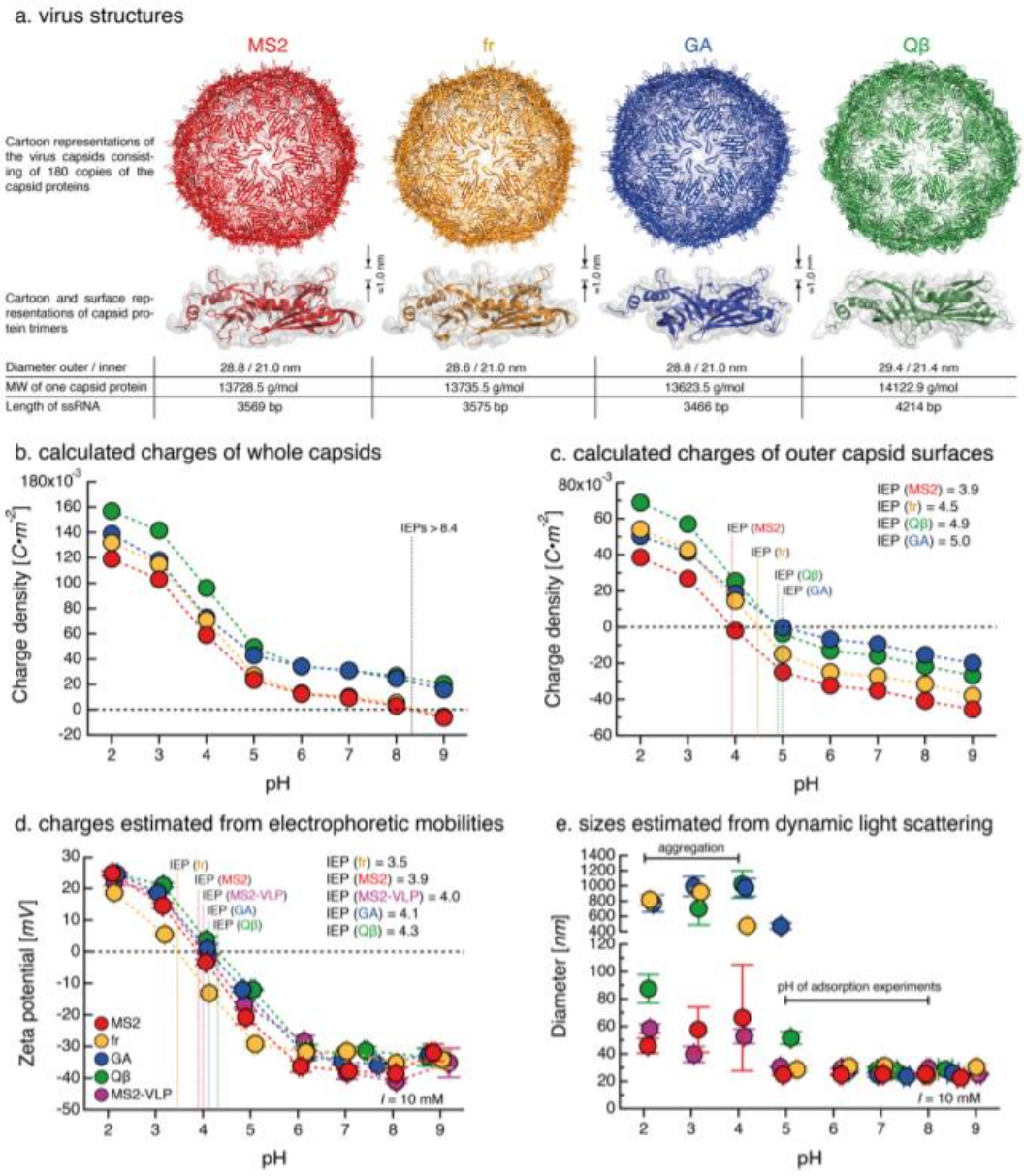

Figure 1.3 Comparison of the a) capsid structure, b) theoretical charge of the whole capsid, c) theoretical charge of just the capsid outer surface, d) zeta potential calculated from measured electrophoretic mobility, and e) size of four f-specific bacteriophages.[46]

Care must be taken when reporting theoretically and experimentally determined isoelectric points as they can be greatly influenced by the presence or absence of nucleic acid and the inclusion of total or partial capsid proteins in analysis. Armanious *et al*. calculated the charge of both the entire capsid and just the exposed capsid surface of four bacteriophages (Figure 1.3a) by taking into account the crystallographic structure of the viruses.[46] The isoelectric points estimated from zeta potentials calculated based on measured electrophoretic mobility closely matched the charge calculated using just the exposed capsid surface (Figure 1.3c,d). The isoelectric point values of just the exposed capsid ranged from 3.5 to 5.0 for all four phages, whereas values greater than 8.4 were calculated using the entire capsid (Figure 1.3b).

Nguyen *et al.*[47] and Dika *et al.*[48] compared the electrostatic interactions of MS2 virus-like particles (VLPs) devoid of internal RNA and purified viable MS2 phages. Dika *et al.* found significant differences in interaction behavior with VLPs demonstrating greater stability at a wider range of conditions than viable phages. Conversely, Nguyen *et al*. discovered only minor effects of the RNA core on MS2 interactions.[49] It has been later determined that the methods used to generate VLPs and to purify both phages and VLPs have a profound impact on interaction behavior, which could account for the difference in results between the two groups.[50] This study revealed that viable phage purification by dialysis and PEG precipitation results in aggregation of particles, depending on the ionic strength and pH of the medium. Ultracentrifugation with a CsCl gradient has resulted in dispersed virus particles at all conditions studied. When applied to VLP suspensions, aggregation has been reduced for both dialysis and PEG precipitation methods, indicating that internal RNA is an important factor in

virus interactions. It is therefore also important to consider the effects of VLP generation because of resultant variations in the composition of the particle core.

Viruses have been studied as nanoparticles of a kind in applications where polymer-based particles were traditionally used because of their defined morphologies and toughness.[51] Viral capsid toughness is predominately measured by nanoindentation using atomic force microscopy (AFM) and has been reviewed by Roos *et al.*[52] and by Mateu.[53] The sum of the forces acting between two biomolecules or surfaces can similarly be measured by atomic force microscopy (AFM), a surface force apparatus, bioforce probe, or optical tweezers.[26] AFM is perhaps the most utilized of these methods, where biomolecules can be attached to both the cantilever tip and sample stage. The forces required to unbind ligands or stretch folded proteins can then be measured. Virus properties have been characterized using dynamic and electrophoretic light scattering,[46-48] isoelectric focusing,[45] AFM,[52,53] electrospray-differential mobility analysis (ES-DMA),[54] electron microscopy,[15] mass spectrometry,[55] and other techniques.

1.2.3 Capsid Assembly and Properties

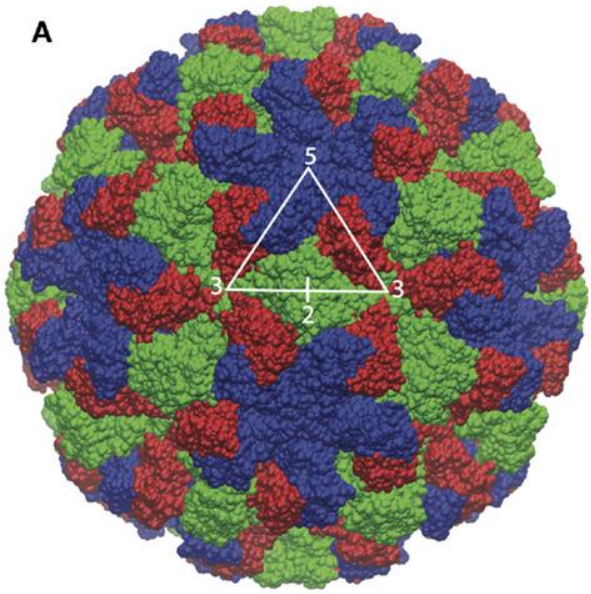

Figure 1.4 Structure of the Norwalk Virus capsid with T=3 symmetry. Five blue subunits form the pentagonal facets, and 3 red and 3 green subunits form the hexagonal facets. The drawn triangle represents one face of the base icosahedron.[56]

Virus capsid assembly has been studied extensively by both computational and experimental approaches, and we briefly summarize here the important colloidal forces involved, namely electrostatic, hydrophobic, and entropic contributions.[57] For more comprehensive reviews, refer to Mateu[58] and Perlmutter.[59] All of the viruses discussed in this review chapter have icosahedral geometry, so they are comprised of 20 triangular faces. These triangles are drawn between hexagons and pentagons composed of proteins that arrange based on the virus's T symmetry, where T is the triangulation number.[60] There are 60T proteins that make up 20T hexagonal and pentagonal facets of the capsid structure.[60] Studies of human

norovirus capsid assembly have shown that capsid proteins form dimers that arrange into larger intermediates composed of two pentagons connected by a dimer. These intermediates then combine to form a complete capsid.[61] An example of a human norovirus structure, which has T=3 icosahedral symmetry, is shown in Figure 1.4.

The assembly of an icosahedral capsid structure is largely dependent on a balance between capsid protein interactions with each other and with nucleic acid,[55,62] which all depend on protein, nucleic acid, and solution properties.[63] The nucleic acid of ssRNA viruses has strong electrostatic attraction to the capsid proteins,[64] whereas protein-protein interactions encompass repulsive electrostatic forces and attractive hydrophobic forces.[65] Because of its strong interaction with capsid proteins, the genome RNA core has an important role in the capsid assembly process. Importantly, it is more energetically favorable for proteins to encapsulate a single large RNA molecule rather than smaller RNA molecules amounting to the same number of nucleotides.[66] Viral RNA molecules are also more compact than random RNA molecules, and capsid proteins prefer to self-assemble around the viral RNA.[67] The tendency of capsid proteins to assemble around viral RNA is driven by nonspecific biomolecular forces and ensures the formation of complete infectious viruses during self-assembly. While RNA is an important component in the formation of infectious viruses, capsid proteins cloned and expressed *in vitro* self-assemble into capsid structures in the absence of viral RNA.[68,69] Termed virus-like particles (VLPs), these structures are useful as surrogates for investigating virus behavior and as vaccines or drug delivery vehicles.

Garmann *et al*. demonstrated by using Cowpea Chlorotic Mottle Virus (CCMV) that the self-assembly of capsids is pathway-dependent. At neutral pH, protein-protein interactions

have been weak enough so that the stronger protein-RNA forces led to protein saturation around each RNA and a resultant small "protocapsid". When the pH was later reduced to a level where protein-protein interactions were stronger, these protocapsids rearranged into fully formed capsid structures. If the pH was initially at the lower value, interconnected aggregates of disordered capsid structures were formed instead of dispersed capsids.[61] Electrostatics play a large role in capsid assembly,[70] and Siber *et al*. reviewed the energetics of the ionic charge contributions.[3] Entropy has also been demonstrated as a significant contributor to capsid self-assembly.[71] Small spheres have been shown to arrange into icosahedral structures under spherical confinement as a result of entropic favorability.[72]

1.2.4 Virus Aggregation – Origins and Impact

The presence of viruses as aggregates or dispersed particles has numerous implications for disinfection, separation, detection, and other applications of viruses that are discussed in Section 1.3. Viral aggregation has been shown to follow classical colloid aggregation models, with aggregation kinetics governed by particle diffusion.[73-75] Solution conditions, including pH, ionic strength, and surfactant concentration, greatly influence the behavior of viruses in aqueous media. The pI of virus capsids is a key factor in determining the electrostatic component of their interactions and is especially important in predicting aggregation. In the absence of sufficiently large alternative stabilizing forces, such as steric repulsion, viruses tend to aggregate near the pI as a result of attractive VdW and hydrophobic forces. This phenomenon has been demonstrated for multiple viruses by measuring electrophoretic mobility and particle size over a range of pH.[36,50,76,77] Virus aggregation induced by low

electrostatic repulsion near the isoelectric point results in lowered plaque-forming unit (pfu) counts in plaque assays of MS2.[78]

Salt conditions also significantly impact virus aggregation behavior. The bacteriophage MS2 remains stable even at very high ionic strength in solutions of monovalent ions. Electrostatic forces are shielded at high ionic strength due to a small Debye length, so Mylon *et al.* have attributed the observed virus stability to steric forces resulting from polypeptide loops that extend from the capsid.[79] Similar steric stabilization has been observed for rotaviruses, and it has been suggested that VP4 on the capsid surface is responsible for these steric forces.[80] Increasing the concentration of divalent calcium ions induced aggregation of MS2, likely due to ion complexation and charge neutralization in addition to ion bridging. Adsorption of organic matter to the virus surface leads to decreased particle stability in divalent ion solutions.[79]

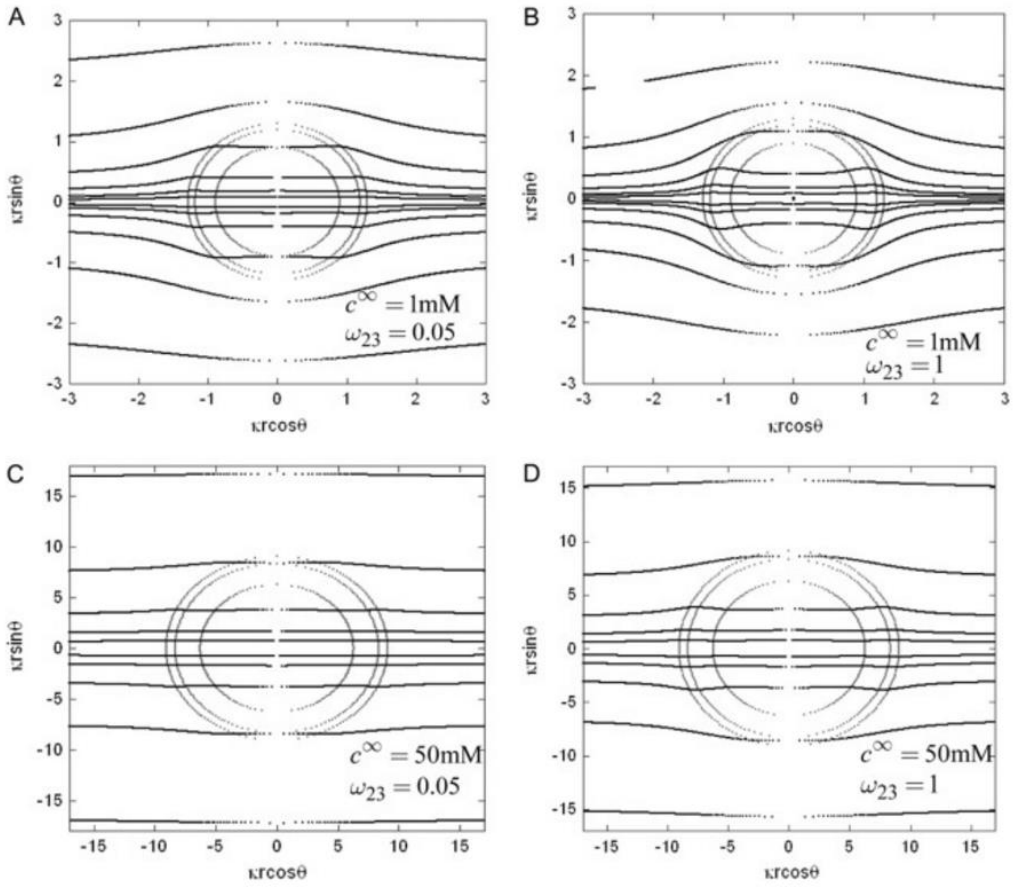

Figure 1.5 Simulated streamlines through virus particles. Streamlines vary as a function of the particle permeability and solution ionic strength.[81]

A similar study comparing MS2 and three other F-specific bacteriophages has indicated that MS2 is the most stable of the four phages evaluated, possibly due to its low hydrophobicity.[81] It has also been suggested that the porosity of the phages affects their behavior in response to solution chemistry,[81] as variations in porosity affects the permeability and the related electro-osmotic flow within dispersed viruses or aggregates (Figure 1.5).[82]

Specifically, isoelectric point has been found to vary as a function of salt concentration more significantly for specific phages than others.[36,81]

Viruses and surfactants display interesting behavior in the mutual presence of both species because they both have amphiphilic properties, while one is large and spherical and the other is small and linear in geometry. The large viruses have hydrophobic patches as well as areas of both positive and negative charge that depend on solution pH and salt conditions, whereas surfactants have a hydrophilic headgroup that may be charged and a hydrophobic part usually composed of a hydrocarbon tail. Surfactants are commonly used in cleaning and disinfectant products, so understanding their interactions with viruses is especially important from an applied biotechnology perspective. The hydrophobic tails of surfactants can associate with hydrophobic regions on the capsid surface, and the head group of an ionic surfactant has attractive interactions with opposite charges and repulsive interactions with similar charges on the capsid.[83] The head group of nonionic surfactants can more weakly associate with charged or polar regions on the capsid surface. The adsorption of common charged and nonionic surfactants onto the capsid surface of human norovirus VLPs that results from these interactions was evaluated in terms of particle size and charge by Mertens *et al.*[76] Briefly, at a pH where the virus has net negative surface charge, cationic surfactant at low concentration adsorbs and induces aggregation due to lowering the electrostatic repulsion between particles, whereas adsorption of anionic surfactant at low concentration keeps particles dispersed. Above the surfactants' critical micelle concentration, aggregates are broken apart and capsid proteins are solubilized by surfactant micelles. Panyukov *et al.* have shown that tobacco mosaic virus retains its structure upon aggregation by low concentration of cationic surfactant.[84]

1.2.5 Virus Adsorption

At its most basic level, particle adsorption to a surface involves the formation of a particle-surface interface area, alongside the removal of particle-liquid and surface-liquid interfaces.[85] The energy of adhesion per unit area is then given by Equation 1.3,

$$W_{PS}^{adh} = \gamma_{PS} - (\gamma_{PL} - \gamma_{SL}) \quad (1.3)$$

where γ represents the interfacial energies between the particle (P), surface (S), and liquid (L), and W_{PS}^{adh} represents the work of particle-surface adhesion.[85] Protein adsorption to surfaces has been shown to follow similar behavior as nanoparticles, and it can be modeled relatively well using traditional colloidal theory.[86] In aqueous solution, the interaction of a predominantly hydrophobic protein and surface will result in strong adsorption, and a predominantly hydrophilic protein and surface will result in weak adsorption. Electrostatic interactions may be positive or negative depending on the relative charge of the protein and surface. Increased surface roughness introduces more sites of attachment for proteins and generally enhances protein adsorption.[85] Virus adsorption to waste treatment pond solids was shown to be reversible.[87] It has been shown that such virus adsorption could be commonly represented by a Freundlich adsorption isotherm.[87-89] Viruses adsorbed onto particles may remain viable for longer than dispersed viruses,[90] increasing their persistence in the environment.

Armanious *et al*. demonstrated that electrostatic interactions and hydrophobic effects are most important in determining virus adsorption to varying surface types.[46] Van der Waals interactions, hydrogen bonding, and steric forces have been found to have lesser impact on virus adsorption to abiotic surfaces. Increasing electrostatic effects by lowering bulk ionic strength results in lower virus adsorption of bacteriophages to varying surface types. The

hydrophobicity of phages and surface roughness determines their propensity to adsorb to hydrophobic surfaces, with higher phage hydrophobicity and surface roughness leading to higher adsorption.[91,92] The influence of hydrophobic interactions on virus adsorption to surfaces has also been demonstrated and characterized in terms of total free energy for HAV.[93] The significance of hydrophobic interactions for bacteriophage and HAV adsorption to surfaces demonstrates the importance of non-DLVO interactions for virus behavior and stability.

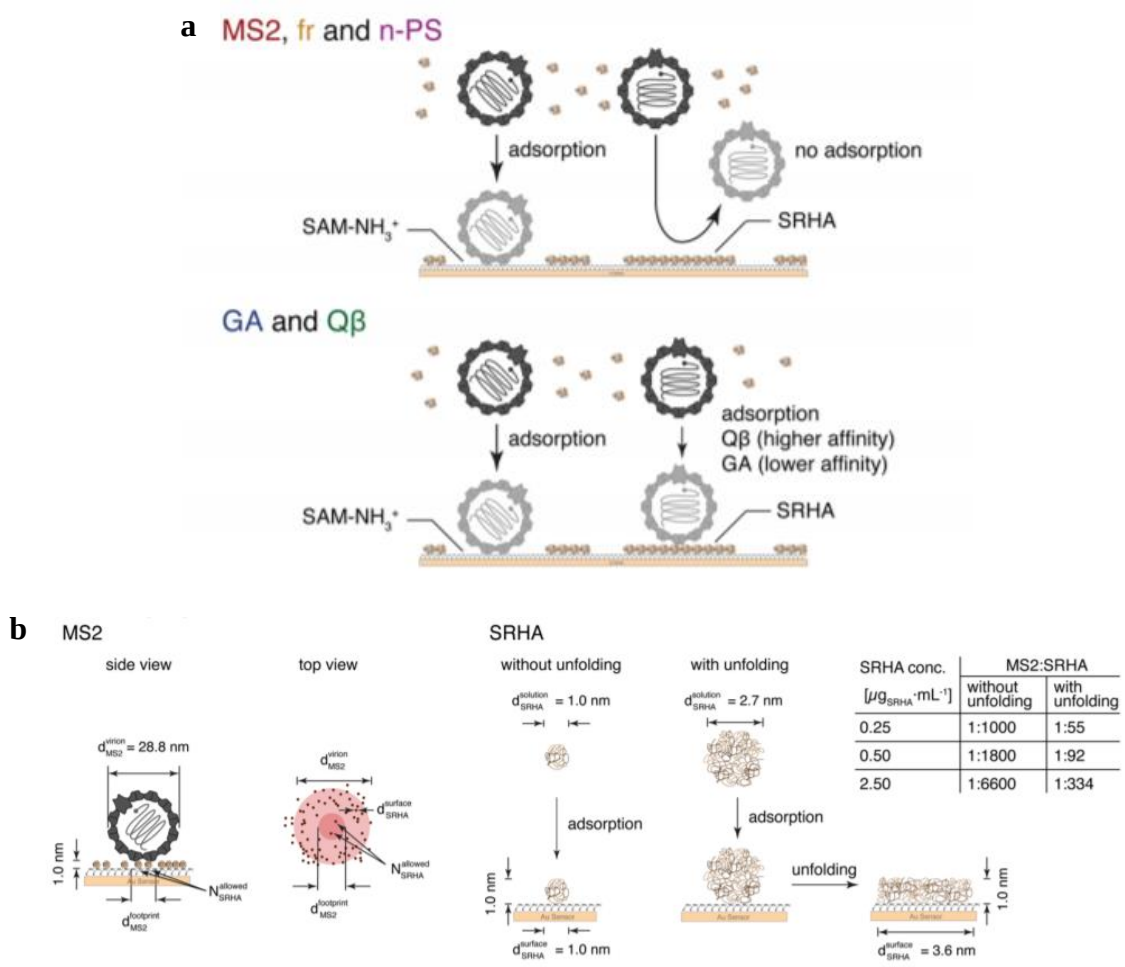

Figure 1.6 a) Comparison of competitive binding and coadsorption of MS2 and organic matter, Suwannee River humic acid (SRHA). b) Comparison of virus binding to surfaces with adsorbed organic matter with and without protein unfolding.[95]

Electrokinetic measurements are also useful in determining colloid and protein adsorption onto surfaces.[94] Viruses with net-negative surface charge readily adsorb to positively-charged surfaces, but organic matter with negative charge competes for adsorption sites (Figure 1.6a).[95] Depending on their relative charge, viruses may also bind onto the surface

of organic matter. Protein unfolding can result in stronger binding to certain surfaces (Figure 1.6b). Contributions by divalent cations in solution are important in rotavirus deposition onto organic matter.[96] These dynamics are important in water filtration and influence the persistence of waterborne viruses in the environment. High concentrations of organic matter encourage rotavirus aggregation and deposition, so viruses may remain dispersed and continue spreading in places with low concentrations of organic matter.[96] Rotavirus adsorption onto organic dispersed matter was shown to be driven by hydrogen bonding between carboxyl and hydroxyl groups,[97] whereas bacteriophage adsorption onto model clay colloids was driven largely by hydrophobic interactions.[88]

Virus adsorption to surfaces also varies between strains of a virus and is a strong function of the valency of the ions present in solution. A comparison of GI.7 and GII.4 norovirus VLPs has demonstrated that phosphate ions decreased attachment of GII.4 VLPs and increased attachment of GI.7 VLPs to silica.[98] The adsorption of both strains has been enhanced by increases in divalent cation concentration, possibly due to specific interactions with the capsids[98] or ion bridging. It has also been shown that non-enveloped icosahedral viruses irreversibly adsorb at air/water interfaces depending on their pH-dependent surface properties.[99] The amphiphilic properties of the capsid proteins facilitate adsorption at air/water interfaces.

Foodborne virus binding to produce presents an enhanced risk for human infection because produce is often not subject to thermal cooking prior to being consumed. Fresh fruits and vegetables can bind high amounts of up to 2% of all viruses exposed to the surface[100] and retain up to 11% of bound viruses even after washing multiple times.[101] Binding and removal

of viruses depends on the properties of the produce and washing solution. Several studies have been performed evaluating the effects of disinfectant or washing solution properties and of produce surface and coating properties on virus binding and removal.

Virus binding to produce surfaces has been attributed to both specific and non-specific surface interactions. Increasing the ionic strength of washing solutions results in decreased attachment of enteric virus surrogates to the surface of lettuce above the isoelectric point of the viruses, indicating that electrostatic interactions are important in nonspecific binding of these viruses to lettuce leaves.[102] Vegetables with crystallized wax coating their surface exhibit lower surface roughness and higher contact angles compared with vegetables without a wax coating, resulting in less rotavirus adsorption.[101] The presence of wax on produce is also important in determining disinfectant efficiency. An oxidizing disinfectant has been shown to have greater activity when used on produce leaves with greater levels of surface wax as compared with produce leaves with low levels of surface wax.[103] A surfactant-based disinfectant exhibited similar disinfectant efficiency on both produce types,[103] likely due to its amphiphilic properties. The presence of cell receptor-like carbohydrates has been reported within the cell wall of lettuce, allowing for specific binding of human noroviruses to the lettuce surface.[104] Surfactants significantly enhance removal of murine norovirus from produce surfaces, providing an increase of up to 2 logs as compared to washing solutions without surfactant.[105] Physical methods, such as scrubbing and peeling, also enhance removal of MNV and HAV from contaminated produce by up to 3 logs.[106]

1.3 Impacts of Virus Colloidal Characteristics

1.3.1 Impact of Colloidal Interactions on Disinfection

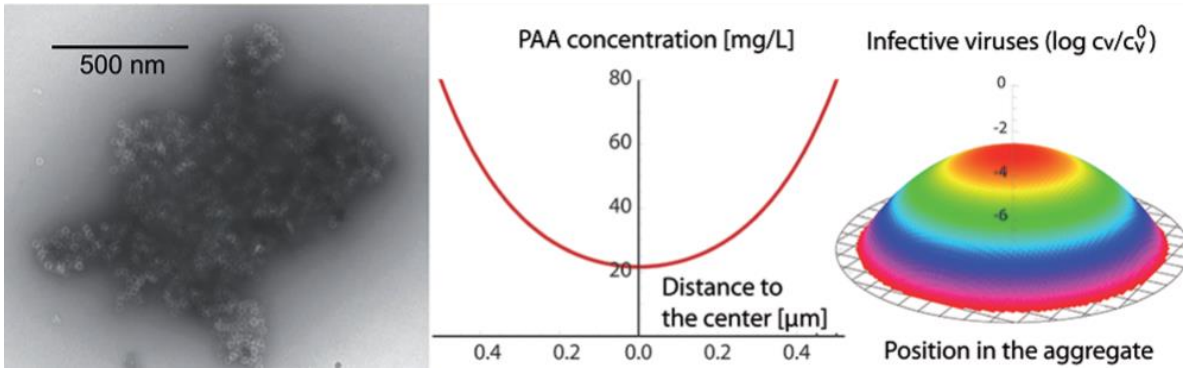

Figure 1.7 Impacts of virus aggregation on disinfection by peracetic acid (PAA). PAA concentration is lower at the center of aggregates, and as a result the viruses at the center of aggregates may remain infectious.[107]

The colloidal characteristics of viruses impact disinfection mainly through the effects of virus aggregation, adsorption onto particles, and capsid conformation. Aggregation inhibits the efficacy of highly reactive disinfectants, as the antiviral agent may be depleted before it reaches viruses on the inside of aggregates (Figure 1.7).[107] Effectively, viruses situated on the outside of aggregates protect those on the inside, so mildly reactive disinfectants are suggested instead of highly reactive ones to ensure diffusion of treatment into aggregates before depletion.[107] Also, permanent fusion of aggregated viruses by certain treatments may allow synergistic behavior of multiple partially inactivated viruses to infect a host cell (multiple infection).[108] Virus-particle association can inhibit virus inactivation, depending on the

conditions.[90] In one study, up to 67% of human noroviruses detected in wastewater treatment pond effluent streams have been bound to particles of diameter in the range 0.45 to 180 μm.[109]

Virus capsid composition impacts disinfection kinetics, but its 3-dimensional structure also plays a very important role as it determines the solvent-accessibility of each amino acid[110] and the proximity of reactive amino acids.[111] Residues that are susceptible to oxidation may form free radicals in the presence of an oxidant, and proximity to other susceptible residues could result in radical propagation.[112] The capsid conformation dependence of disinfection could explain differences in the susceptibilities of similar viruses to the same disinfectant.[110,113,114] Heat treatment of MS2 caused temporary exposure of hydrophobic residues and increased capsid permeability,[115] so the intactness and conformation of the capsid proteins is important in their stability. Inactivated virus particles may still remain intact, but the rearrangement or covalent damaging of the capsid surface may prevent binding and entry to the host cell.[115-117]

1.3.2 Separation and Detection Applications

Many diverse separation and detection methods exist and more are continually being developed for viruses,[118-120] so they are not all mentioned here. We present the most commonly used methods for separation and detection of viruses based on colloidal properties and interactions.

Precipitation is a common protein separation method. Virus precipitation can be achieved by making hydrophobic interactions between particles more dominant. Increasing the dominance of hydrophobic interactions can be accomplished by increasing ionic strength to

shield electrostatic repulsion, adjusting pH to the isoelectric point to reduce electrostatic interactions, dehydrating the protein surface by adding a cosolvent such as ethanol,[121] and neutralizing surface charges by adding oppositely-charged surfactant or multivalent ions.[122] The phenomenon of ions of higher valency having very strong effects on colloid aggregation is known as the Schulze-Hardy rule. Poly(ethylene glycol) (PEG) precipitation is commonly used to separate proteins[123] and viruses.[124-127] PEG is highly hydrophilic, so depletion exclusion of viruses from the dissolved polymer phase results in their precipitation as PEG concentration is increased. Phase separation of viruses between two immiscible polymer aqueous phases can be achieved for viruses with preference for one of the phases.[128]

Separation methods based on the size or density of virus particles include gradient ultracentrifugation and filtration. Density gradient ultracentrifugation using cesium chloride (CsCl) is commonly used to concentrate and purify VLPs of various viruses.[129,130] Viruses can be simultaneously concentrated and filtered from smaller particles, molecules, and salts using centrifugal filters.[131] Microporous filters with positive charge are commonly used to process large volumes of liquid and operate based on size exclusion.[132] Unless multi-step differential filtration is used, density gradient ultracentrifugation offers much more precise particle purification as it separates particles of varying density into distinct bands. Each filtration step only offers separation of particles that are larger or smaller than a single diameter or molecular weight cutoff. Following separation and concentration, viruses are enumerated in a laboratory using cell culture or reverse transcriptase (for RNA viruses) quantitative polymerase chain reaction (RT-qPCR) methods.[132] Laboratory-based purification methods also include affinity chromatography, which exploits the highly-specific interactions between virus and antibody

or other receptor to bind and subsequently elute virus particles.[133,134] Affinity chromatography tends to be quite expensive due to the gel and receptor components, so other methods are often preferred in cases where somewhat lower purity is acceptable.

Development of rapid field-based approaches for separation and detection of viruses is of research interest as well. These methods are usually based on the electrokinetic or specific binding properties of viruses rather than their size. Perhaps the simplest field-based biological detection method is the immunoassay,[135] which takes advantage of the high specificity of antibody-antigen interactions. Immunoassays have been performed in various formats, including microfluidic devices,[136] plate-based assays,[137] flow chambers,[138] and other platforms. Latex microspheres can be coated with antibodies and either achieve simple threshold detection by visible agglutination in the presence of antigen[139] or concentration-dependent impedance detection after precipitation onto electrodes.[140,141] High antigen specificity has also been demonstrated for other receptors, including aptamers,[142-145] carbohydrate cell receptors,[146,147] and bacterial proteins.[148] Receptors or non-specific binding agents can be adsorbed onto magnetic particles for collection and concentration of viruses with a magnetic field[149-153] and subsequent detection.

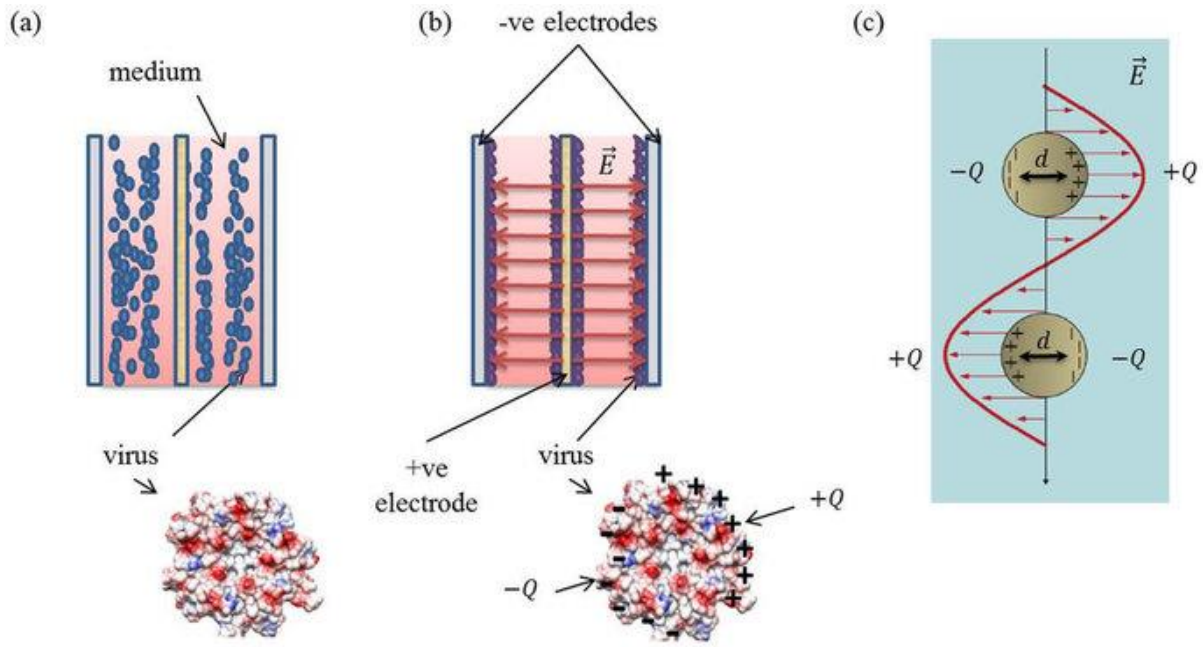

Figure 1.8 Depiction of virus detection enabled by electric field techniques. a) The viruses remain dispersed when the electric field is off. b) Viruses become polarized when the alternating current (AC) electric field is turned on and migrate to the electrodes with higher or lower field intensity based on the difference with the medium polarization. c) Polarization of virus particles within an AC electric field.[154]

More recent advances in detection use the unique electrical properties of viruses to distinguish specific viruses from other particles (Figure 1.8).[154] Capacitance-based virus detection has been achieved by determining the characteristic dielectric constant of a virus type that is dependent on its composition.[155] The dielectric constant of viruses is used in dielectrophoresis (DEP) based separation and detection methods.[156] DEP involves the polarization of particles in a nonuniform electric field that results in their manipulation based on electric field frequency. Viruses move towards the high field electrodes (positive DEP

behavior) or away from the electrodes (negative DEP behavior) depending on whether the electric field frequency is above or below the crossover frequency, which is where DEP forces are zero.[157]

1.3.3 Colloidal Implications for Vaccine Development

Viral vaccines can be composed of attenuated viruses, inactivated viruses, protein antigens, or virus-based or virus-like particles (VLPs).[158] VLPs are attractive candidates for vaccines because they are both immunogenic and noninfectious.[159,160] VLPs are also expressed in non-host vectors using the genes for one or more capsid proteins, so they can be engineered to have enhanced properties such as increased stability, greater immunogenicity, and epitopes for other antigens.[158]

Adjuvants are additives to vaccine formulations that aid in eliciting a sufficient immune response to achieve immunity.[161] These additives are especially important for protein antigens that may be too small to be efficiently recognized by the immune system.[162] Adjuvants decrease the amount of antigen necessary, reducing the cost of vaccine production. The immune response can be increased by slow release of antigen at the immunization site, promoting inflammation at the immunization site to activate an immune cascade, and enhancing antigen uptake by immune cells that stimulate the immune response further.[161] Adjuvants take many forms, including aluminum compounds,[163] complexes of saponins,[164] emulsions,[165] and combinations of these carriers.[164-166] Some adjuvants, such as liposomes, are being developed for delivery of antigens for vaccines as well as other drugs.[166]

Vaccine formulations must facilitate effective antigen loading onto adjuvants, effective antigen release under physiological conditions, and antigen stability during storage and use.[167] Electrostatic interactions, but not hydrophobic interactions, were found to influence antigen adsorption onto aluminum-based adjuvants.[163] The tested aluminum-based adjuvants were hydrogel suspensions, so hydrophobic-mediated protein binding would not have been expected. Ligand exchange is another important effect involved in the interaction of antigen adsorption to aluminum-based adjuvants and involves the competitive binding of phosphate or other groups that are present both in solution and on the antigen.[163,168]

1.3.4 Water Purification from Viruses

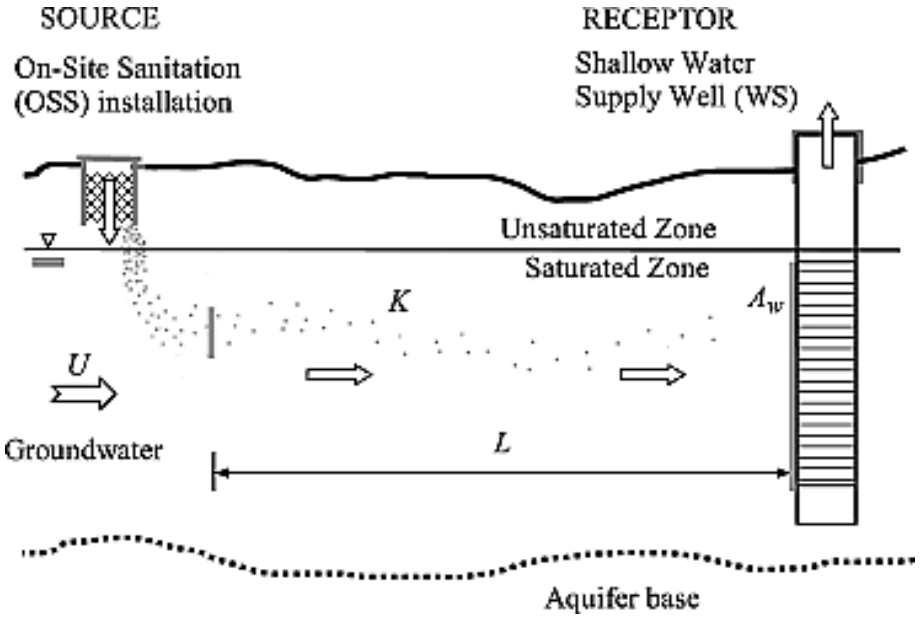

Figure 1.9 Schematic of pathogen transfer from a contamination source to drinking water through various barriers.[169]

Drinking water could become contaminated by fecal pathogens from various sources including sewage pipes, manure fertilizers, reuse of treated wastewater, and aquifers.[169,170] Molin *et al*. completed a risk assessment for the transfer of pathogens from contamination source to ingestion by a human host as they pass through barriers such as groundwater and soil (Figure 1.9).[169] These barriers are capable of naturally inactivating and capturing viral pathogens, and many of the same mechanisms observed in natural water purification are used in wastewater treatment.

Wastewater treatment ponds, activated sludge, and trickling filtration are among the most commonly used methods for water decontamination.[171] Adsorption to solids and resultant sedimentation, predation by other organisms, and sunlight irradiation have been identified as mechanisms by which viruses are removed from wastewater treatment ponds.[172] Enteric viruses were found adsorbed most abundantly onto small colloidal particles with diameter in the range of 0.45 to 180 μm, which suggests that sedimentation is not a major mechanism responsible for the virus removal from wastewater treatment ponds.[109,173] Viruses also adsorb onto algae and bacteria[174] and are inactivated by bacterial growth.[87] Sunlight irradiation is dependent on temperature and the presence of organic matter and can either directly damage virus structures or stimulate the formation of reactive oxygen species from dissolved oxygen that then cause damage.[175] Pond effluents may also be treated by chlorine and UV lamps for additional inactivation.[172]

Coagulation is a strategy used to reduce virus particle numbers and enhance virus filtration. Virus coagulation reduces bacteriophage titer by up to 7 logs[176] and is accomplished by introducing metal salts using chemical dissolution[177] or electro-oxidation of a "sacrificial

electrode" (electrocoagulation).[178] All of the colloidal interactions previously described for virus adsorption and aggregation impact virus removal from contaminated water by coagulation and have been reviewed by Heffron and Mayer.[176] Filtration processes often follow virus coagulation and include membrane bioreactors[179] and biosand filters.[180] New technologies for water treatment that are based on virus adsorption continue to emerge, including materials such as functionalized nanofibers[89] and nonwovens.[181]

1.4 Thesis Overview

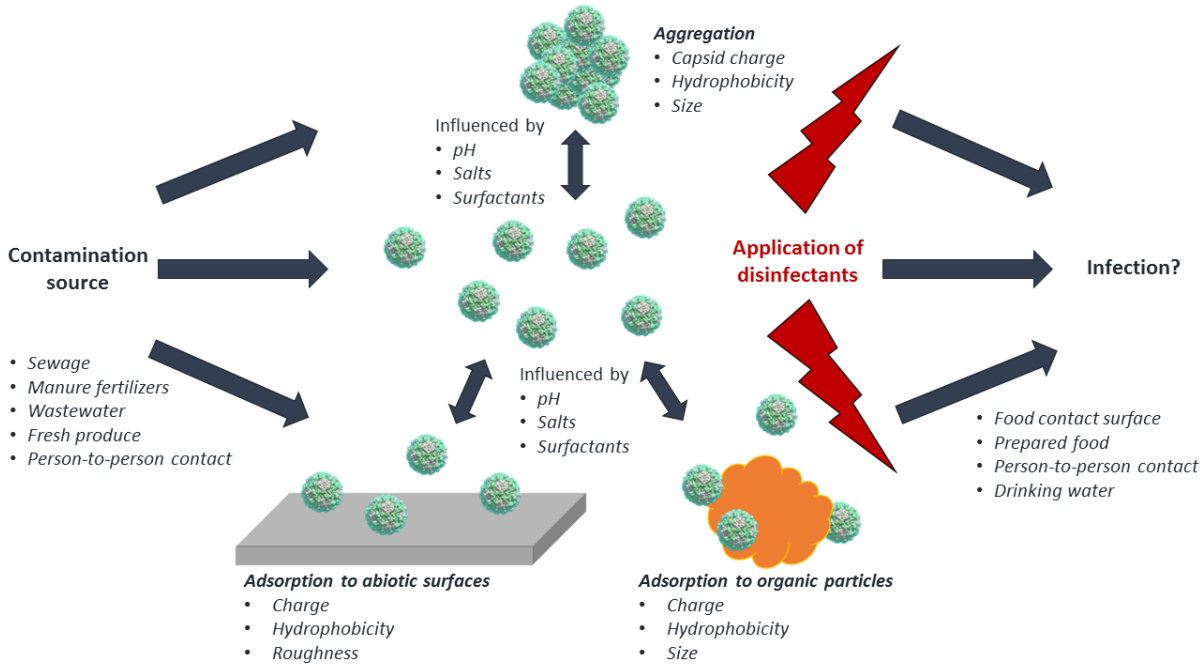

Figure 1.10 Summary of the interactions involved in virus dispersal, adsorption, and persistence in the environment.

Virus interactions with each other and with surfaces of varying types affect their persistence in the environment. Virus and surface properties in addition to solution pH, salt

conditions, and presence of surfactants dictate virus adsorption and aggregation by numerous mechanisms, as shown in Figure 1.10. The resultant state of the viruses affects their susceptibility to disinfectants, infectivity, and further transmission. Human noroviruses are of specific interest as they are the leading cause of foodborne illness in the US and worldwide.[182] Human norovirus is estimated to cause 685 million illnesses and over 200,000 deaths globally annually.[183] Noroviruses pose a major threat to public health and cause billions of dollars in losses to the US alone annually.[184] They are also considered a potential bioterrorism hazard due to the acute and debilitating symptoms of infection.[185] The capsid structure of these viruses is a T=3 icosahedron ranging between 30-38 nm in diameter.[186,187] As an enteric virus, human norovirus is stable in nature at a wide range of pH levels and therefore can be present as dispersed particles or aggregates with varying sizes.[188] Human noroviruses also have astounding persistence with the ability to withstand a wide range of temperatures, pH levels, and chemical treatments in the environment.[189] They can remain on dry surfaces for weeks without losing significant infectivity.[190] Because of the resistance properties that noroviruses possess, they fail to respond to neutralizing methods effective against many other pathogens.[191-194] Noroviruses require more potent disinfection strategies and longer contact times in comparison to other foodborne pathogens.[195]

We aim to reduce the dissemination of human noroviruses in the environment using surfactant and copper ion-based particle modifications. Surfactant adsorption to the capsid surface changes particle interactions with other particles and with surfaces. These solution behaviors have implications for the efficacy of surfactant-based cleaners in removing noroviruses. Aqueous copper can catalyze redox reactions that cause permanent damage to the

capsid and nucleic acid. Capsid damage removes the infectivity of the virus by rendering it unable to bind to and infect a cell or by entirely destroying the virus particle. Inactivation reduces virus titer and thereby lessens its spread in the environment. The development of a new generation of metal ion-based disinfectants could reduce the number of infectious norovirus particles and thus prevent their spread in the environment.

Chapter 2 describes how surfactants can be used to modify and control human norovirus interactions to improve virus clearing. Human norovirus interactions are controlled by its surface properties in addition to the properties of the suspending medium and contact surfaces. The impacts of surfactants commonly used in household antimicrobials and cleaning products on human norovirus dispersion state is not well understood and has implications for virus persistence as well as cleaning and disinfection efforts. Chapter 3 describes the behavior of human norovirus VLPs in the presence of divalent copper ions, and Chapter 4 provides evidence of human norovirus inactivation by copper ions in the presence of sodium ascorbate as a reducing agent. Chapter 5 presents alternative reducing agents to sodium ascorbate in order to improve the formulations introduced in Chapter 4. Chapter 6 summarizes the results presented in this dissertation and provides suggestions for future research on the use of surfactant and copper ion-based approaches to reduce the spread of human norovirus.

1.5 References

1 Sen, T. K. Processes in Pathogenic Biocolloidal Contaminants Transport in Saturated and Unsaturated Porous Media: A Review. *Water Air Soil Pollut.* **216**, 239-256 (2011).

2 Gelderblom, H. R. in Medical Microbiology. 4th Edition.(ed Baron, S.) University of Texas Medical Branch at Galveston, Galveston, TX, (1996).

3 Siber, A., Bozic, A. L. & Podgornik, R. Energies and pressures in viruses: contribution of nonspecific electrostatic interactions. *Phys. Chem. Chem. Phys.* **14**, 3746-3765 (2012).

4 Palacios, G. & Oberste, M. Enteroviruses as agents of emerging infectious diseases. *J. Neurovirol*. **11**, 424-433 (2005).

5 Tapparel, C., Siegrist, F., Petty, T. J. & Kaiser, L. Picornavirus and enterovirus diversity with associated human diseases. *Infection Genetics and Evolution* **14**, 282-293 (2013).

6 Vaughan, G. et al. Hepatitis A virus: Host interactions, molecular epidemiology and evolution. *Infect. Genet. Evol.* **21**, 227-243 (2014).

7 Bondarenko, T. Y., Ternovoi, V. A. & Netesov, S. V. Hepatitis A virus: Structure-functional features of genome, molecular diagnostics, and cultivation. *Molecular Genetics Microbiology and Virology* **28**, 99-109 (2013).

8 Leung, A., Kellner, J. & Davies, H. Rotavirus gastroenteritis. *Adv. Ther.* **22**, 476-487 (2005).

9 Yen, C. et al. Rotavirus vaccines Update on global impact and future priorities. *Human Vaccines* **7**, 1282-1290 (2011).

10 Moore, M. D., Goulter, R. M. & Jaykus, L. Human Norovirus as a Foodborne Pathogen: Challenges and Developments. *Ann. Rev. Food Sci. Technol.* **6,** 411-433 (2015).

11 Robilotti, E., Deresinski, S. & Pinsky, B. A. Norovirus. *Clin. Microbiol. Rev.* **28**, 134-164 (2015).

12 Hall, A. J. *et al.* Norovirus Disease in the United States. *Emerg. Infect. Diseases*. **19**, 1198-1205 (2013).

13 Vasickova, P., Pavlik, I., Verani, M. & Carducci, A. Issues Concerning Survival of Viruses on Surfaces. *Food Environ. Virol.* **2**, 24-34 (2010).

14 Vasickova, P. & Kovarcik, K. Natural persistence of food- and waterborne viruses. *Viruses in Food and Water: Risks, Surveillance and Control*, 179-204 (2013).

15 Carter, M. Enterically infecting viruses: pathogenicity, transmission and significance for food and waterborne infection. *J. Appl. Microbiol*. **98**, 1354-1380 (2005).

16 Seitz, S.R. et al. Norovirus Infectivity in Humans and Persistence in Water. *Appl. Environ. Microbiol.* **77**, 6884-6888 (2011).

17 Teunis, P. F. M. et al. Norwalk virus: How infectious is it? *J. Med. Virol*. **80**, 1468-1476 (2008).

18 Yang, Y. & Griffiths, M. W. Comparative Persistence of Subgroups of F-Specific RNA Phages in River Water. *Appl. Environ. Microbiol*. **79**, 4564-4567 (2013).

19 Stockley, P., Stonehouse, N. & Valegard, K. Molecular Mechanism of Rna Phage Morphogenesis. *Int. J. Biochem*. **26**, 1249-1260 (1994).

20 Baert, L. Foodborne virus inactivation by thermal and non-thermal processes. *Viruses in Food and Water: Risks, Surveillance and Control*, 237-260 (2013).

21 Cromeans, T. et al. Comprehensive Comparison of Cultivable Norovirus Surrogates in Response to Different Inactivation and Disinfection Treatments. *Appl. Environ. Microbiol*. **80**, 5743-5751 (2014).

22 Arthur, S. E. & Gibson, K. E. Physicochemical stability profile of Tulane virus: a human norovirus surrogate. *J. Appl. Microbiol*. **119**, 868-75 (2015).

23 Ettayebi, K. et al. Replication of human noroviruses in stem cell–derived human enteroids. *Science* **353,** 1387-1393 (2016).

24 Jones, M.K. *et al*. Enteric bacteria promote human and mouse norovirus infection of B cells. *Science* **346**, 755-759 (2014).

25 Jones, M.K. *et al*. Human norovirus culture in B cells. *Nat. Protoc.* **10**, 1939-1947 (2015).

26 Leckband, D. Measuring the forces that control protein interactions. *Annu. Rev. Biophys. Biomol. Struct*. **29**, 1-26 (2000).

27 Leckband, D. & Israelachvili, J. Intermolecular forces in biology. *Q. Rev. Biophys*. **34**, 105-267 (2001).

28 Israelachvili, J. N. in Intermolecular and Surface Forces, Third Edition 503-534 Elsevier, Inc., Waltham, MA, (2011).

29 Valle-Delgado, J. J., Molina-Bolivar, J. A., Galisteo-Gonzalez, F. & Galvez-Ruiz, M. J. Evidence of hydration forces between proteins. *Curr. Opin. Colloid Interface Sci.* **16**, 572-578 (2011).

30 Huggins, D. J. Studying the role of cooperative hydration in stabilizing folded protein states. *J. Struct. Biol.* **196**, 394-406 (2016).

31 Penrod, S., Olson, T. & Grant, S. Deposition kinetics of two viruses in packed beds of quartz granular media. *Langmuir* **12**, 5576-5587 (1996).

32 Piazza, R. Protein interactions and association: an open challenge for colloid science. *Curr. Opin. Colloid Interface Sci.* **8**, 515-522 (2004).

33 Ohshima, H. Electrical Phenomena of Soft Particles. A Soft Step Function Model. *J. Phys. Chem. A* **116**, 6473-6480 (2012).

34 Ohshima, H. Electrokinetic phenomena of soft particles. *Curr. Opin. Colloid Interface Sci.* **18**, 73-82 (2013).

35 Gopmandal, P. P., Bhattacharyya, S. & Ohshima, H. Effect of core charge density on the electrophoresis of a soft particle coated with polyelectrolyte layer. *Colloid Polym. Sci.* **294**, 727-733 (2016).

36 Langlet, J., Gaboriaud, F., Duval, J. F. L. & Gantzer, C. Aggregation and surface properties of F-specific RNA phages: Implication for membrane filtration processes. *Water Res.* **42**, 2769-2777 (2008).

37 Duval, J. F. L. & Gaboriaud, F. Progress in electrohydrodynamics of soft microbial particle interphases. *Curr. Opin. Colloid Interface Sci*. **15**, 184-195 (2010).

38 Bozic, A. L., Siber, A. & Podgornik, R. How simple can a model of an empty viral capsid be? Charge distributions in viral capsids. *J. Biol. Phys*. **38**, 657-671 (2012).

39 Hernando-Perez, M. et al. Quantitative nanoscale electrostatics of viruses. *Nanoscale* **7**, 17289-17298 (2015).

40 De, S., Bhattacharyya, S. & Gopmandal, P. P. Importance of core electrostatic properties on the electrophoresis of a soft particle. *Phys. Rev. E* **94**, 022611 (2016).

41 Helfricht, N., Doblhofer, E., Duval, J. F. L., Scheibel, T. & Papastavrou, G. Colloidal Properties of Recombinant Spider Silk Protein Particles. *J. Phys. Chem. C* **120**, 18015-18027 (2016).

42 Duval, J. F. L. Dynamics of metal uptake by charged biointerphases: bioavailability and bulk depletion. *Phys. Chem. Chem. Phys*. **15**, 7873-7888 (2013).

43 Bozic, A. L. & Podgornik, R. Symmetry effects in electrostatic interactions between two arbitrarily charged spherical shells in the Debye-Huckel approximation. *J. Chem. Phys*. **138**, 074902 (2013).

44 Yeh, L., Tai, Y., Wang, N., Hsu, J. & Qian, S. Electrokinetics of pH-regulated zwitterionic polyelectrolyte nanoparticles. *Nanoscale* **4**, 7575-7584 (2012).

45 Michen, B. & Graule, T. Isoelectric points of viruses. *J. Appl. Microbiol*. **109**, 388-397 (2010).

46 Armanious, A. et al. Viruses at Solid Water Interfaces: A Systematic Assessment of Interactions Driving Adsorption. *Environ. Sci. Technol*. **50**, 732-743 (2016).

47 Nguyen, T. H. et al. The RNA core weakly influences the interactions of the bacteriophage MS2 at key environmental interfaces. *Soft Matter* **7**, 10449-10456 (2011).

48 Dika, C., Duval, J. F. L., Ly-Chatain, H. M., Merlin, C. & Gantzer, C. Impact of Internal RNA on Aggregation and Electrokinetics of Viruses: Comparison between MS2 Phage and Corresponding Virus-Like Particles. *Appl. Environ. Microbiol*. **77**, 4939-4948 (2011).

49 Phan, A. D. et al. Electric potential profile of a spherical soft particle with a charged core. *J. Chem. Phys*. **139**, 244908 (2013).

50 Dika, C., Gantzer, C., Perrin, A. & Duval, J. F. L. Impact of the virus purification protocol on aggregation and electrokinetics of MS2 phages and corresponding virus-like particles. *Phys. Chem. Chem. Phys*. **15**, 5691-5700 (2013).

51 Sirotkin, S., Mermet, A., Bergoin, M., Ward, V. & Van Etten, J. L. Viruses as nanoparticles: Structure versus collective dynamics. *Phys. Rev. E* **90**, 022718 (2014).

52 Roos, W. H., Bruinsma, R. & Wuite, G. J. L. Physical virology. *Nature Phys*. **6**, 733-743 (2010).

53 Mateu, M. G. Mechanical properties of viruses analyzed by atomic force microscopy: A virological perspective. *Virus Res*. **168**, 1-22 (2012).

54 Guha, S., Li, M., Tarlov, M. J. & Zechariah, M. R. Electrospray-differential mobility analysis of bionanoparticles. *Trends Biotechnol*. **30**, 291-300 (2012).

55 Snijder, J. et al. Probing the biophysical interplay between a viral genome and its capsid. *Nat. Chem.* **5**, 502-509 (2013).

56 Boyd, K. J., Bansal, P., Feng, J. & May, E. R. Stability of Norwalk Virus Capsid Protein Interfaces Evaluated by in Silico Nanoindentation. *Front. Bioeng. Biotechnol.* **3**, 103 (2015).

57 Bishop, K. J. M., Wilmer, C. E., Soh, S. & Grzybowski, B. A. Nanoscale Forces and Their Uses in Self-Assembly. *Small* **5**, 1600-1630 (2009).

58 Mateu, M. G. Assembly, stability and dynamics of virus capsids. *Arch. Biochem. Biophys.* **531**, 65-79 (2013).

59 Perlmutter, J. D. & Hagan, M. F. Mechanisms of Virus Assembly. *Ann. Rev. Phys. Chem.* **66**, 217-239 (2015).

60 Caspar, D. & Klug, A. Physical Principles in Construction of Regular Viruses. *Cold Spring Harb. Symp. Quant. Biol.* **27**, 1 (1962).

61 Tresset, G. et al. Norovirus Capsid Proteins Self-Assemble through Biphasic Kinetics via Long-Lived Stave-like Intermediates. *J. Am. Chem. Soc.* **135**, 15373-15381 (2013).

62 Garmann, R. F., Comas-Garcia, M., Knobler, C. M. & Gelbart, W. M. Physical Principles in the Self-Assembly of a Simple Spherical Virus. *Acc. Chem. Res*. **49**, 48-55 (2016).

63 Shojaei, H. R., Bozic, A. L., Muthukumar, M. & Podgornik, R. Effects of long-range interactions on curvature energies of viral shells. *Phys. Rev. E* **93**, 052415 (2016).

64 Belyi, V. A. & Muthukumar, M. Electrostatic origin of the genome packing in viruses. *Proc. Natl. Acad. Sci. U. S. A.* **103**, 17174-17178 (2006).

65 Bruinsma, R. F., Comas-Garcia, M., Garmann, R. F. & Grosberg, A. Y. Equilibrium self-assembly of small RNA viruses. *Phys. Rev. E* **93**, 032405 (2016).

66 Kelly, J., Grosberg, A. Y. & Bruinsma, R. Sequence Dependence of Viral RNA Encapsidation. *J. Phys. Chem. B* **120**, 6038-6050 (2016).

67 Tubiana, L., Bozic, A. L., Micheletti, C. & Podgornik, R. Synonymous Mutations Reduce Genome Compactness in Icosahedral ssRNA Viruses. *Biophys. J.* **108**, 194-202 (2015).

68 Ceres, P. & Zlotnick, A. Weak protein-protein interactions are sufficient to drive assembly of hepatitis B virus capsids. *Biochemistry* **41**, 11525-11531 (2002).

69 Glasgow, J. & Tullman-Ercek, D. Production and applications of engineered viral capsids. *Appl. Microbiol. Biotechnol.* **98**, 5847-5858 (2014).

70 Vega-Acosta, J. R., Cadena-Nava, R. D., Gelbar, W. M., Knobler, C. M. & Ruiz-Garcia, J. Electrophoretic Mobilities of a Viral Capsid, Its Capsid Protein, and Their Relation to Viral Assembly. *J Phys Chem B* **118**, 1984-1989 (2014).

71 Damasceno, P. F., Engel, M. & Glotzer, S. C. Predictive Self-Assembly of Polyhedra into Complex Structures. *Science* **337**, 453-457 (2012).

72 de Nijs, B. et al. Entropy-driven formation of large icosahedral colloidal clusters by spherical confinement. *Nat. Mater.* **14**, 56-60 (2015).

73 Floyd, R. & Sharp, D. Viral Aggregation - Quantitation and Kinetics of Aggregation of Poliovirus and Reovirus. *Appl. Environ. Microbiol.* **35**, 1079-1083 (1978).

74 Kurganov, B. I., Rafikova, E. R. & Dobrov, E. N. Kinetics of thermal aggregation of tobacco mosaic virus coat protein. *Biochemistry-Moscow* **67**, 525-533 (2002).

75 Panyukov, Y., Yudin, I., Drachev, V., Dobrov, E. & Kurganov, B. The study of amorphous aggregation of tobacco mosaic virus coat protein by dynamic light scattering. *Biophys. Chem*. **127**, 9-18 (2007).

76 Mertens, B. S. & Velev, O. D. Characterization and control of surfactant-mediated Norovirus interactions. *Soft Matter* **11,** 8621-8631 (2015).

77 Samandoulgou, I., Fliss, I. & Jean, J. Zeta Potential and Aggregation of Virus-Like Particle of Human Norovirus and Feline Calicivirus Under Different Physicochemical Conditions. *Food Environ. Virol.* **7**, 249-260 (2015).

78 Langlet, J., Gaboriaud, F. & Gantzer, C. Effects of pH on plaque forming unit counts and aggregation of MS2 bacteriophage. *J. Appl. Microbiol*. **103**, 1632-1638 (2007).

79 Mylon, S. E. et al. Influence of Salts and Natural Organic Matter on the Stability of Bacteriophage MS2. *Langmuir* **26**, 1035-1042 (2010).

80 Gutierrez, L., Mylon, S. E., Nash, B. & Nguyen, T. H. Deposition and Aggregation Kinetics of Rotavirus in Divalent Cation Solutions. *Environ. Sci. Technol*. **44**, 4552-4557 (2010).

81 Langlet, J., Gaboriaud, F., Gantzer, C. & Duval, J. F. L. Impact of chemical and structural anisotropy on the electrophoretic mobility of spherical soft multilayer particles: The case of bacteriophage MS2. *Biophys. J*. **94**, 3293-3312 (2008).

82 Duval, J. F. L., and H. Ohshima. 2006. Electrophoresis of diffuse soft particles. *Langmuir* **22**, 3533–3546.

83 Stenstam, A., Topgaard, D. & Wennerstrom, H. Aggregation in a protein-surfactant system. The interplay between hydrophobic and electrostatic interactions. *J. Phys. Chem. B* **107**, 7987-7992 (2003).

84 Panyukov, Y. V., Nemykh, M. A., Dobrov, E. N. & Drachev, V. A. Surfactant-induced amorphous aggregation of tobacco mosaic virus coat protein: A physical methods approach. *Macromol. Biosci*. **8**, 199-209 (2008).

85 Palacio, M. L. B. & Bhushan, B. Bioadhesion: a review of concepts and applications. *Philosophical Transactions of the Royal Society A-Mathematical Physical and Engineering Sciences* **370**, 2321-2347 (2012).

86 Adamczyk, Z., Nattich-Rak, M., Sadowska, M., Michna, A. & Szczepaniak, K. Mechanisms of nanoparticle and bioparticle deposition - Kinetic aspects. *Colloids and Surf. A-Physicochem. Eng. Asp.* **439**, 3-22 (2013).

87 Sobsey, M. & Cooper, R. Enteric Virus Survival in Algal-Bacterial Wastewater Treatment Systems 1. Laboratory Studies. *Water Res*. **7**, 669-685 (1973).

88 Chrysikopoulos, C. V. & Syngouna, V. I. Attachment of bacteriophages MS2 and Phi X174 onto kaolinite and montmorillonite: Extended-DLVO interactions. *Colloids and Surfaces B-Biointerfaces* **92**, 74-83 (2012).

89 Mi, X. & Heldt, C. L. Adsorption of a non-enveloped mammalian virus to functionalized nanofibers. *Colloids Surf. B Biointerfaces* **121**, 319-324 (2014).

90 Templeton, M. R., Andrews, R. C. & Hofmann, R. Particle-associated viruses in water: Impacts on disinfection processes. *Crit. Rev. Environ. Sci. Technol*. **38**, 137-164 (2008).

91 Dika, C., Ly-Chatain, M. H., Francius, G., Duval, J. F. L. & Gantzer, C. Non-DLVO adhesion of F-specific RNA bacteriophages to abiotic surfaces: Importance of surface roughness, hydrophobic and electrostatic interactions. *Colloids Surf. A Physicochem. Eng. Asp.* **435**, 178-187 (2013).

92 Dika, C., Duval, J. F. L., Francius, G., Perrin, A. & Gantzer, C. Isoelectric point is an inadequate descriptor of MS2, Phi X 174 and PRD1 phages adhesion on abiotic surfaces. *J. Colloid Interface Sci*. **446**, 327-334 (2015).

93 Kukavica-Ibrulj, I., Darveau, A., Jean, J. & Fliss, I. Hepatitis A virus attachment to agri-food surfaces using immunological, virological and thermodynamic assays. *J. Appl. Microbiol.* **97**, 923-934 (2004).

94 Adamczyk, Z., Nattich, M., Wasilewska, M. & Zaucha, M. Colloid particle and protein deposition - Electrokinetic studies. *Adv. Colloid Interface Sci*. **168**, 3-28 (2011).

95 Armanious, A., Muench, M., Kohn, T. & Sander, M. Competitive Coadsorption Dynamics of Viruses and Dissolved Organic Matter to Positively Charged Sorbent Surfaces. *Environ. Sci. Technol*. **50**, 3597-3606 (2016).

96 Gutierrez, L. & Nguyen, T. H. Interactions between Rotavirus and Suwannee River Organic Matter: Aggregation, Deposition, and Adhesion Force Measurement. *Environ. Sci. Technol*. **46**, 8705-8713 (2012).

97 Gutierrez, L. & Nguyen, T. H. Interactions between Rotavirus and Natural Organic Matter Isolates with Different Physicochemical Characteristics. *Langmuir* **29**, 14460-14468 (2013).

98 da Silva, A. K., Kavanagh, O. V., Estes, M. K. & Elimelech, M. Adsorption and Aggregation Properties of Norovirus GI and GII Virus-like Particles Demonstrate Differing Responses to Solution Chemistry. *Environ. Sci. Technol*. **45**, 520-526 (2011).

99 Torres-Salgado, J. F. *et al*. Physicochemical Study of Viral Nanoparticles at the Air/Water Interface. *J Phys Chem B* **120**, 5864-5873 (2016).

100 Deboosere, N. *et al*. Adhesion of human pathogenic enteric viruses and surrogate viruses to inert and vegetal food surfaces. *Food Microbiol*. **32**, 48-56 (2012).

101 Lu, L. *et al*. Influence of Epicuticular Physicochemical Properties on Porcine Rotavirus Adsorption to 24 Leafy Green Vegetables and Tomatoes. *PloS One* **10**, e0132841 (2015).

102 Vega, E., Garland, J. & Pillai, S. D. Electrostatic forces control nonspecific virus attachment to lettuce. *J. Food Prot*. **71**, 522-529 (2008).

103 Fuzawa, M. et al. Effect of Leaf Surface Chemical Properties on Efficacy of Sanitizer for Rotavirus Inactivation. *Appl. Environ. Microbiol*. **82**, 6214-6222 (2016).

104 Gao, X., Esseili, M. A., Lu, Z., Saif, L. J. & Wang, Q. Recognition of Histo-Blood Group Antigen-Like Carbohydrates in Lettuce by Human GII.4 Norovirus. *Appl. Environ. Microbiol*. **82**, 2966-2974 (2016).

105 Predmore, A. & Li, J. Enhanced Removal of a Human Norovirus Surrogate from Fresh Vegetables and Fruits by a Combination of Surfactants and Sanitizers. *Appl. Environ. Microbiol*. **77**, 4829-4838 (2011).

106 Wang, Q., Erickson, M. C., Ortega, Y. & Cannon, J. L. Physical Removal and Transfer of Murine Norovirus and Hepatitis A Virus from Contaminated Produce by Scrubbing and Peeling. *J. Food Prot.* **76**, 85-92 (2013).

107 Mattle, M. J. *et al*. Impact of Virus Aggregation on Inactivation by Peracetic Acid and Implications for Other Disinfectants. *Environ. Sci. Technol*. **45**, 7710-7717 (2011).

108 Mattle, M. J. & Kohn, T. Inactivation and Tailing during UV254 Disinfection of Viruses: Contributions of Viral Aggregation, Light Shielding within Viral Aggregates, and Recombination. *Environ. Sci. Technol*. **46**, 10022-10030 (2012).

109 Da Silva, A. K. *et al*. Norovirus Removal and Particle Association in a Waste Stabilization Pond. *Environ. Sci. Technol*. **42**, 9151-9157 (2008).

110 Sigstam, T. *et al*. Subtle Differences in Virus Composition Affect Disinfection Kinetics and Mechanisms. *Appl. Environ. Microbiol*. **79**, 3455-3467 (2013).

111 Choe, J. K., Richards, D. H., Wilson, C. J. & Mitch, W. A. Degradation of Amino Acids and Structure in Model Proteins and Bacteriophage MS2 by Chlorine, Bromine, and Ozone. *Environ. Sci. Technol*. **49**, 13331-13339 (2015).

112 Miller, D., Buettner, G. & Aust, S. Transition-Metals as Catalysts of Autoxidation Reactions. *Free Radic. Biol. Med.* **8**, 95-108 (1990).

113 Park, G. W. *et al*. Strain-Specific Virolysis Patterns of Human Noroviruses in Response to Alcohols. *PloS One* **11**, e0157787 (2016).

114 Li, D. *et al*. Evaluation of methods measuring the capsid integrity and/or functions of noroviruses by heat inactivation. *J. Virol. Methods* **181**, 1-5 (2012).

115 Brie, A., Bertrand, I., Meo, M., Boudaud, N. & Gantzer, C. The Effect of Heat on the Physicochemical Properties of Bacteriophage MS2. *Food Environ. Virol.* **8**, 251-261 (2016).

116 Li, X. & Chen, H. Evaluation of the Porcine Gastric Mucin Binding Assay for High-Pressure-Inactivation Studies Using Murine Norovirus and Tulane Virus. *Appl. Environ. Microbiol*. **81**, 515-521 (2015).

117 Hirneisen, K. A. & Kniel, K. E. Comparison of ELISA attachment and infectivity assays for murine norovirus. *J. Virol. Methods* **186**, 14-20 (2012).

118 Knight, A., Li, D., Uyttendaele, M. & Jaykus, L. A critical review of methods for detecting human noroviruses and predicting their infectivity. *Crit. Rev. Microbiol*. **39**, 295-309 (2013).

119 Sidoti, F., Ritta, M., Costa, C. & Cavallo, R. Diagnosis of viral gastroenteritis: limits and potential of currently available procedures. *J. Infect. Dev. Ctries.* **9**, 551-561 (2015).

120 Schrader, C., Johne, R., Schielke, A. & Ellerbroek, L. Food associated viruses and their detection - a review. *Archiv Fur Lebensmittelhygiene* **62**, 36-51 (2011).

121 Yoshizawa, S., Arakawa, T. & Shiraki, K. Dependence of ethanol effects on protein charges. *Int. J. Biol. Macromol*. **68**, 169-172 (2014).

122 van Oss, C. J. & Giese, R. F. Role of the Polar Properties of Water in Separation Methods. *Sep. Purif. Rev.* **40**, 163-208 (2011).

123 Ingham, K. Protein Precipitation with Polyethylene-Glycol. *Meth. Enzymol*. **104**, 351-356 (1984).

124 Fontes, L., Campos, G., Beck, P., Brandao, C. & Sardi, S. Precipitation of bovine rotavirus by polyethylen glycol (PEG) and its application to produce polyclonal and monoclonal antibodies. *J. Virol. Methods* **123**, 147-153 (2005).

125 Jaykus, L., DeLeon, R. & Sobsey, M. Development of a molecular method for the detection of enteric viruses in oysters. *J. Food Prot*. **58**, 1357-1362 (1995).

126 Summa, M., von Bonsdorff, C. & Maunula, L. Evaluation of four virus recovery methods for detecting noroviruses on fresh lettuce, sliced ham, and frozen raspberries. *J. Virol. Methods* **183**, 154-160 (2012).

127 Hafliger, D., Gilgen, M., Luthy, J. & Hubner, P. Seminested RT-PCR systems for small round structured viruses and detection of enteric viruses in seafood. *Int. J. Food Microbiol.* **37**, 27-36 (1997).

128 Shuval, H., Fattal, B., Cymbalis, S. & Goldblum, N. Phase-Separation Method for Concentration and Detection of Viruses in Water. *Water Res*. **3**, 225-& (1969).

129 Crawford, S. et al. Characterization of Virus-Like Particles Produced by the Expression of Rotavirus Capsid Proteins in Insect Cells. *J. Virol*. **68**, 5945-5952 (1994).

130 Xi, J., Min, W., Graham, D. & Estes, M. Expression, Self-Assembly, and Antigenicity of the Norwalk Virus Capsid Protein. *J. Virol*. **66**, 6527-6532 (1992).

131 Qiu, Y. et al. A one-step centrifugal ultrafiltration method to concentrate enteric viruses from wastewater. *J. Virol. Methods* **237**, 150-153 (2016).

132 Ikner, L. A., Gerba, C. P. & Bright, K. R. Concentration and Recovery of Viruses from Water: A Comprehensive Review. *Food Environ. Virol.* **4**, 41-67 (2012).

133 Elkana, Y., Thornton, A. & Zuckerman, A. Purification of Hepatitis-a Virus by Affinity Chromatography. *J. Immunol. Methods* **25**, 185-187 (1979).

134 Oneil, P. & Balkovic, E. Virus Harvesting and Affinity-Based Liquid-Chromatography - a Method for Virus Concentration and Purification. *Bio-Technology* **11**, 173-178 (1993).

135 Andreotti, P. E. *et al.* Immunoassay of infectious agents. *BioTechniques* **35**, 850-859 (2003).

136 Leng Chuan, Zhang Xiaoqing & Jue Huangxian. Microfluidic Chip-Based Immunoassay. *Prog. Chem.* **21**, 687-695 (2009).

137 Denis, F. *et al*. Virus associated with the gastrointestinal tract. *Ann. Biol. Clin.* (Paris) **55**, 275-287 (1997).

138 Gupta, S., Huda, S., Kilpatrick, P. K. & Velev, O. D. Characterization and optimization of gold nanoparticle-based silver-enhanced immunoassays. *Anal. Chem*. **79**, 3810-3820 (2007).

139 Molina-Bolivar, J. A. & Galisteo-Gonzalez, F. Latex immunoagglutination assays. *J. Macromol. Sci. Polymer Rev* **45**, 59-98 (2005).

140 Pejcic, B. & De Marco, R. Impedance spectroscopy: Over 35 years of electrochemical sensor optimization. *Electrochim. Acta* **51**, 6217-6229 (2006).

141 Gupta, S., Kilpatrick, P. K., Melvin, E. & Velev, O. D. On-chip latex agglutination immunoassay readout by electrochemical impedance spectroscopy. *Lab Chip* **12**, 4279-4286 (2012).

142 Moore, M. D., Bobay, B. G., Mertens, B. & Jaykus, L. A. Human Norovirus Aptamer Exhibits High Degree of Target Conformation-Dependent Binding Similar to That of Receptors and Discriminates Particle Functionality. *mSphere* (2016).

143 Escudero-Abarca, B. I., Suh, S. H., Moore, M. D., Dwivedi, H. P. & Jaykus, L. Selection, Characterization and Application of Nucleic Acid Aptamers for the Capture and Detection of Human Norovirus Strains. *PloS One* **9**, e106805 (2014).

144 Giamberardino, A. *et al*. Ultrasensitive Norovirus Detection Using DNA Aptasensor Technology. *PLoS One* **8**, e79087 (2013).

145 Moore, M.D., Bobay, B.G., Mertens, B. & Jaykus, L.A. Human Norovirus Aptamer Exhibits High Degree of Target Conformation-Dependent Binding Similar to That of Receptors and Discriminates Particle Functionality. *mSphere* **1**, e00298-16 (2016).

146 Hutson, A. M., Atmar, R. L., Marcus, D. M. & Estes, M. K. Norwalk virus-like particle hemagglutination by binding to H histo-blood group antigens. *J. Virol*. **77**, 405-415 (2003).

147 Tan, M. & Jiang, X. Histo-blood group antigens: a common niche for norovirus and rotavirus. *Expert Rev. Mol. Med.* **16**, e5 (2014).

148 Imai, T. et al. Adsorption characteristics of an enteric virus-binding protein to norovirus, rotavirus and poliovirus. *Bmc Biotechnology* **11**, 123 (2011).

149 Sakudo, A. & Onodera, T. Virus capture using anionic polymer-coated magnetic beads (Review). *Int. J. Mol. Med*. **30**, 3-7 (2012).

150 Elaissari, A. Magnetic Latex Particles in Nanobiotechnologies for Biomedical Diagnostic Applications: State of the Art. *Macromolecular Symposia* **281**, 14-19 (2009).

151 Monceyron, C. & Grinde, B. Detection of Hepatitis-a Virus in Clinical and Environmental-Samples by Immunomagnetic Separation and Pcr. *J. Virol. Methods* **46**, 157-166 (1994).

152 Yang, W. et al. Development of a combined immunomagnetic separation and quantitative reverse transcription-PCR assay for sensitive detection of infectious rotavirus in water samples. *J. Microbiol. Methods* **84**, 447-453 (2011).

153 Yao, L., Wu, Q., Wang, D., Kou, X. & Zhang, J. Development of monoclonal antibody-coated immunomagnetic beads for separation and detection of norovirus (genogroup II) in faecal extract samples. *Lett. Appl. Microbiol*. **49**, 173-178 (2009).

154 Al Ahmad, M., Mustafa, F., Ali, L. M. & Rizvi, T. A. Virus detection and quantification using electrical parameters. *Sci. Rep.* **4**, 6831 (2014).

155 Al Ahmad, M., Mustafa, F., Ali, L. M., Karakkat, J. V. & Rizvi, T. A. Label-Free Capacitance-Based Identification of Viruses. *Sci. Rep.* **5**, 9809 (2015).

156 Nakano, M., Obara, R., Ding, Z. & Suehiro, J. Detection of norovirus and rotavirus by dielectrophoretic impedance measurement. *2013 Seventh International Conference on Sensing Technology (Icst)*, 374-378 (2013).

157 Lapizco-Encinas, B. H. & Rito-Palomares, M. Dielectrophoresis for the manipulation of nanobioparticles. *Electrophoresis* **28**, 4521-4538 (2007).

158 Lee, K. L., Twyman, R. M., Fiering, S. & Steinmetz, N. F. Virus-based nanoparticles as platform technologies for modern vaccines. *Wiley Interdiscip. Rev. Nanomed. Nanobiotechnol.* **8**, 554-578 (2016).

159 Lua, L. H. L. et al. Bioengineering Virus-Like Particles as Vaccines. *Biotechnol. Bioeng.* **111**, 425-440 (2014).

160 Yan, D., Wei, Y., Guo, H. & Sun, S. The application of virus-like particles as vaccines and biological vehicles. *Appl. Microbiol. Biotechnol.* **99**, 10415-10432 (2015).

161 Gupta, A., Das, S., Schanen, B. & Seal, S. Adjuvants in micro- to nanoscale: current state and future direction. *Wiley Interdiscip. Rev. Nanomed. Nanobiotechnol.* **8**, 61-84 (2016).

162 Bobbala, S. & Hook, S. Is There an Optimal Formulation and Delivery Strategy for Subunit Vaccines? *Pharm. Res.* **33**, 2078-2097 (2016).

163 Huang, M. & Wang, W. Factors affecting alum-protein interactions. *Int. J. Pharm.* **466**, 139-146 (2014).

164 Sjolander, A., Cox, J. & Barr, I. ISCOMs: an adjuvant with multiple functions. *J. Leukoc. Biol.* **64**, 713-723 (1998).

165 Garcon, N., Chomez, P. & Van Mechelen, M. GlaxoSmithKline Adjuvant systems in vaccines: concepts, achievements and perspectives. *Expert Rev. Vaccines* **6**, 723-739 (2007).

166 Peek, L. J., Middaugh, C. R. & Berkland, C. Nanotechnology in vaccine delivery. *Adv. Drug Deliv. Rev.* **60**, 915-928 (2008).

167 Wahome, N., Hickey, J. M., Volkin, D. B. & Middaugh, C. R. Formulation Studies During Preclinical Development of Influenza Hemagglutinin and Virus-Like Particle Vaccine Candidates. *Vaccine Design: Methods and Protocols, Vol 2: Vaccines for Veterinary Diseases* **1404**, 393-421 (2016).

168 Jully, V., Mathot, F., Moniotte, N., Preat, V. & Lemoine, D. Mechanisms of Antigen Adsorption Onto an Aluminum-Hydroxide Adjuvant Evaluated by High-Throughput Screening. *J. Pharm. Sci.* **105**, 1829-1836 (2016).

169 Molin, S., Cvetkovic, V. & Stenstrom, T. A. Microbial risk assessment in heterogeneous aquifers: 2. Infection risk sensitivity. *Water Resour. Res.* **46**, W05519 (2010).

170 Petrovic, T. Prevalence of viruses in food and the environment. *Viruses in Food and Water: Risks, Surveillance and Control*, 19-46 (2013).

171 Cook, N. & Richards, G. P. An introduction to food- and waterborne viral disease. *Viruses in Food and Water: Risks, Surveillance and Control*, 3-18 (2013).

172 Verbyla, M. E. & Mihelcic, J. R. A review of virus removal in wastewater treatment pond systems. *Water Res.* **71**, 107-124 (2015).

173 Symonds, E. M. et al. A case study of enteric virus removal and insights into the associated risk of water reuse for two wastewater treatment pond systems in Bolivia. *Water Res*. **65**, 257-270 (2014).

174 Zemb, O., Manefield, M., Thomas, F. & Jacquet, S. Phage adsorption to bacteria in the light of the electrostatics: A case study using E. coli, T2 and flow cytometry. *J. Virol. Methods* **189**, 283-289 (2013).

175 Romero, O. C., Straub, A. P., Kohn, T. & Nguyen, T. H. Role of Temperature and Suwannee River Natural Organic Matter on Inactivation Kinetics of Rotavirus and Bacteriophage MS2 by Solar Irradiation. *Environ. Sci. Technol*. **45**, 10385-10393 (2011).

176 Heffron, J. & Mayer, B. K. Emerging investigators series: virus mitigation by coagulation: recent discoveries and future directions. *Env. Sci. Water Res. Technol.* **2**, 443-459 (2016).

177 Shirasaki, N., Matsushita, T., Matsui, Y., Murai, K. & Aochi, A. Elimination of representative contaminant candidate list viruses, coxsackievirus, echovirus, hepatitis A virus, and norovirus, from water by coagulation processes. *J. Hazard. Mater.* **326**, 110-119 (2017).

178 Chellam, S. & Sari, M. A. Aluminum electrocoagulation as pretreatment during microfiltration of surface water containing NOM: A review of fouling, NOM, DBP, and virus control. *J. Hazard. Mater.* **304**, 490-501 (2016).

179 Visvanathan, C., Ben Aim, R. & Parameshwaran, K. Membrane separation bioreactors for wastewater treatment. *Crit. Rev. Environ. Sci. Technol.* **30**, 1-48 (2000).

180 Wang, H., Li, M., Brockman, K. & Nguyen, T. H. Reduction of MS2 bacteriophage and rotavirus in biosand filters. *Env. Sci. Water Res. Technol.* **2**, 483-491 (2016).

181 Tanioka, A. and Takahashi, M. Highly Productive Systems of Nanofibers for Novel Applications. *Ind Eng Chem Res* **55**, 3759-3764 (2016).

182 Atmar, R.L. and Estes M.K. The epidemiologic and clinical importance of norovirus infection. *Gastroenterol Clin North Am* **35**, 275–90 (2006).

183 Torgerson, P. R. *et al*. World Health Organization Estimates of the Global and Regional Disease Burden of 11 Foodborne Parasitic Diseases, 2010: A Data Synthesis. *PloS Medicine* **12**, e1001920 (2015).

184 Scharff, R.L. Economic Burden from Health Losses Due to Foodborne Illness in the United States. *J. Food Prot.* **75**, 123-31 (2012).

185 E. M. Hartmann and R. U. Halden, in *Detection of biological agents for the prevention of bioterrorism*, ed. J. Banoub, Springer, Dordrecht, The Netherlands, 2011, 158.

186 B. V. V. Prasad, Rothnagel, R., Jiang, X. and Estes M. K. Three-dimensional structure of baculovirus-expressed Norwalk virus capsids. *J. Virol.* **68**, 5117-5125 (1994).

187 J. Choi, A. M. Hutson, M. K. Estes and Prasad B.V.V. Atomic resolution structural characterization of recognition of histo-blood group antigens by Norwalk virus. *Proc. Natl. Acad. Sci. U. S. A.* **105**, 9175-9180 (2008).

188 I. Xagoraraki, Yin, Z. and Svambayev Z. Fate of Viruses in Water Systems *J. Environ. Eng.* **140**, 04014020 (2014).

189 K. Seo, Lee, J.E., Lim, M.Y. and G. Ko G. Effect of temperature, pH, and NaCl on the inactivation kinetics of murine norovirus *J. Food Prot.* **75**, 533-540 (2012).

190 B. I. Escudero, Rawsthorne, H., Gensel, C. and Jaykus, L.A. Persistence and Transferability of Noroviruses on and between Common Surfaces and Food. *J. Food Prot.* **75**, 927-935 (2012).

191 P. Liu, Yuen, Y., Hsiao, H., Jaykus, L.A. and Moe, C. Effectiveness of liquid soap and hand sanitizer against Norwalk virus on contaminated hands *Appl. Environ. Microbiol.* **76**, 394-399 (2010).

192 P. Nowak, Topping, J.R., Fotheringham, V., Gallimore, C.I., Gray, J.J., Iturriza-Gomara, M. and Knight, A.I. Measurement of the virolysis of human GII.4 norovirus in response to disinfectants and sanitisers. *J. Virol. Methods* **174**, 7-11 (2011).

193 G. W. Park, Barclay, L., Macinga, D., Charbonneau, D., Pettigrew, C.A. and J. Vinje, J. Comparative efficacy of seven hand sanitizers against murine norovirus, feline calicivirus, and GII.4 Norovirus. *J. Food Prot.* **73**, 2232-2238 (2010).

194 G. Tung, Macinga, D., Arbogast, J. and Jaykus, L.A. Efficacy of commonly used disinfectants for inactivation of human noroviruses and their surrogates. *J. Food Prot.* **76**, 1210-1217 (2013).

195 K. Whitehead and McCue, K.A. Virucidal efficacy of disinfectant actives against feline calicivirus, a surrogate for norovirus, in a short contact time. *Am. J. Infect. Control* **38**, 26-30 (2010).

CHAPTER 2

Characterization and Control of Surfactant-Mediated Norovirus Interactions

A version of this chapter has been published in

Soft Matter **11,** 8621-8631 (2015).

2.1 Introduction

We report and analyze data on the colloidal interactions of human noroviruses as soft nanoparticles in water using common colloidal characterization techniques such as dynamic light scattering (DLS) and transmission electron microscopy (TEM). The colloidal state of virus particles under various conditions is an aspect of virus behavior that complicates disinfection,[1] so we have investigated the behavior of norovirus-like particles in the presence of different classes of surfactants. Studies have shown that virus aggregates help sustain and may even enhance infectivity by shielding viruses on the inside of aggregates from virucidal treatments.[2,3] Virus aggregation at different pH values and ionic strengths has been well documented in relation to membrane filtration processes,[4-7] but less research has been conducted to elucidate the impact of surfactant type and concentration on virus particle aggregation and subsequent deactivation.[8-10]

As mentioned in Chapter 1, virus-like particles (VLPs) are a useful alternative to viable noroviruses for studying particle surface properties and interactions.[11,12] During their preparation, norovirus major capsid protein is produced in a separate expression vector and spontaneously assembles into the virus capsid structure without infectious RNA inside.[11]

Because the VLPs lack internal RNA that can contribute to particle stability and interactions, VLPs have not been considered as suitable substitutes for viable viruses in disinfection studies.[13] It has been shown that the method used to purify viruses and VLPs also has an impact on virus-virus interactions.[14,15] Instead VLPs may be used as predictors of virus capsid interactions in the presence of differing solution chemistries and possible vaccine agents.[16,17] Norovirus VLPs have been used to study conformational capsid changes that facilitate disassembly over a range of pH levels and temperatures,[12,18-21] and virus surface charge has been previously shown to govern particle behavior.[22] The assembly and disassembly of norovirus VLPs has been shown to mostly involve stable protein dimers, intermediates containing about 11 dimers, and complete capsids composed of 90 dimers.[23] The P domain of the major capsid protein, which forms protrusions on the capsid, is involved in the interactions that form stable dimers, and the S domain is involved in the interactions between dimers to form the icosahedral structure.[24] The capsid protrusions may contribute to VLP stability by adding rigidity to the particles.[25]

Because the outermost layer of norovirus is the protein capsid, its aggregation behavior will have similarities to that of general proteins. Protein interactions are complex and can be influenced by electrostatic double-layer forces, van der Waals forces, hydration, and steric forces.[26] The complexity of protein interactions arises from the characteristic and diverse amino acid compositions that produce hydrophobic, hydrophilic, anionic, and cationic regions on the protein.[27] Slight differences in the sequences of the virus capsid proteins result in perceptible differences in virus susceptibility to certain disinfectants,[28] so understanding virus surface properties is especially important. The factors and interactions related to protein

aggregation have been extensively investigated[29] as they have relevance to food processing[30] and drug development and delivery.[31,32] We use this knowledge and similar experimental techniques to characterize virus aggregation and dispersion.[33]

Electrostatic interactions in water medium strongly influence general colloidal particle behavior, including that of viruses. Non-enveloped viruses have been extensively modeled as soft, porous colloids[34,35] with three shells of charge density, including the protein capsid, capsid-bound RNA, and free RNA.[36,37] Because of the porosity of some virus capsids, the charge of internal RNA has a significant effect on their apparent isoelectric point and therefore would also influence virus stability and binding behavior. Capsid porosity complicates the use of zeta potential as a means of describing particle surface charge even in the absence of internal RNA.[36] Here we use zeta potential data to evaluate the effect of surfactant-altered apparent capsid charge on Norovirus capsid aggregation, dispersion, and disassembly.

Naturally-occurring surface-active molecules such as proteins that behave as surfactants[38] and saponins[39] have been shown to exhibit significant bactericidal and virucidal behavior. These surfactants provide motivation to study the interactions between virus particles and various classes of surfactants to elucidate possible mechanisms of deactivation or stabilization. Surfactants concentrated above their critical micelle concentration (CMC) in aqueous solution form micellar aggregates, which can vary depending on the molecular and electrolytic solvent environment. Surfactant binding to folded or unfolded proteins can influence micelle formation by the development of surfactant-protein structures in addition to free micelles.[40,41] Some micelles have the ability to entrap and solubilize other molecules or particles.[42] Bound surfactants can modify the apparent surface charge of nanoparticles[43] and

therefore influence the interactions and aggregation of these particles in solution. Because proteins are electrostatically diverse and possess hydrophobic, hydrophilic, anionic, and cationic regions, they can bind both anionic and cationic surfactants strongly. Surfactants with charged head groups can alter the effective surface charge of surfaces or particles by shielding opposite charges or adding charge to a hydrophobic site.[44] The high surface activity of surfactants allows them to dictate protein stability and interactions.

We use norovirus VLPs as a model system of specific practical relevance to study surfactant-imposed colloidal interactions of virus capsids. These VLPs are from a GII.4 Houston strain (Houston/TCH186/02) of norovirus that has not yet been characterized by crystallography. The diameter of the VLPs is assumed to be close to that of the GI.1 Norwalk strain, which has been characterized at 38.0 nm in diameter.[45] The intact virus strain contains a genome 7559 base pairs in length and is infectious to humans.[46] We selected one common and widespread anionic, cationic, and nonionic surfactant to represent each surfactant type. We used sodium dodecyl sulfate (SDS) as an anionic surfactant because of its common use in hand soaps, dish detergents, and other household products. We selected cetyltrimethylammonium bromide (CTAB) as a cationic surfactant because of its use as an antimicrobial in many cleaning products. The nonionic surfactant was Tween 20 (polysorbate 20), which is extensively used in many processed food and drink products (which eventually may also be carriers for noroviruses). For varying concentrations of each of these surfactants, we used DLS to determine the sizes of particles in solution and analyzed each peak of intensity distributions to represent either virus aggregates, dispersed viruses, or disassembled virus capsids. We then present electrophoretic light scattering (ELS) data and compare it to the theoretically calculated

capsid charges to explain the mechanisms behind each observed colloidal behavior. Finally, we confirm the presence of VLP aggregation, dispersion, and disassembly with TEM images and describe the impact that each behavior makes on virus infectivity, persistence, and disinfection.

2.2 Results and Discussion

2.2.1 Dynamic Light Scattering (DLS) Characterization of Virus Aggregation State at Varying pH

We used DLS to measure the size of particles present in VLP suspensions in phosphate-buffered saline (PBS). The VLPs concentration was fixed, while pH, surfactant type, and surfactant concentration were varied. For the surfactant effect studies, SDS, CTAB, and Tween 20 were each added individually at concentrations ranging from 0.01% to 0.5% by weight. All of the suspensions containing surfactant were produced at pH 7.4. These data were used to determine whether the VLPs were aggregated, dispersed, or disassembled at each pH or surfactant concentration. We also used ELS to measure the zeta potential of particles present in VLP suspensions with varying pH and surfactant concentrations below 0.05%. Micelles would interfere with the measurement of VLP zeta potential, so higher surfactant concentrations were excluded. These data were used to correlate the electrostatic properties of the particles with their interactions observed by DLS. Finally, we used TEM to view aggregated, dispersed, or disassembled VLPs under selected surfactant conditions.

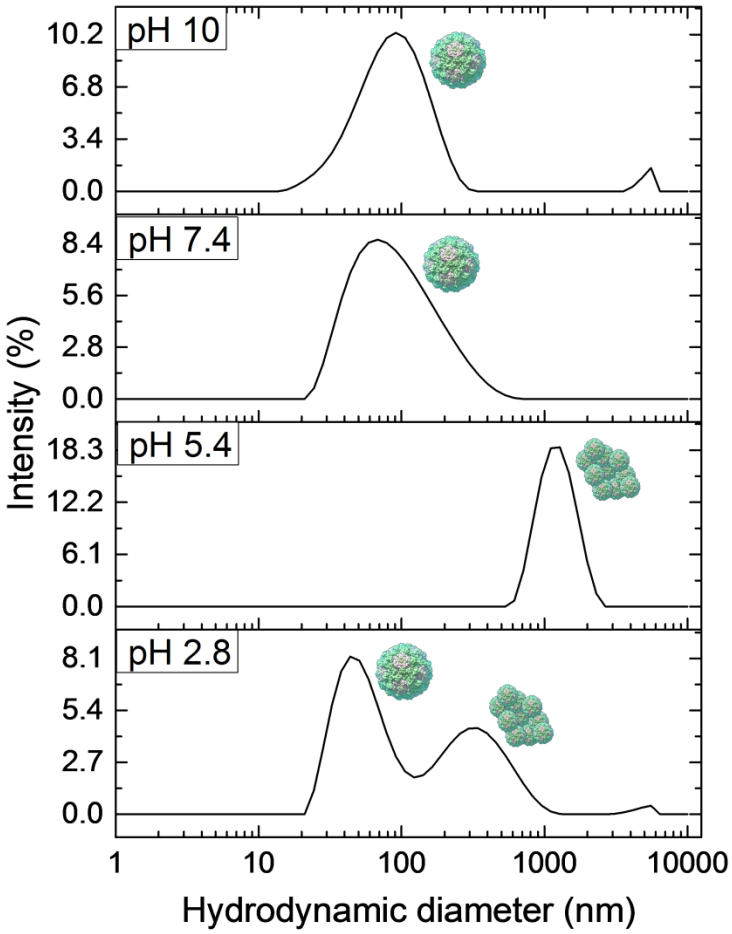

Figure 2.1 Intensity distributions determined by DLS of Norovirus VLPs in PBS of varying pH. The peaks are matched to the schematic presentations of the types of detected species. Data sets are representative curves from 3 repeated measurements for each of 3 different samples at each pH.

DLS data can be represented as intensity, volume, or number distributions of the particle size. We determined that with the concentration of VLPs and surfactants used, the intensity distribution gives an accurate representation of the relative amount of dispersed or aggregated VLPs remaining in solution after each treatment. For the intensity of scattered light,

$I \sim r^6$, so a VLP that is 40 nm in diameter will scatter about 90,000 times more light than a micelle or protein that is 6 nm in diameter. For our VLP and surfactant mixtures, all DLS data are presented as plots of the intensity distributions because the concentration of surfactant micelles in solution is high enough to scatter light proportional to the amount scattered by dispersed VLPs or aggregates. Micelles would be the only particles represented in a volume distribution, where $V \sim r^3$. Details of these calculations are presented in Section 2.4. The corresponding DLS correlation function data are presented in Appendix A.

Because the capsid protein dimers are very similar in size to surfactant micelles, the proteins and micelles overlap in the same peak in the intensity distributions. Therefore these peaks cannot be used to determine the relative amounts of capsid protein dimers produced from VLPs by each treatment. Instead we evaluate the presence or absence of peaks attributed to dispersed or aggregated VLPs to determine the efficacy of each additive to disrupt the particles. Also, because most samples in this study are polydisperse, the algorithms used by the DLS software to determine exact particle size are not precise. The same particle may be reported by the software as slightly different in size in separate measurements. We therefore use ranges of particle sizes to define three categories of peaks in the DLS distributions presented here. A peak in the region of 5-10 nm most likely arises from surfactant micelles, capsid protein dimers, or both; a peak in the region of 30-70 nm represents disperse VLPs; and a peak above 100 nm indicates the presence of VLP aggregates. The data shown in Figure 2.1 demonstrate that the VLPs are well dispersed at low and high pH, while aggregation is prevalent at pH values close to the isoelectric point of the capsid proteins (pH~4.5). Some aggregation is present at neutral pH due to lower magnitude of surface charge compared to low pH. This

slight aggregation accounts for broader peaks for mostly dispersed viruses at 70-80 nm. We analyze further these observations in terms of protein charge and aggregation state after presenting the effects of surfactants on VLP interactions.

2.2.2 Norovirus Integrity and Aggregation in the Presence of Nonionic, Cationic, and Anionic Surfactants

The behavior of VLPs at varying concentrations of added nonionic surfactant, Tween 20, is shown in Figure 2.2. The nonionic surfactant shows little impact on the state of the virus in suspension. A peak indicating the presence of dispersed VLPs exists for each concentration used, and no significant amounts of aggregated VLPs are present. A peak indicating the presence of a micelle or capsid protein dimer emerges at all Tween 20 concentrations greater than 0.05%. However the addition of cationic surfactant, CTAB, had a large effect on VLP behavior, stability, and integrity as shown by the DLS data in Figure 2.3. These data indicate that this surfactant induces much more vigorous and diverse effects. Peaks representing particle aggregates are present at all concentrations below 0.5%, and peaks indicating the presence of surfactant micelles and/or capsid protein dimers are observed at all concentrations above 0.01%. Peaks representing dispersed viruses are observed at intermediate CTAB concentrations of 0.05% and 0.1%. Finally, the data for VLP behavior in the presence of varying concentrations of the anionic surfactant, SDS, are plotted in Figure 2.4. Peaks representing the dispersed virus are present at all concentrations below 0.5%, and micelle or capsid protein dimer peaks are present at all concentrations above 0.01%. Significant aggregate

peaks appear at concentrations of 0.05% and 0.1%, which reduce to a small aggregate peak at 0.5%.

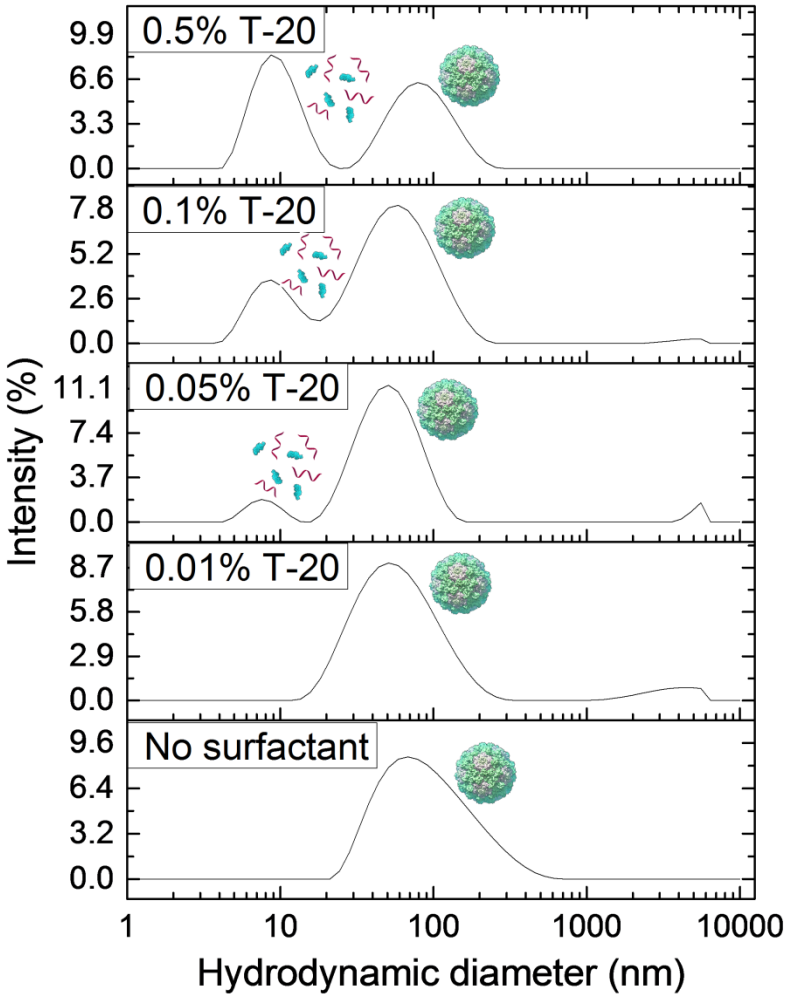

Figure 2.2 Intensity distributions from DLS experiment of norovirus VLPs in PBS media at pH 7.4 containing 0.01%, 0.05%, 0.1%, and 0.5% Tween 20. The peaks are visually labelled with the schematic presentations of the types of detected species. The data sets are representative curves from 3 repeated measurements for each of 3 different samples at each concentration. The norovirus VLPs remain stable and well-dispersed at all Tween 20 concentrations tested.

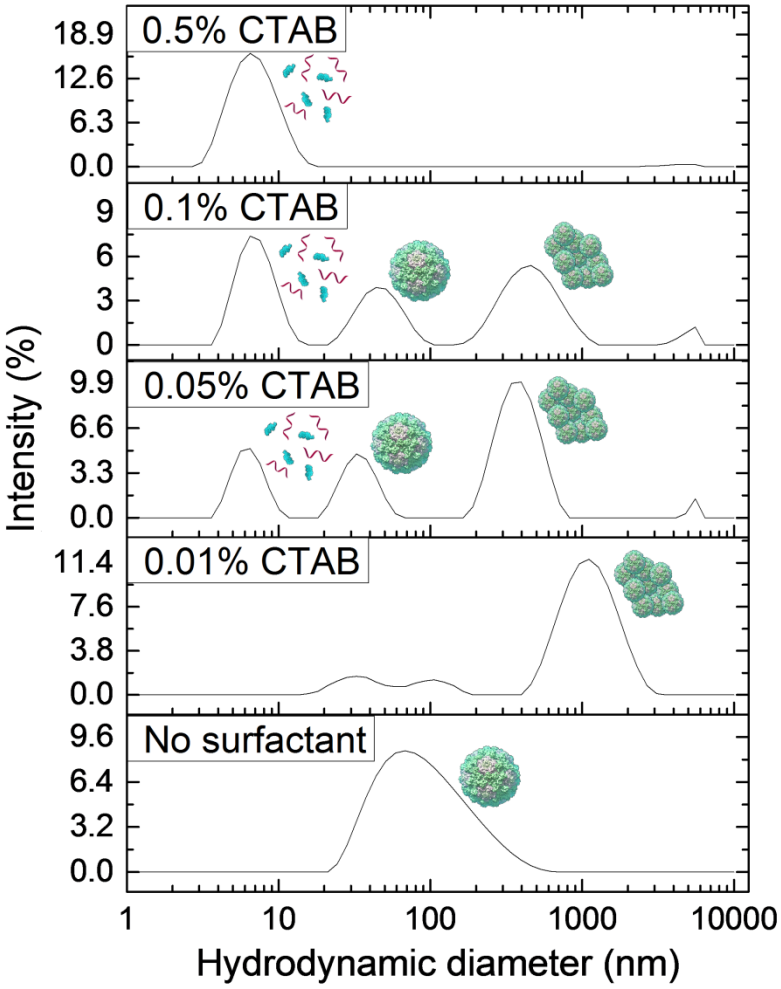

Figure 2.3 Intensity distributions from DLS experiment of norovirus VLPs in PBS solutions at pH 7.4 containing 0.01%, 0.05%, 0.1%, and 0.5% CTAB. The data sets are representative curves from 3 repeated measurements for each of 3 different samples at each concentration. Norovirus VLPs aggregate in the presence of low concentrations of CTAB and disassemble at high CTAB concentrations.

These data reveal multiple mechanisms behind the action of these surfactants on the virus dispersions. Norovirus VLPs behave similarly at all concentrations of Tween 20 studied, with a distinct peak representing intact and dispersed particles at each concentration. The critical micelle concentration (CMC) of Tween-20 is 0.005%,[47] and a micelle or protein peak is observed above 0.01%. This discrepancy is probably due to the low concentration of micelles at CMC. The peak of species of diameter < 10 nm most likely represents only surfactant micelles because the peak representing dispersed viruses is present consistently at all concentrations and does not appear to be reduced due to virus loss by capsid disassembly. Even at high concentrations, Tween 20 does not appear to disassemble norovirus VLPs and may even serve to stabilize them in a well-dispersed, single-virus form.

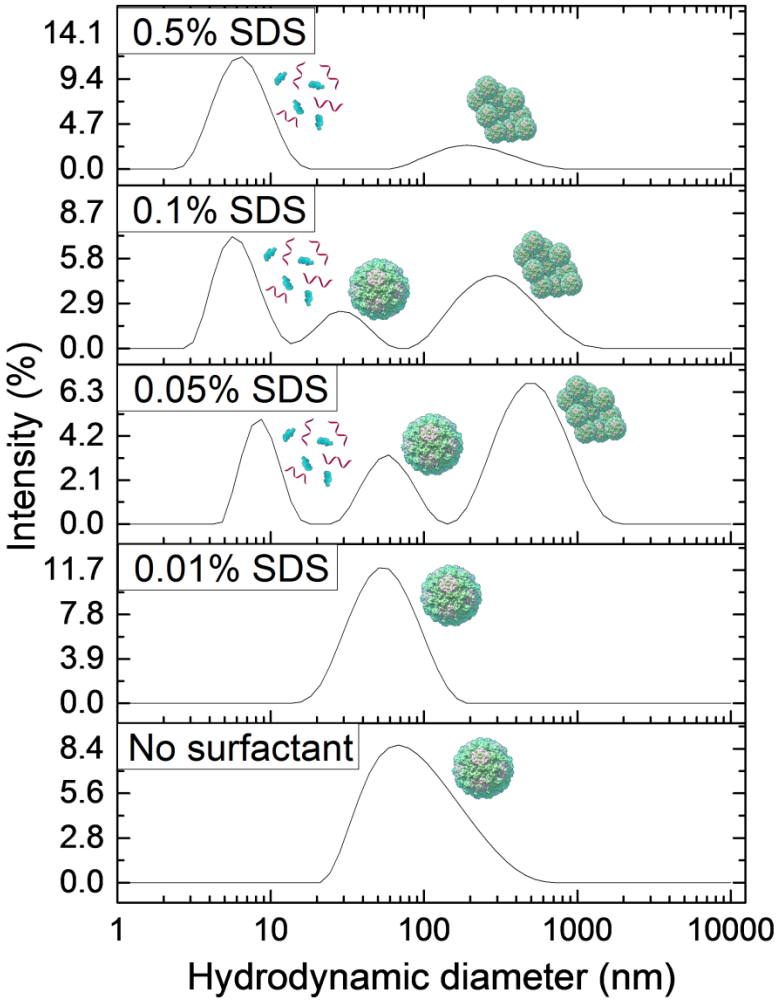

Figure 2.4 Intensity distributions from DLS experiments of norovirus VLPs in PBS at pH 7.4 containing 0.01%, 0.05%, 0.1%, and 0.5% of anionic surfactant, SDS. The plots are representative data sets from 3 repeated measurements for each of 3 different samples at each concentration. Norovirus VLPs remain dispersed in the presence of low concentrations of SDS, while they first partially aggregate and then disassemble in the presence of high SDS concentrations.

CTAB has a different effect on VLPs depending on its concentration. Aggregates are present at low concentrations because of heterocoagulation between the surfactant molecules and VLPs. The CMC of CTAB in PBS has been measured at 0.034 wt%.[48] At surfactant concentrations above CMC, we observe the appearance of a peak in intensity indicating the presence of micelles or capsid protein dimers. The disappearance of both dispersed VLP peaks and aggregate peaks at high concentrations of CTAB indicates that this cationic surfactant can disassemble the VLPs above its CMC. This VLP disassembly suggests that CTAB micelles have the ability to disrupt interactions between proteins within the capsid structure and solubilize capsid protein dimers. It is likely that the surfactant molecules assemble around the protein dimers to form a larger micelle-like structure including the dimers. During this *de facto* solubilization process, the capsid proteins may partially unfold and reveal more hydrophobic regions. As the concentration of CTAB micelles increases, more VLPs and VLP aggregates are broken apart and solubilized. The appearance of dispersed VLP peaks above CTAB CMC may be attributed to full capsid recharging and electrostatic repulsion between positively charged virus particles with adsorbed CTAB molecules, which we discuss further in the next section.

The anionic surfactant, SDS, also has a distinctly varying effect on VLPs depending on its concentration. SDS adsorption to the capsid surface will increase the apparent magnitude of the VLP net negative surface charge by binding to cationic areas on the surface, which causes increased electrostatic repulsion and dispersion at low concentration. The intensity peaks for particles of large diameter seen at SDS concentrations greater than 0.01% may represent aggregates that form as partially unfolded capsid proteins with exposed hydrophobic

regions stick together. The CMC of SDS in pure PBS is about 0.13%,[48] and the peak for particles of diameter 5-10 nm is detected at 0.1% SDS. Therefore this peak most likely represents dimerized proteins from disassembled capsids. VLPs in solution may also alter the CMC of SDS, so micelles may form at lower concentration than in pure PBS. A lower CMC would enable virus disassembly and capsid protein solubilization at a lower SDS concentration than expected.

We observed that the nonionic surfactant, Tween 20, induced VLPs stabilization at all concentrations studied. Many processed food products contain Tween 20 (polysorbate 20) as an emulsifier or stabilizer, so the results lead to the unexpected conclusions that common food additives similar to Tween 20 may actually contribute to the persistence of noroviruses and perhaps other foodborne viral pathogens. Norovirus VLPs have potential use as vaccines, so these results indicate why nonionic surfactants such as Tween 20 could also be successful candidates for nontoxic vaccine excipients.[16] Conversely, both charged surfactants studied were able to disassemble VLPs at high concentration and solubilize them in surfactant micelles. These strong ionic surfactants are therefore good candidates for virus cleaners and disinfectants. Their differences in behavior at low concentration need to be considered in the context of specific applications and are discussed in more detail in subsequent sections.

2.2.3 Evaluation of the Electrostatic Interaction Contributions to Virus Dispersion State

The data for the aggregation state of VLPs at varying pH and surfactant concentrations point out that many of the observed effects are a result of the charging of the capsids and their electrostatic interactions in water medium. To interpret the results we evaluated the capsid

charge on the basis of its peptide sequence and dissociation properties. The capsid surface charge of the VLPs was calculated based on the number of charged amino acids within the capsid protein and their respective pK_a[49] values using a modification of the Henderson-Hasselbach equation.

$$C_p = -\sum_{iA} n_{iA}\left(1+10^{-(pH-pKa_{iA})}\right)^{-1} + \sum_{iB} n_{iB}\left(1+10^{(pH-pKa_{iB})}\right)^{-1} \quad (2.1)$$

In Equation 2.1, the summation in the first term is done over the number of negatively charged residues of different types, n_{iA}, and the second term accounts for the sum of the pH-dependent positively charged residues, n_{iB}. The pH at which this charge equals zero is the theoretical isoelectric point (pI) for the virus capsid. Above the pI, the capsid has a net negative charge due to a higher number of negatively charged amino acids, and below the pI the capsid has a net positive charge due to a higher number of positively charged amino acids. The above formula provides a reasonable estimate of the protein charge and interactions in solution.[29,49]

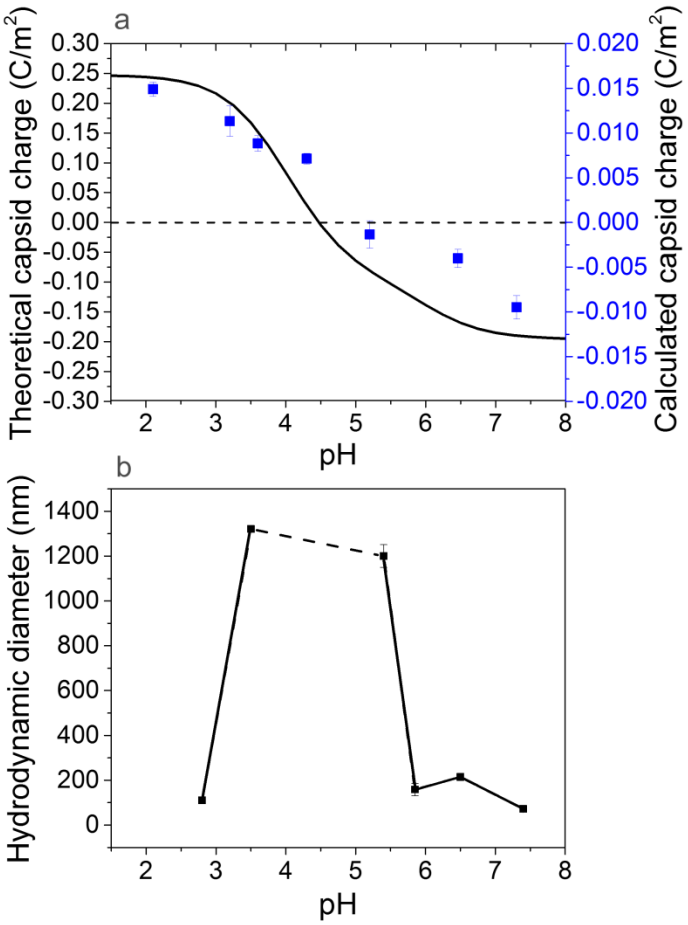

Figure 2.5 Comparison of a) theoretically evaluated capsid charge (curve) and capsid charge calculated from zeta potential measurements (points) and b) diameter of VLPs or VLP aggregates at varying pH revealing capsid isoelectric point. The error bars represent the standard error of three measurements at each condition. Theoretical capsid charges at varying pH were calculated using a modification of the Henderson-Hasselbach equation (Equation 2.1). There is a very good correlation between the virus capsid surface charge with pH and the aggregation behavior observed by DLS near the isoelectric point.

Significant changes in surface charge of proteins and colloids can be induced by altering the solution pH or adding charged surfactant. The theoretical capsid charge as a function of pH shown in Figure 2.5a proves that the norovirus capsids have a net negative surface charge at low pH, and a net positive surface charge at high pH. This theoretical capsid charge curve predicts that the isoelectric point of the major capsid protein is around 4.5. We see a similar trend in the calculated capsid charge, which is determined from measured zeta potential and also shown in Figure 2.5a. We converted zeta potential to capsid charge using the Grahame equation,[42]

$$\sigma^2 = 2\varepsilon_0 \varepsilon kT(\sum_i \rho_{0i} - \sum_i \rho_{\infty i}) \tag{2.2}$$

where σ is the surface charge density, ε_0 represents vacuum permittivity, ε represents the relative permittivity of water, k is the Boltzmann constant, T the temperature, and ρ_i represents the ion density. Ion density is defined by a Boltzmann distribution,[42]

$$\rho_{0i} = \rho_{\infty i} e^{\frac{-z_i e \psi_0}{kT}} \tag{2.3}$$

where ρ_{0i} represents the density of ion i at the VLP surface, $\rho_{\infty i}$ represents the density of ion i in the bulk liquid, z_i represents the valence of ion i, e represents the electron charge, and ψ_0 represents the VLP surface potential. The zeta potential equals the surface potential when the slipping plane is located at the particle surface, but this potential is often used as an approximation of surface potential as it can be easily measured.[50]

For simplicity and because we are mainly interested in trends in surface charge as a function of pH and surfactant concentration, we approximated the VLP surface potential in Equation 2.3 with the measured zeta potential. These data suggest that the isoelectric point of the VLPs is about 4.9. Calculated and theoretical capsid charges differ by approximately an

order of magnitude likely due to assumptions in the model that the surfaces of the particles are hard spheres. Norovirus particles have protrusions and are slightly porous, so they will not precisely follow DLVO theory. Also, theoretical capsid charge is calculated for the entire capsid protein, much of which is *not* part of the exposed surface, and thus is likely overestimated. By comparing these capsid charge trends with the diameter of particles as a function of pH as shown in Figure 2.5b, it is straightforward to correlate the capsid charge to the VLP aggregation. Net capsid charge is lowest in magnitude, and the measured size is highest (obviously resulting from virus aggregation) around the isoelectric point. Net capsid charge is highest in magnitude, and the measured particle size is closest to that of individual VLPs farther away from the isoelectric point. These observations indicate that high capsid charge facilitates electrostatic repulsion between particles that results in dispersed VLPs, and low capsid charge reduces electrostatic repulsion between particles that results in VLP aggregation by van der Waals and hydrophobic attraction. Thus, the VLPs exhibit a behavior common to many colloidal particles and their behavior and stability can be conveniently interpreted on this basis.

We now apply colloidal fundamentals in interpreting how the apparent capsid charge of the VLPs is altered by the addition of charged surfactant. To demonstrate charged surfactant adsorption onto the capsid surface, we measured the zeta potential of VLPs in the presence of different concentrations of CTAB or SDS. We converted this zeta potential into charge density using Equations 2.2 and 2.3, then interpreted the difference between the charge density at each surfactant concentration and the charge density without surfactant as the number of charges that were added as a result of surfactant adsorption. Surfactant molecules that adsorb could add

a charge or neutralize an opposite charge on the capsid. Both mechanisms result in a loss of one net surface charge. Therefore we assumed that each charge added or subtracted corresponds to the adsorption of one surfactant molecule.

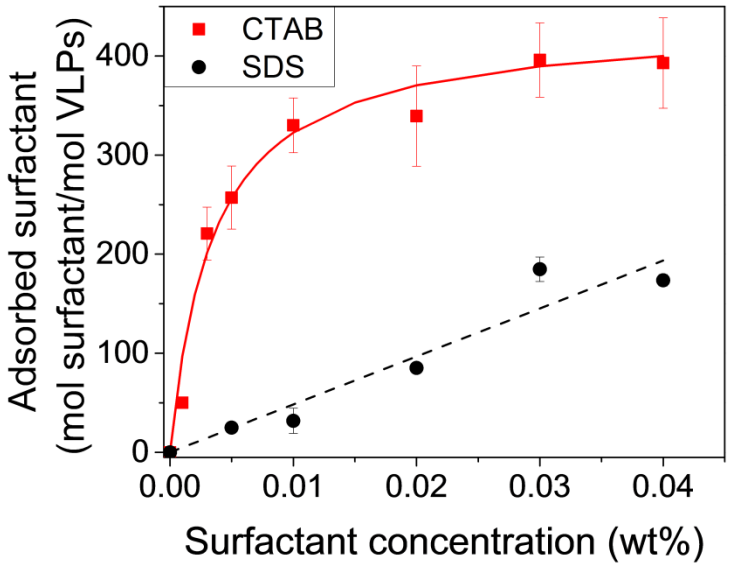

Figure 2.6 Calculated and modeled surfactant adsorption onto VLPs at varying surfactant concentration at pH 7.4. The amount of adsorbed surfactant was calculated by converting the measured zeta potential to charge density with the Grahame equation and then converting the change in charge density to number of surfactant molecules. Error bars represent the standard error of three measurements at each condition. The apparent virus capsid charge can be controlled by adding charged surfactant. Both simple adsorption models interpret adequately the amount of surfactant binding to the model viruses.

The estimated amount of charged surfactant adsorbed onto VLPs as a function of surfactant concentration is shown in Figure 2.6. The addition of oppositely-charged surfactant, CTAB, reduces the magnitude of the zeta potential at low concentration. At concentrations higher than about 0.005%, the amount of CTAB adsorbed on the VLPs is high enough to reverse the sign of the apparent capsid zeta potential. We fit the adsorption data of CTAB onto the VLP surfaces with a simple Langmuir-type adsorption isotherm,

$$\Gamma = \Gamma_{max} \frac{k_{ads} C}{1 + k_{ads} C} \tag{2.4}$$

where Γ represents mass adsorbed per area, Γ_{max} represents mass adsorbed per unit area at saturation, k_{ads} represents the adsorption constant, and C represents the surfactant concentration in the bulk liquid. We used the surface area of a sphere of diameter 35 nm to approximate the available surface area for surfactant adsorption on the capsid. Because CTAB has positive charge and the capsid has a net negative charge at pH 7.2, the magnitude of the surface charge density first decreases with CTAB adsorption, then increases as the surface becomes saturated. These surfactant-induced changes in VLP surface charge could well describe the particle behaviors shown in Figure 2.3. The decrease in magnitude of apparent capsid charge at low CTAB concentration explains the presence of large particle aggregates observed in Figure 2.3. As the CTAB concentration is increased, we begin to observe the presence of dispersed particles. An increase in magnitude of the effective positive surface charge by more CTAB adsorption likely enables this re-dispersion process.

The charge shift data for SDS plotted in Figure 2.6 indicate a much weaker adsorption likely resulting from hydrophobic interactions (as the SDS has the same sign of charge as the

capsid). We used a linear adsorption isotherm (Equation 2.5) to model the binding of some SDS molecules onto the VLP surface.

$$\Gamma = \Gamma_{max} k_{ads} C \tag{2.5}$$

A linear isotherm describes systems where the adsorbent has low affinity for the surface or where the concentration of adsorbent is low. We assumed that the affinity of SDS for the VLP surface is low at pH 7.2 because the capsid already has a net negative surface charge. Due to micellization, SDS concentrations in the bulk liquid may never become high enough to reach high surface adsorption density. Even low SDS adsorption to the VLP surface causes an increase in magnitude of apparent surface charge. Particle dispersion at low SDS concentration shown in Figure 2.4 is facilitated by electrostatic repulsion resulting from this increased magnitude of apparent surface charge. Finally, adsorption data for Tween 20 are not included because the addition of nonionic surfactant does not induce a significant change in measured zeta potential and apparent surface charge.

Overall, the data prove that many of the aqueous VLP interactions reported here depend on the apparent surface charge of the virus capsids. As we observed while varying pH variations and adding charged surfactant, virus aggregation tends to occur where the magnitude of surface charge is low, and conversely, virus dispersion is facilitated by a high magnitude of capsid surface charge and resultant electrostatic repulsion. A decrease in magnitude of the apparent surface charge suppresses the electrostatic repulsion between the dispersed virus particles in solution and subsequently enables their aggregation. Surfactant adsorption to the VLP surface can have multiple origins. For charged surfactants, the head group can bind to an opposite charge on the capsid surface. This mode of adsorption implies a fixed number of

surfactant binding sites on the capsid at each pH, which will result in charge neutralization at the right (typically very low) surfactant concentration. In addition, for all classes of surfactant, the hydrophobic tail can adsorb to hydrophobic regions on the capsid surface. This type of adsorption does not imply a fixed number of binding sites and will result in additional charges on the surface in the case of charged surfactants. The head groups of all classes of surfactants can also bind to polar regions on the capsid surface, or any combination of these modes of adsorption can occur. We also obtained data on the combined effects of pH and surfactant, which illustrate complex, but expected trends, and are briefly introduced in Figures A.2 and A.3.

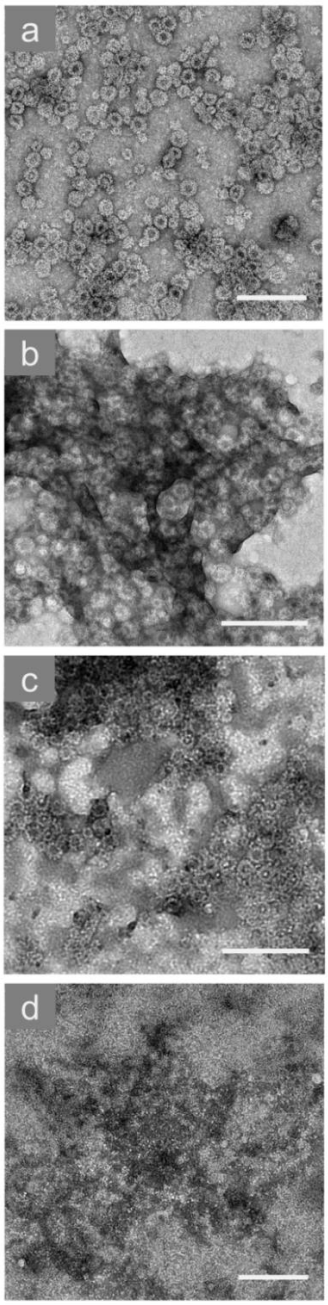

Figure 2.7 TEM images of GII.4 norovirus VLPs in 0.15 M NaCl, including a) intact and dispersed capsids without surfactant, b) intact capsids stabilized by 0.01% SDS, c) intact capsids aggregated by 0.01% CTAB, and d) capsids disassembled by 0.5% SDS. The scale bars are equal to 200 nm.

We could also observe directly these patterns of VLP behaviors using electron microscopy. TEM images of each type of system mentioned above are shown in Figure 2.7. Dispersed VLPs without surfactant are shown in Figure 2.7a, and intact VLPs in the presence of a low concentration of SDS are shown in Figure 2.7b. A low concentration of CTAB induces the formation of large aggregates ranging from about 0.2 to 1 μm in size formed by intact capsids, which are illustrated in Figure 2.7c. These aggregates are separated by areas free of any single VLPs. At high SDS concentration VLP disassembly occurs, and intact capsids are no longer distinguishable, as seen in Figure 2.7d. The three potential mechanisms observed after surfactant addition to VLP solutions are summarized in Section 2.3. These mechanisms include capsid disassembly due to protein dimer solubilization in surfactant micelles, capsid recharging by surfactant adsorption leading to VLP aggregation, and capsid recharging by surfactant adsorption leading to VLP dispersion and possible blocking of binding receptors. We discuss the biological implications of these results in the next section.

2.2.3 Surfactant-mediated VLP Removal from Hydrophilized Glass Slides

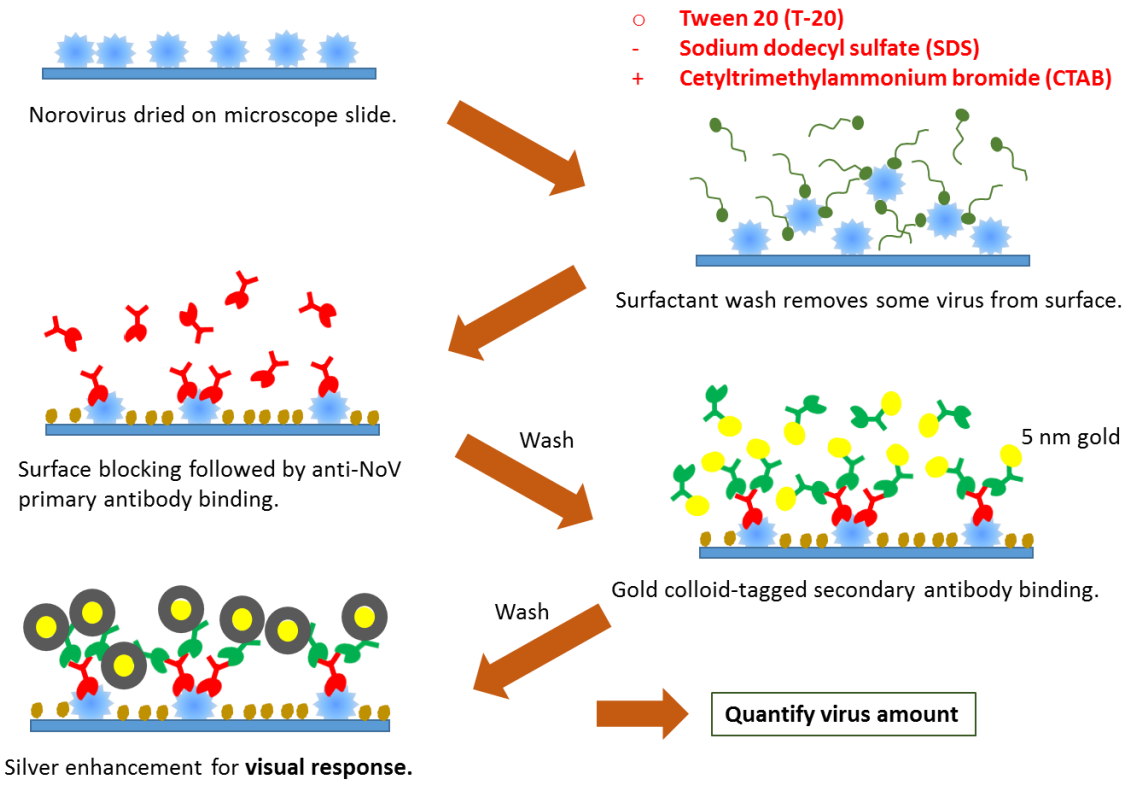

Figure 2.8 Schematic of surface immunoassay used to evaluate VLP amount remaining on a surface after washing with various surfactant solutions. Silver enhancement of gold nanoparticles produces a visual response. The intensity of this visual response is proportional to the amount of VLPs on the surface.

Different classes of surfactants also influence virus adsorption to and desorption from surfaces. A surface immunoassay was used to determine the amount of virus particles that remained on a hydrophilized glass microscope slide with negative charge after washing with Tween 20, SDS, and CTAB. The VLPs were dried from solution onto the surface, incubated

with surfactant for 10 minutes, and detected using an immunoassay with silver enhancement of gold nanoparticles. This assay is summarized in Figure 2.8 and results in a dark spot that is visible to the naked eye. The intensity of this spot normalized to the intensity of the spot from a control assay represents the relative amount of VLPs left on the surface after washing.

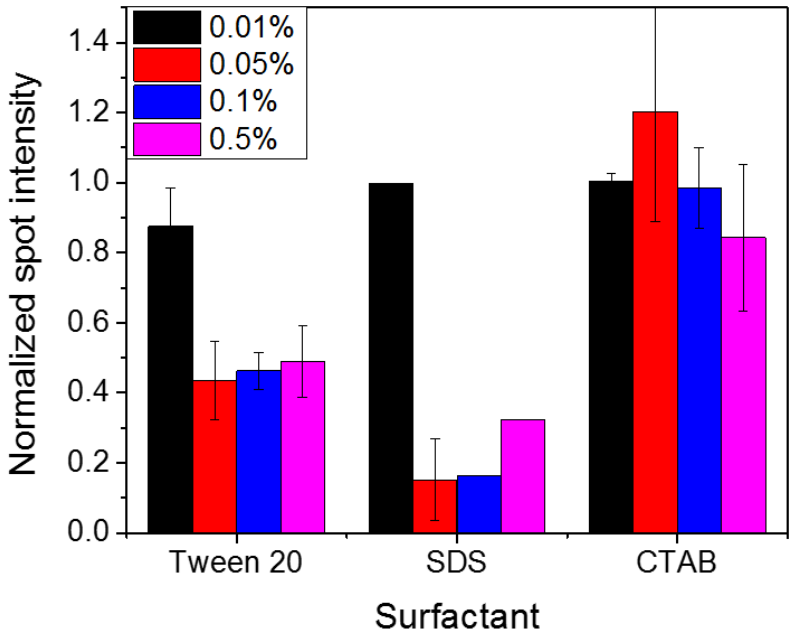

Figure 2.9 Relative intensity of spots from silver enhancement-based surface immunoassay after washing with varying concentrations of Tween 20, SDS, and CTAB. Error bars represent the standard error of at least 2 replicate samples.

Washing with low concentration of all three surfactants resulted in little change in the amount of VLPs left on the surface. Above CMC, VLPs were removed from the surface after washing with Tween 20 and SDS. Tween 20 resulted in about 50% VLP removal, whereas

SDS resulted in about 80% VLP removal. Tween 20 was expected to remove a small amount of VLPs from the surface as it is a mild, nonionic surfactant. Tween 20 molecules and micelles may enhance particle desorption due to polar interactions between the surfactant head group and the hydroxyl groups on the glass surface and hydrophobic interactions between the surfactant tail and regions on the VLP surface. SDS was expected to remove a larger amount of VLPs from the surface as it is a stronger, anionic surfactant. SDS micelles may solubilize individual capsid proteins or dimers, as shown in Figure 2.4, causing a decrease in the amount of VLPs detected. SDS molecules adsorbed to the VLP surface may evoke electrostatic repulsion between the VLP and the negatively-charged microscope slide surface, resulting in particle desorption and clearing. CTAB was not able to remove a substantial amount of VLPs from the slide surface even above CMC. Increased VLP retention was even observed at 0.5% CTAB as compared with the control wash using buffer solution. This increase in VLP retention suggests that electrostatic attraction between VLPs with adsorbed cationic surfactant and the negatively-charged surface reduced virus desorption. Evidence of increased virus retention on surfaces after washing with CTAB could indicate the possibility of some adverse effects of commonly used antimicrobial cleaning products that contain quaternary ammonium compounds.

2.3 General Discussion and Conclusions

Based on our results evaluating the aggregation state of human norovirus VLPs in the presence of different classes of surfactants, we summarize the mechanisms that we identified as governing the VLP properties in Figure 2.10. We conclude that positively-charged surfactants

at low concentrations reduce the magnitude of the apparent capsid surface charge enough to induce particle aggregation for capsids with a net negative surface charge. Negatively-charged surfactants at low concentrations increase the magnitude of the apparent capsid surface charge and enhance electrostatic repulsion between the particles. As the concentration of charged surfactant is increased beyond its CMC, the micelles can solubilize capsid protein dimers and therefore disassemble the capsid structure. Thus the surfactants are efficient in disrupting the virus structure only above their CMC, an important finding that should be taken into account when formulating virus cleaning and disinfectant systems with surfactants. Surfactant micellization results in the ability of strong surfactants to disrupt interactions between virus capsid proteins and solubilize individual proteins or dimers. Mild nonionic surfactants can slightly increase repulsion between particles, reducing aggregation and adsorption to surfaces. As mild nonionic surfactants are commonly used in stabilizing food and drink products, our data suggest that their addition to such products may have the undesired potential consequence of stabilizing virus contaminants as well.

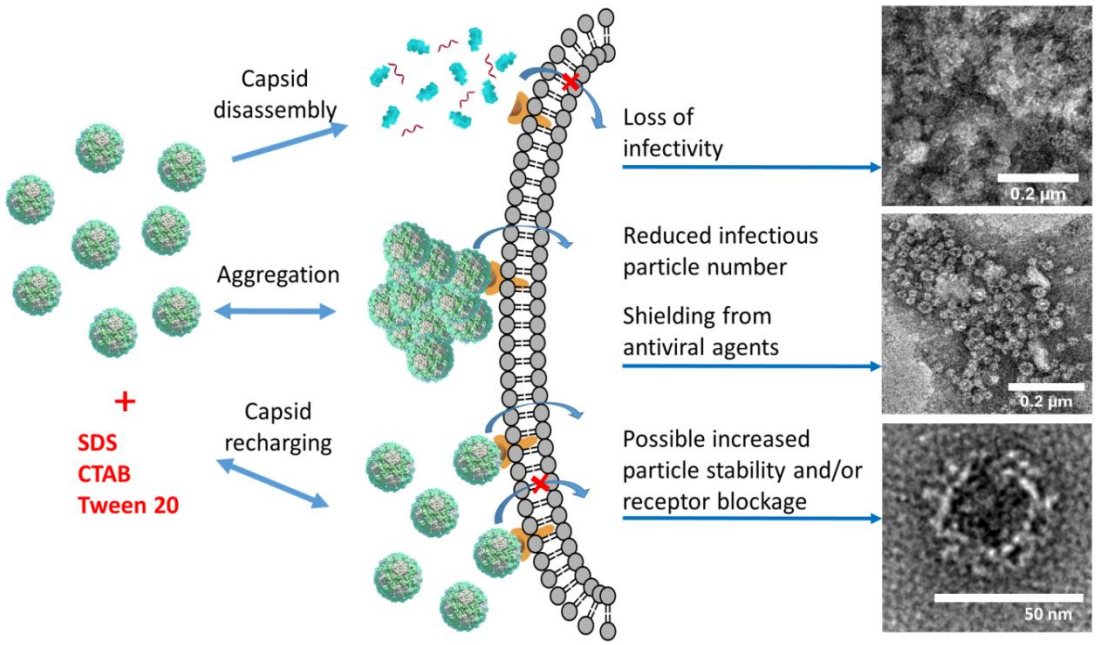

Figure 2.10 Summary of the mechanisms responsible for human norovirus VLP behavior after exposure to three different surfactant types. TEM images represent VLPs stained with uranyl acetate after treatment with 0.5% CTAB (top), 0.01% CTAB (middle), and no surfactant (bottom).

The insights on colloidal stability of viruses may also have importance to understanding their biological activity (Figure 2.10). We hypothesize that the changes in the virus charge and aggregation could have a profound effect on virus infectivity. Virus particle disassembly by surfactant is likely to lead to complete loss of infectivity, which can also be severely disrupted by the dramatic apparent surface charge alteration and aggregation caused by ionic surfactant. Low concentrations of ionic surfactants (below CMC) are likely to disrupt the virus infectivity much less, while low to moderate amounts of mild nonionic surfactants such as Tween 20 are

even likely to enhance virus dispersivity, while potentially increasing their infectivity to some extent. It should be noted, however, that the data reported here are obtained with reconstituted virus capsids, which are likely to be less stable than the native RNA-containing virus assemblies. While the charge and aggregation state of real noroviruses are likely to be similar to the ones reported here, the natural virus particles may be more stable against surfactant-driven disassembly, contributing to the notoriously large ability for norovirus to withstand cleanup and disinfection efforts.

The colloidal behavior of human norovirus revealed here should be considered when formulating disinfectants and cleaning agents. The types and concentrations of surfactants used to enhance rinsing of produce should be evaluated with regards to their CMC to determine the optimum concentration for a dispersion state that promotes effective norovirus clearing. Dispersion state can also influence disinfectant efficiency, so surfactant selection based on colloidal interactions is important in maximizing the accessibility of virucides to virus particles. Capsid recharging by surfactants is also important in evaluating the effectiveness of water membrane filtration processes. Surfactant adsorption may enhance the long-range dispersion of noroviruses by protecting them from damage through the reversible formation of aggregates or enhancing particle stability through increased dispersion.

Overall, the characterization of the colloidal interactions, dispersion state, and integrity of the virus particles may provide valuable data in understanding pathogenicity trends and aiding in the development of strategies to prevent virus spread. Characterizing human norovirus behavior is especially important due to its unique resiliency in many different chemical environments. It appears that simple adjustments in the pH, salt conditions, and

addition of common surfactants to cleaning and antiviral products can assist in preventing outbreaks and treating norovirus as an infectious agent.

2.4 Experimental

2.4.1 VLPs and Surfactants

All experiments were carried out with Houston norovirus VLPs from genogroup GII.4. The VLPs were provided courtesy of R. Atmar (Baylor College of Medicine, Houston, TX). Sodium dodecyl sulfate (SDS, Sigma Aldrich), cetyltrimethylammonium bromide (CTAB, Sigma Aldrich, St. Louis, MO), and Tween 20 (Sigma Aldrich, St. Louis, MO) were used as surfactant additives. Unless otherwise indicated, all experiments were performed in 0.01 M PBS prepared by adding a PBS tablet (Sigma Aldrich, St. Louis, MO) to deionized water. pH adjustments were achieved by adding small aliquots of 0.1 M sodium hydroxide (Fisher Scientific, Pittsburgh, PA) or hydrochloric acid (Acros Chemical, Pittsburgh, PA).

2.4.2 TEM Images

For viewing under TEM, 100 μg ml^{-1} norovirus VLPs in 0.15 M NaCl (Sigma Aldrich, St. Louis, MO) containing various surfactant concentrations were adsorbed onto nickel grids with a carbon support film (Ladd Research, Williston, VT). A droplet of VLP solution was applied to each grid for 2 minutes to allow for adsorption. Excess liquid was then removed, followed by 5-10 seconds of negative staining with 2% uranyl acetate. For the images in Figure 2.7, the grid-mounted samples were imaged by field emission TEM using a 2010F S/TEM (JEOL,

Tokyo, Japan) at 200 kV. For the images in Figure 2.10, the grids were imaged by conventional TEM using a 2000FX S/TEM (JEOL, Tokyo, Japan) at 200 kV.

2.4.3 DLS Measurements

Protein, micelle, VLP, and aggregate sizes were determined by DLS. VLPs were added to small volume cuvettes (40-70 ul) containing various surfactant concentrations in PBS to a final VLP concentration of 10 µg ml^{-1}. After 30 minutes incubation at room temperature, each sample was measured in triplicate using a Zetasizer Nano ZS (Malvern Instruments) with a 10 mW He-Ne laser at 633 nm and a photodiode located 173° from the incident laser beam. Zetasizer software calculated a size distribution of particles in each sample from light scattering intensity data. Representative graphs of these size distributions for each surfactant conditions are presented. At least 3 replicates of measurements at each surfactant condition were obtained.

Using the CMC and aggregation number[51] of each surfactant and Equation 2.6, we calculated the number of micelles at each surfactant concentration:

$$M = \frac{C_s - CMC}{N} \tag{2.6}$$

where M = micelle concentration, C_s= total molar surfactant concentration, CMC = critical micelle concentration, and N = aggregation number. We then compared the relative signal that would be produced by volume and intensity distributions from micelles and VLPs using their respective diameters and concentrations in Equation 2.7 and Equation 2.8:

$$R_V = \frac{d_m^3}{d_{VLP}^3} * \frac{M}{C_{VLP}} \tag{2.7}$$

$$R_I = \frac{d_m^6}{d_{VLP}^6} * \frac{M}{C_{VLP}} \quad (2.8)$$

where R_V = micelle to VLP ratio of signal from a volume distribution, d_m = diameter of a micelle, d_{VLP} = diameter of a VLP, C_{VLP} = molar VLP concentration, and R_I = micelle to VLP ratio of signal from an intensity distribution. We then related the ratios of concentrations and scattering signals for micelles and VLPs. For each surfactant, $R_I \leq 1$ and $R_V > 1$. Based on these calculations, an intensity distribution expresses VLP behavior more accurately than a volume distribution because micelles scatter as much or less light than VLPs at each concentration.

2.4.4 Zeta Potential Measurements

VLP electrophoretic mobility was determined by a Zetasizer Nano ZSP (Malvern Instruments) with a 10 mW HeNe laser at 633 nm and a photodiode located 173° from the incident laser beam. Zetasizer software calculated zeta potential from electrophoretic mobility using the Smoluchowski formula. The Smoluchowski formula was assumed to be a reasonable approximation because the Debye length in 0.01 M PBS is 0.76 nm, which is about 50-fold smaller than the VLP radius. VLPs were placed into a glass cuvette containing PBS solutions of varying pH or surfactant concentration to a final concentration of 5 μg ml^{-1} and immediately measured to determine zeta potential before significant aggregation occurred. 0.1 M hydrochloric acid and sodium hydroxide were used for pH adjustments. Each sample was measured in triplicate.

2.4.5 Surface Immunoassay

The protocol described by Gupta *et al*. was followed with some revisions. Microscope slides were hydrophilized by submersion in Nochromix for 24 hours followed by rinsing in DI water and drying. Two 0.5 µl droplets of 50 µg/mL GII.4 VLPs in PBS were dried onto the slide surface. An 18 µl volume flow chamber (Grace Biolabs) was placed over the drops, and a peristaltic pump was used to pump fluid through the chamber. A specific surfactant type and concentration was pumped into the chamber and incubated for 10 minutes. Then PBS containing 0.3 wt% bovine serum albumin (PBSA) was incubated for 10 minutes, followed by 10 minutes with PBSA and 0.25% Tween 20 for blocking. Primary mouse anti-NoV antibody (Abcam) at µg/mL was incubated for 30 minutes, followed by a 3 minute wash step with PBSA and 0.25% Tween 20. Secondary goat anti-mouse antibody at $2x10^{13}$ particles/mL with a 5 nm gold nanoparticle tag was then incubated for 30 minutes, followed a wash with 20 µl PBSA and 0.25% Tween 20. Samples were then washed with 200 µl DI water. Silver enhancement solution was prepared by mixing solutions A and B at a 1:1 ratio as described by the manufacturer (Cytodiagnostics) 15 minutes before use. The final silver enhancement solution was then added to the flow chamber and incubated for 15 minutes. Samples were then subjected to a final wash with 200µl DI water. Enhanced spots were imaged using a Canon camera and analyzed using Photoshop software (Adobe). The lasso tool within Photoshop software was used to outline each spot, and the histogram analysis tool was then used to determine the average intensity of the spot. Normalized spot intensity was calculated by first normalizing the intensity to the background intensity of the image to obtain an optical density ratio (ODR),

$$ODR = \frac{(I_{spot} - I_{background})}{I_{background}} \tag{2.7}$$

where I_{spot} represents the intensity of a spot and $I_{background}$ represents the intensity of the image background. Then the ODR of each sample was divided by the ODR of a control sample where buffer was used in place of a surfactant wash to obtain normalized spot intensity (I_n),

$$I_n = \frac{ODR_{sample}}{ODR_{control}} \tag{2.8}$$

where ODR_{sample} represents the ODR of a sample with a surfactant wash and $ODR_{control}$ represents the ODR of a control sample with a buffer wash.

2.5 Acknowledgments

The authors acknowledge funding from the USDA-NIFA Food Virology Collaborative (NoroCORE), supported by the National Institute of Food and Agriculture, U.S. Department of Agriculture, under award number 2011-68003-30395. We also thank the Molecular Biotechnology Training Program (MBTP) sponsored by the National Institutes of Health and the Graduate School at North Carolina State University (5 T32 GM008776-15). The authors acknowledge the use of the Analytical Instrumentation Facility (AIF) at North Carolina State University, which is supported by the State of North Carolina and the NSF and the use of the Zetasizer Nano ZSP, which was purchased by the NSF Triangle Materials Research Science and Engineering Center (NSF DMR-1121107).

2.6 References

1 Pinto, F., Maillard, J. & Denyer, S. P. Effect of surfactants, temperature, and sonication on the virucidal activity of polyhexamethylene biguanide against the bacteriophage MS2. *Am. J. Infect. Control* **38**, 393-398 (2010).

2 Mattle, M. J. *et al*. Impact of Virus Aggregation on Inactivation by Peracetic Acid and Implications for Other Disinfectants. *Environ. Sci. Technol.* **45**, 7710-7717 (2011).

3 Mattle, M. J. & Kohn, T. Inactivation and Tailing during UV254 Disinfection of Viruses: Contributions of Viral Aggregation, Light Shielding within Viral Aggregates, and Recombination. *Environ. Sci. Technol.* **46**, 10022-10030 (2012).

4 Langlet, J., Gaboriaud, F., Duval, J. F. L. & Gantzer, C. Aggregation and surface properties of F-specific RNA phages: Implication for membrane filtration processes. *Water Res.* **42**, 2769-2777 (2008).

5 Mylon, S. E. *et al*. Influence of Salts and Natural Organic Matter on the Stability of Bacteriophage MS2. *Langmuir* **26**, 1035-1042 (2010).

6 Redman, J., Grant, S., Olson, T., Hardy, M. & Estes, M. Filtration of recombinant Norwalk virus particles and bacteriophage MS2 in quartz sand: Importance of electrostatic interactions. *Environ. Sci. Technol.* **31**, 3378-3383 (1997).

7 Wong, K., Mukherjee, B., Kahler, A. M., Zepp, R. & Molina, M. Influence of Inorganic Ions on Aggregation and Adsorption Behaviors of Human Adenovirus. *Environ. Sci. Technol.* **46**, 11145-11153 (2012).

8 Panyukov, Y. V., Nemykh, M. A., Dobrov, E. N. & Drachev, V. A. Surfactant-induced amorphous aggregation of tobacco mosaic virus coat protein: A physical methods approach. *Macromol. Biosci.* **8**, 199-209 (2008).

9 Panyukov, Y. *et al*. Low cetyltrimethylammonium bromide concentrations induce reversible amorphous aggregation of tobacco mosaic virus and its coat protein at room temperature. *Int. J. Biochem. Cell Biol.* **38**, 533-543 (2006).

10 Predmore, A. & Li, J. Enhanced Removal of a Human Norovirus Surrogate from Fresh Vegetables and Fruits by a Combination of Surfactants and Sanitizers. *Appl. Environ. Microbiol.* **77**, 4829-4838 (2011).

11 Zeltins, A. Construction and Characterization of Virus-Like Particles: A Review. *Mol. Biotechnol.* **53**, 92-107 (2013).

12 Ausar, S. F., Foubert, T. R., Hudson, M. H., Vedvick, T. S. & Middaugh, C. R. Conformational stability and disassembly of Norwalk virus-like particles - Effect of pH and temperature. *J. Biol. Chem.* **281**, 19478-19488 (2006).

13 Dika, C., Duval, J. F. L., Ly-Chatain, H. M., Merlin, C. & Gantzer, C. Impact of Internal RNA on Aggregation and Electrokinetics of Viruses: Comparison between MS2 Phage and Corresponding Virus-Like Particles. *Appl. Environ. Microbiol.* **77**, 4939-4948 (2011).

14 Dika, C., Gantzer, C., Perrin, A. & Duval, J. F. L. Impact of the virus purification protocol on aggregation and electrokinetics of MS2 phages and corresponding virus-like particles. *Phys. Chem. Chem. Phys.* **15**, 5691-5700 (2013).

15 Nguyen, T. H. *et al*. The RNA core weakly influences the interactions of the bacteriophage MS2 at key environmental interfaces. *Soft Matter* **7**, 10449-10456 (2011).

16 Kissmann, J. *et al*. Physical stabilization of Norwalk virus-like particles. *J. Pharm. Sci.* **97**, 4208-4218 (2008).

17 Shi, L. *et al*. Stabilization of human papillomavirus virus-like particles by non-ionic surfactants. *J. Pharm. Sci.* **94**, 1538-1551 (2005).

18 Cuellar, J. L., Meinhoevel, F., Hoehne, M. & Donath, E. Size and mechanical stability of norovirus capsids depend on pH: a nanoindentation study. *J. Gen. Virol.* **91**, 2449-2456 (2010).

19 da Silva, A. K., Kavanagh, O. V., Estes, M. K. & Elimelech, M. Adsorption and Aggregation Properties of Norovirus GI and GII Virus-like Particles Demonstrate Differing Responses to Solution Chemistry. *Environ. Sci. Technol.* **45**, 520-526 (2011).

20 Shoemaker, G. K. *et al*. Norwalk Virus Assembly and Stability Monitored by Mass Spectrometry. *Molec. Cell. Proteom.* **9**, 1742-1751 (2010).

21 Uetrecht, C., Barbu, I. M., Shoemaker, G. K., van Duijn, E. & Heck, A. J. R. Interrogating viral capsid assembly with ion mobility-mass spectrometry. *Nat. Chem.* **3**, 126-132 (2011).

22 Vandenbossche, G. Alteration of Viral Infectious Behavior by Surface-Active Agents. *Microbiol. Res.* **149**, 105-114 (1994).

23 Tresset, G. *et al*. Norovirus Capsid Proteins Self-Assemble through Biphasic Kinetics via Long-Lived Stave-like Intermediates. *J. Am. Chem. Soc.* **135**, 15373-15381 (2013).

24 Prasad, B. V. V. *et al*. X-ray crystallographic structure of the Norwalk virus capsid. *Science* **286**, 287-290 (1999).

25 Baclayon, M. *et al*. Prestress Strengthens the Shell of Norwalk Virus Nanoparticles. *Nano Letters* **11**, 4865-4869 (2011).

26 Leckband, D. Measuring the forces that control protein interactions. *Annu. Rev. Biophys. Biomol. Struct.* **29**, 1-26 (2000).

27 Gitlin, I., Carbeck, J. D. & Whitesides, G. M. Why are proteins charged? Networks of charge-charge interactions in proteins measured by charge ladders and capillary electrophoresis. *Angew. Chem. Int. Ed.* **45**, 3022-3060 (2006).

28 Sigstam, T. *et al*. Subtle Differences in Virus Composition Affect Disinfection Kinetics and Mechanisms. *Appl. Environ. Microbiol.* **79**, 3455-3467 (2013).

29 Velev, O. D., Kaler, E. W. & Lenhoff, A. M. Protein interactions in solution characterized by light and neutron scattering: Comparison of lysozyme and chymotrypsinogen. *Biophys. J.* **75**, 2682-2697 (1998).

30 Velev, O. D. *et al*. Investigation of the mechanisms of stabilization of food emulsions by vegetable proteins. *Food Hydrocoll.* **7**, 55-71 (1993).

31 Saluja, A. & Kalonia, D. S. Nature and consequences of protein-protein interactions in high protein concentration solutions. *Int. J. Pharm.* **358**, 1-15 (2008).

32 Kamerzell, T. J., Esfandiary, R., Joshi, S. B., Middaugh, C. R. & Volkin, D. B. Protein-excipient interactions: Mechanisms and biophysical characterization applied to protein formulation development. *Adv. Drug Deliv. Rev.* **63**, 1118-1159 (2011).

33 Wang, W., Nema, S. & Teagarden, D. Protein aggregation-Pathways and influencing factors. *Int. J. Pharm.* **390**, 89-99 (2010).

34 Duval, J. F. L. & Gaboriaud, F. Progress in electrohydrodynamics of soft microbial particle interphases. *Curr. Opin. Colloid Interface Sci.* **15**, 184-195 (2010).

35 Ohshima, H. Electrokinetic phenomena of soft particles. *Curr. Opin. Colloid Interface Sci.* **18**, 73-82 (2013).

36 Langlet, J., Gaboriaud, F., Gantzer, C. & Duval, J. F. L. Impact of chemical and structural anisotropy on the electrophoretic mobility of spherical soft multilayer particles: The case of bacteriophage MS2. *Biophys. J.* **94**, 3293-3312 (2008).

37 Toropova, K., Basnak, G., Twarock, R., Stockley, P. G. & Ranson, N. A. The three-dimensional structure of genomic RNA in bacteriophage MS2: Implications for assembly. *J. Mol. Biol.* **375**, 824-836 (2008).

38 White, M. *et al*. Multimerization of Surfactant Protein D, but Not Its Collagen Domain, Is Required for Antiviral and Opsonic Activities Related to Influenza Virus. *J. Immunol.* **181**, 7936-7943 (2008).

39 Pu Xiu-ying, Liu Yu, Li Yan, Zhang Wei-jie & Wang Heng-rui. Preparation of polyphylla saponins and their antiviral effect on influenza A virus. *Zhongguo Yaolixue Yu Dulixue Zazhi* **27**, 187-192 (2013).

40 Turro, N. J., Lei, X. G., Ananthapadmanabhan, K. P. & Aronson, M. Spectroscopic Probe Analysis of Protein-Surfactant Interactions - the Bsa/sds System. *Langmuir* **11**, 2525-2533 (1995).

41 Otzen, D. Protein unfolding in detergents: Effect of micelle structure, ionic strength, pH, and temperature. *Biophys. J.* **83**, 2219-2230 ER (2002).

42 Israelachvili, J. N. in *Intermolecular and Surfaces Forces, Third Edition* 503-503-534 (Elsevier Inc., Waltham, MA, 2011).

43 Skoglund, S. *et al*. Effect of laundry surfactants on surface charge and colloidal stability of silver nanoparticles. *Langmuir* **29**, 8882-91 (2013).

44 Moren, A. & Khan, A. Surfactant hydrophobic effect on the phase behavior of oppositely charged protein and surfactant mixtures: Lysozyme and sodium alkyl sulfates. *Langmuir* **14**, 6818-6826 (1998).

45 B. V. V. Prasad, R. Rothnagel, X. Jiang and M. K. Estes, *J. Virol.*, 1994, **68**, 5117-5125.

46 Larsson, M. M. *et al*. Antibody prevalence and titer to norovirus (genogroup II) correlate with secretor (FUT2) but not with ABO phenotype or Lewis (FUT3) genotype. *J. Infect. Dis.* **194**, 1422-1427 (2006).

47 Patist, A., Bhagwat, S. S., Penfield, K. W., Aikens, P. & Shah, D. O. On the measurement of critical micelle concentrations of pure and technical-grade nonionic surfactants. *J. Surfactants and Deterg.* **3**, 53-58 (2000).

48 De Paula, R., da Hora Machado, A. E. & de Miranda, J. A. 3-Benzoxazol-2-yl-7-(N,N-diethylamino)-chromen-2-one as a fluorescence probe for the investigation of micellar microenvironments. *J. Photochem. Photobiol. A.* **165**, 109-114 (2004).

49 Stryer, L. in *Biochemistry* (W. H. Freeman and Co., New York, 1988).

50 Somasundaran, P. Encyclopedia of Surface and Colloid Science, 2004 Update Supplement. **5**, 302 (2004).

51 Anachkov, S. E., Danov, K. D., Basheva, E. S., Kralchevsky, P. A. & Ananthapadmanabhan, K. P. Determination of the aggregation number and charge of ionic surfactant micelles from the stepwise thinning of foam films. *Adv. Colloid Interface Sci.* **183–184**, 55-67 (2012).

CHAPTER 3

Aggregation of Human Norovirus Virus-Like-Particles by Divalent Copper and Other Transition Metal Ions

3.1 Introduction

Metallic copper in the form of vessels and kitchenware has long been known empirically as a potent antimicrobial agent.[1,2] Recently, numerous groups have reported that solid copper surfaces are able to induce norovirus inactivation, with viral load reduced by up to 4 logs when measured by RT-qPCR and up to 5 logs when measured by plaque assay of the human norovirus surrogate murine norovirus (MNV). The ability of copper-containing alloys to inactivate noroviruses has been found to depend on the alloy composition, with the copper fraction directly correlated to the degree and rate of virus inactivation.[3-5] Copper surfaces were the first material to be recognized by the US Environmental Protection Agency (US EPA) as having antimicrobial properties.[6] Numerous groups have synthesized copper nanoparticles for their biocidal action[7] and embedded them into materials such as thin-film composite membranes to prevent biofouling.[8] A significantly lower metal amount can be used and released into the environment through the use of copper ions instead of copper alloys and nanoparticles. Cu(II) salts and mixtures have demonstrated biocidal activity[9] and have been loaded onto material matrices such as gels[10] and polymer fibers.[11]

Many proteins are able to chelate copper at specific coordination sites.[12-14] These binding sites have high affinity for copper ions, leaving a very low concentration of copper in solution.[15] Many copper-binding motifs have been identified within various copper transport

proteins. These motifs rely on the 3-dimensional conformation of the folded protein. Most of the copper ions in the body are complexed with proteins.[15] This complexation prevents redox activity between the copper ions and reducing agents within the body that would lead to the formation of damaging oxide radicals.[13,15,16] The redox activity of copper ions is harnessed by the body in a highly regulated way to accomplish certain cell functions,[13] including immune defenses.[16]

We investigated the effects of copper ions on virus-like particles of human norovirus because the mechanism of human norovirus destruction on solid copper is not well understood, and copper ions are less expensive and easier to distribute as antiviral agents. Divalent copper ions are the most stable and prevalent form of solvated copper. We also investigated the differences in behavior between norovirus strains when exposed to divalent copper ions. New human norovirus strains have emerged frequently over time as the virus mutates in response to herd immunity.[17,18] Norovirus strains are placed into genotypes and genogroups based on sequence similarities of the major capsid protein, VP1, and strains within a genogroup have at least 60% sequence homology, while strains within a genotype are more closely related.[19] Of the six Norovirus genogroups, GI, GII, and GIV contain strains that are human pathogens.[17,20] These strains have been found to behave differently in a number of ways. For example, the necessity to include bile to facilitate human norovirus replication in vitro is strain-dependent.[21] Also, individual susceptibility to human norovirus infection is correlated to varying histo-blood group antigen (HBGA) types.[19,22,23] HBGAs are present on the surface of intestinal cells and are important in facilitating infection, although their role in infection is not fully resolved.[24,25] Human norovirus binding to HBGAs is strain-dependent, allowing certain strains

to infect individuals with specific blood types and not others.[18,26] The capsids of new norovirus strains appear to antigenically evade the immune response while still allowing differential binding to HBGAs.[27-29] These capsid changes may also contribute to differences in strain responses to disinfection methods.

3.2 Results and Discussion

Dynamic light scattering was used to evaluate the effects of divalent copper ions on human norovirus VLPs. Dispersed VLPs are represented by a volume distribution peak at a hydrodynamic diameter between 30-40 nm. VLP aggregates are represented by a volume distribution peak at a hydrodynamic diameter larger than 100 nm.

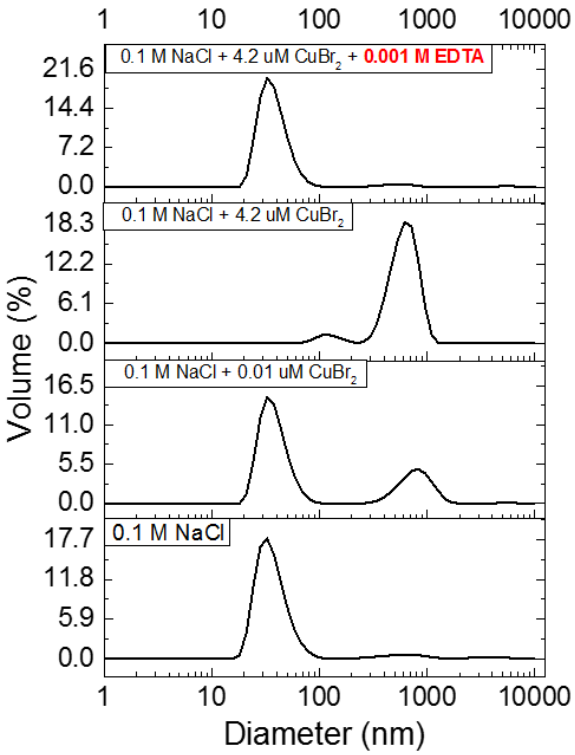

Figure 3.1 Volume distribution of light scattered by human norovirus VLPs as a function of particle diameter. Aggregation of human norovirus VLPs occurs after addition of increasing amounts of copper bromide. Aggregation is reversible by addition of EDTA, a copper chelator.

As seen in Figure 3.1, dispersed VLPs are present in 0.1 M NaCl solution at neutral pH. Dispersed VLPs and a small amount of aggregated VLPs were present after addition of 0.01 µM copper bromide, and all VLPs were aggregated after increasing the copper concentration to 4.2 µM. The human norovirus major capsid protein has a net negative charge at neutral pH,[30,31] so copper binding to the capsid surface decreases the magnitude of charge on the capsid. Less charge on the particle results in decreased electrostatic repulsion between particles and subsequent aggregation. Divalent ions can also facilitate ion bridging between

particles, where the ion binds to charged sites on two separate particles. Ion bridging also results in particle aggregation. VLP aggregation was reversible by adding EDTA, a copper chelator, in excess of the copper ions.

3.2.1 Effects of Salt and pH on Copper-induced VLP Aggregation

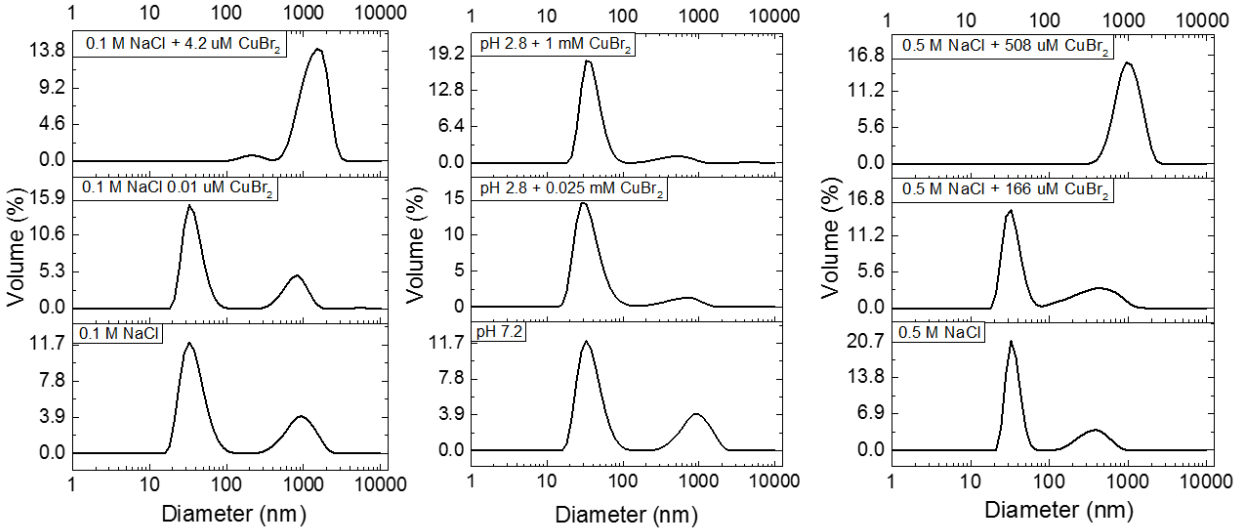

Figure 3.2 Dynamic light scattering data showing the effects of pH and ionic strength on the copper-induced aggregation of VLPs. a) Aggregation occurs at low copper concentration in 0.1 M NaCl solution at neutral pH. b) Aggregation does not occur even at millimolar concentrations of copper at pH below the major capsid protein isoelectric point. c) Aggregation occurs at higher concentration in 0.5 M NaCl solution at neutral pH than in lower ionic strength.

When the pH is dropped below the isoelectric point of the major capsid protein, the capsid has a net positive charge. Copper ions have fewer locations to bind on the capsid surface, so aggregation does not occur. At pH 2.8, which is below the major capsid protein isoelectric point of GII.4 Houston human norovirus VLPs, particles remained dispersed even after addition of up to 1 mM copper bromide (Figure 3.2b). This concentration is almost 1000-fold higher than that required to aggregate the VLPs at neutral pH (Figure 3.2a).

Salt ions shield the surface charges on dispersed particles, so increasing ionic strength is expected to aggregate particles normally dispersed by electrostatic forces. As seen in Figure 3.2, increasing the salt concentration from 0.1 M (Figure 3.2a) to 0.5 M (Figure 3.2c) resulted in a greater resistance of the VLPs to aggregation. Approximately 100-fold lower copper concentration was required to aggregate the VLPs suspended in 0.1 M NaCl solution than in 0.5 M NaCl solution. The NaCl ions may shield copper ions from binding to the particle surface and prevent aggregation from occurring.

3.2.2 VLP Aggregation by Other Transition Metals

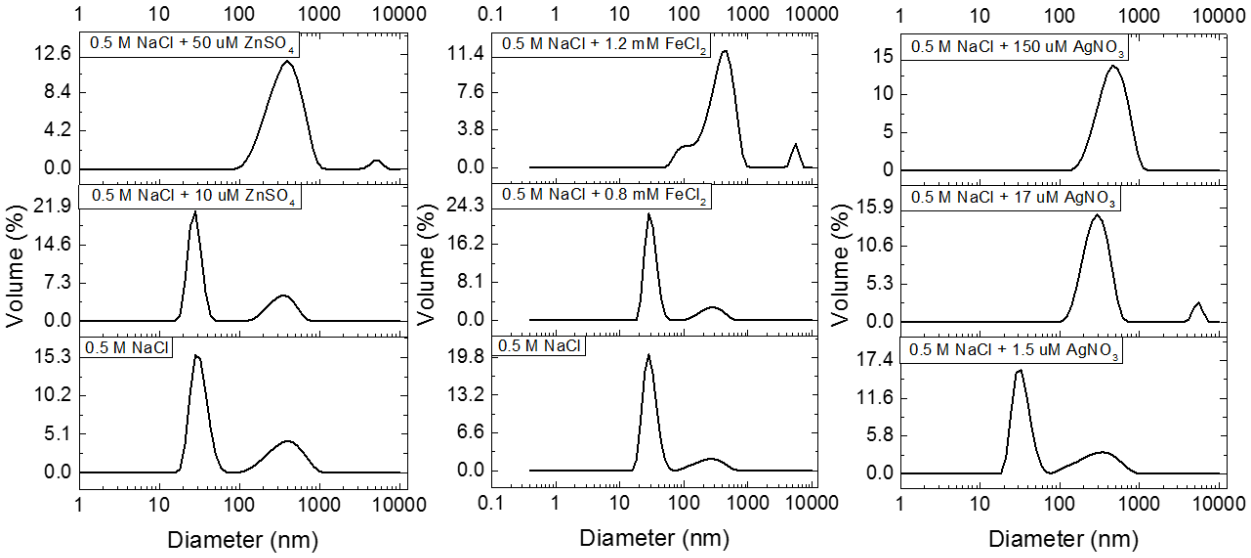

Figure 3.3 Dynamic light scattering data showing aggregation of VLPs after addition of increasing concentrations of a) zinc sulfate, b) iron chloride, and c) silver nitrate.

Other cations, specifically other transition metals, are also capable of binding and aggregating VLPs. We found that in 0.5 M NaCl solution at neutral pH, 50 µM zinc sulfate, 1.2 mM iron chloride, and 17 µM silver nitrate all aggregate the VLPs (Figure 3.3). Therefore, the transition metal ions studied here have the ability to bind and aggregate GII.4 Houston human norovirus VLPs with the following relative strength: silver > zinc > copper > iron. Silver was both the only monovalent metal ion studied and the ion with the strongest ability to bind and aggregate VLPs. Silver has known antimicrobial properties at low concentration[32] that may be aided by its protein-binding capabilities. Zinc[33] and copper[1] have also been used

as antimicrobials and antivirals. It should be noted that the transition metal salts used in this study contain different counterions. As a consequence, ion-specific effects from the counterions may play a role in the binding and aggregation behaviors of the VLPs and metal ions.

3.2.3 Strain-dependent Susceptibility to Aggregation

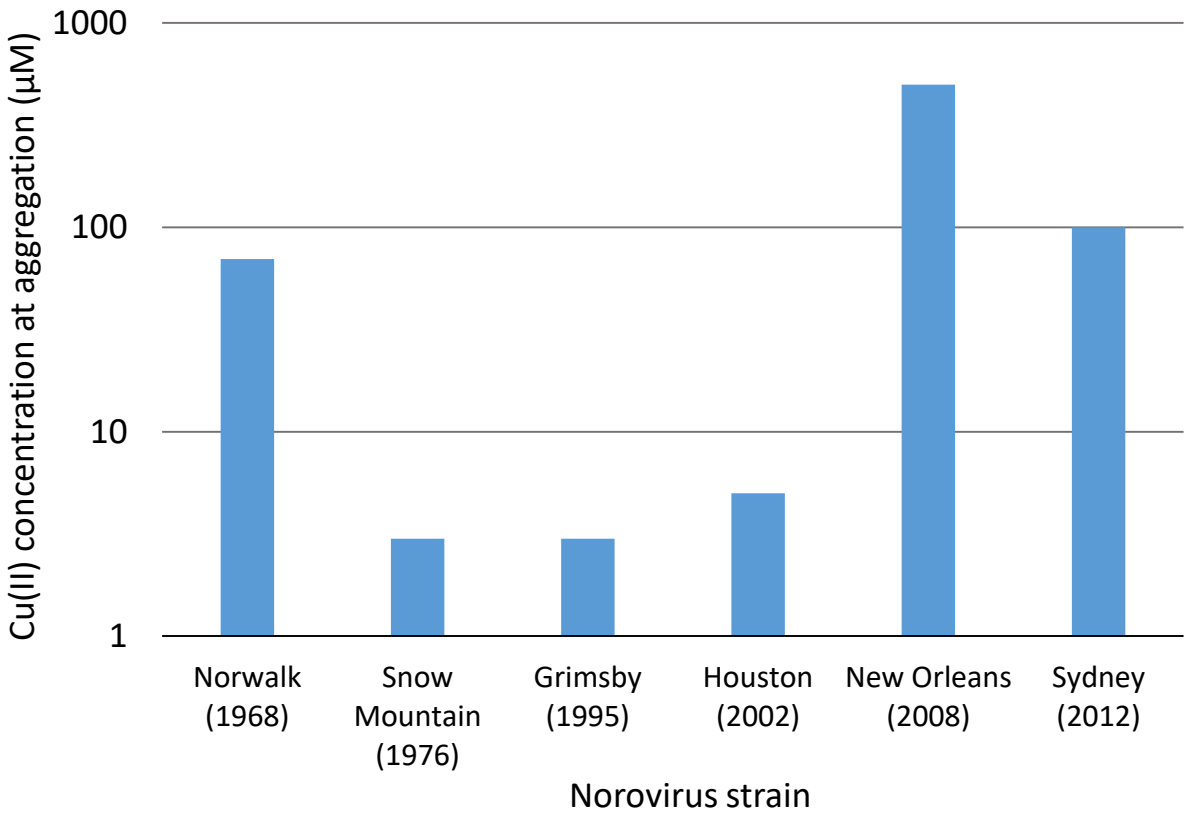

Figure 3.4 Plot of the lowest $CuBr_2$ concentration required to induce aggregation of various strains of human norovirus. The strains are distinguished by the year of emergence, which is provided in parenthesis.

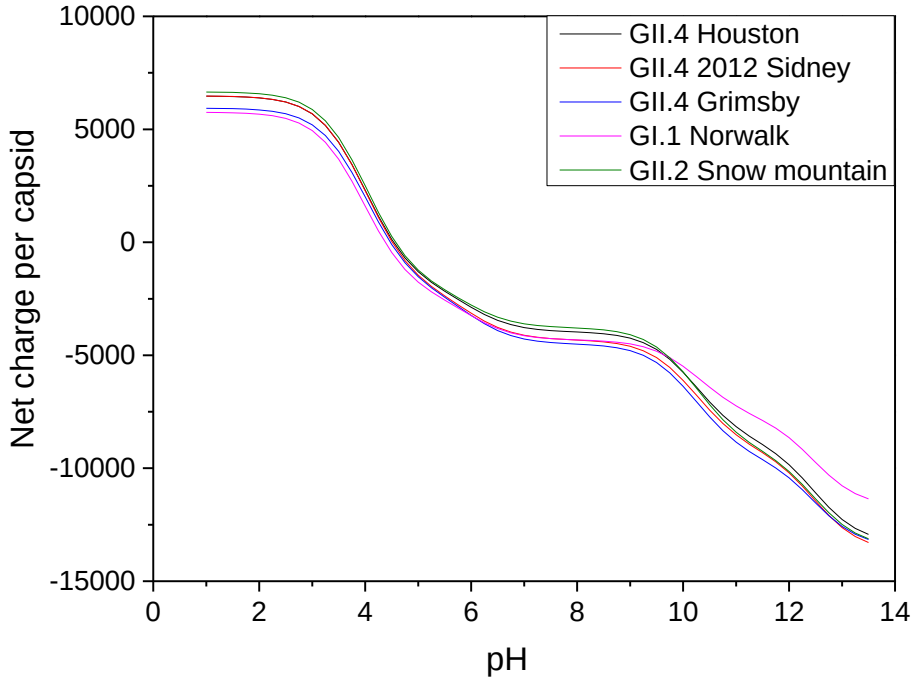

Figure 3.5 Theoretical capsid charge of various human norovirus strains as a function of pH. Capsid charge was calculated using the major capsid protein composition and a derivation of the Henderson-Hasselbach equation, as explained in Chapter 2.

Significant differences exist between the susceptibility of different human norovirus strains to aggregation by divalent copper ions. The minimum concentration of copper bromide necessary to induce aggregation in suspensions of VLPs of six different human norovirus strains are presented in Figure 3.4. This minimum concentration varies by two orders of magnitude, depending on the strain. The differences in the minimum copper concentration required to induce aggregation cannot be explained by differences in capsid charge. The theoretical charge per capsid of each VLP strain as a function of pH is presented in Figure 3.5. These capsid charges were calculated using a derivation of the Henderson-Hasselbach equation

(Equation 2.1). The VLP strains all have very similar charge profiles, so the small variations in charge between strains cannot account for the large variations in VLP behavior in the presence of divalent copper ions.

It is possible that specific copper-binding motifs exist on the surface of human norovirus capsids and that differences in amino acid compositions between strains result in differing numbers of these motifs. Even differences in the number of individual exposed amino acids that have high affinity for copper ions, including histidine, cysteine, and methionine, could exist between strains. Residues with side chains that contain nitrogen, oxygen, and/or sulfur are most commonly involved in copper binding because of the coordination of these atoms with copper ions.[14] Variations in the number of exposed residues with high copper affinity could account for the strain-specific susceptibilities of VLPs to aggregation by divalent copper ions. Specific binding would also explain how copper concentrations as low as micromolar can induce rapid aggregation in VLP suspensions. Further research would need to take into account the 3-dimensional conformations of each capsid and determine copper-binding sites on each strain.

3.3 Conclusions

We showed that divalent copper ions bind and aggregate human norovirus VLPs at low concentration. The minimum copper concentration required to induce aggregation depended on solution ionic strength and pH. At pH values below the isoelectric point where VLPs have a net positive surface charge, aggregation does not occur. Other transition metals commonly considered for disinfection are also able to aggregate VLPs at low concentration. The relative

ability of these metals to induce aggregation has the following trend: silver > zinc > copper > iron. Substantial differences in VLP susceptibility to aggregation by divalent copper ions exist between strains, despite only minor differences in capsid charge. This indicates that specific copper binding motifs or residues are present in greater quantity on the surface of the more susceptible strains. Additional studies comparing the exposed residues on the 3-dimensional structures of the varying strains could elucidate the causes behind significant differences in behavior in the presence of copper ions. Overall, the data prove that copper ion binding and aggregation of VLPs may have large implications in virus transmission and disinfection.

3.4 Materials and Methods

3.4.1 Dynamic Light Scattering Measurements

VLP and aggregate sizes were determined by DLS. VLPs of varying strains were added to cuvettes containing 0.15 M or 0.5 M NaCl at a final VLP concentration of 5 µg ml^{-1}. Small volumes of 1-9 µl of $CuBr_2$, $ZnSO_4$, $FeCl_2$, and $AgNO_3$ stocks ranging in concentration from 10^{-6} to 0.1 M were added to the VLP suspensions, and the particle size was measured after each addition to determine whether aggregation had taken place. Each sample was measured in triplicate using a Zetasizer Nano ZSP (Malvern Instruments) with a 10 mW He-Ne laser at 633 nm and a photodiode located 173° from the incident laser beam. Zetasizer software calculated a size distribution of particles in each sample from light scattering intensity data and then converted these data to a volume distribution.

3.5 Acknowledgments

Funding for this work was provided by the USDA-NIFA Food Virology Collaborative (NoroCORE), supported by the National Institute of Food and Agriculture, U.S. Department of Agriculture, under award number 2011-68003-30395. Additional funds were provided by the Molecular Biotechnology Training Program (MBTP) sponsored by the National Institutes of Health and the Graduate School at North Carolina State University (5 T32 GM008776-15). The Zetasizer Nano ZSP was purchased by the NSF Triangle Materials Research Science and Engineering Center (NSF DMR-1121107).

3.6 References

1 Borkow, G. & Gabbay, J. Copper as a biocidal tool. *Curr. Med. Chem.* **12**, 2163-2175 (2005).

2 Dollwet, H. H. A. & Sorenson, J. R. J. Historic Uses of Copper-Compounds in Medicine. *J. Trace Elem. Med. Biol.* **2**, 80-87 (1985).

3 Warnes, S. L. & Keevil, C. W. Inactivation of Norovirus on Dry Copper Alloy Surfaces. *PloS One* **8**, e75017 (2013).

4 Manuel, C. S., Moore, M. D. & Jaykus, L. A. Destruction of the Capsid and Genome of GII.4 Human Norovirus Occurs during Exposure to Metal Alloys Containing Copper. *Appl. Environ. Microbiol.* **81**, 4940-4946 (2015).

5 Warnes, S. L., Summersgill, E. N. & Keevil, C. W. Inactivation of Murine Norovirus on a Range of Copper Alloy Surfaces Is Accompanied by Loss of Capsid Integrity. *Appl. Environ. Microbiol.* **81**, 1085-1091 (2015).

6 O'Gorman, J. & Humphreys, H. Application of copper to prevent and control infection. Where are we now? *J. Hosp. Infect.* **81**, 217-223 (2012).

7 Ingle, A. P., Duran, N. & Rai, M. Bioactivity, mechanism of action, and cytotoxicity of copper-based nanoparticles: A review. *Appl. Microbiol. Biotechnol.* **98**, 1001-1009 (2014).

8 Ben-Sasson, M. *et al*. Surface Functionalization of Thin-Film Composite Membranes with Copper Nanoparticles for Antimicrobial Surface Properties. *Environ. Sci. Technol.* **48**, 384-393 (2014).

9 Gant, V. A. *et al*. Three novel highly charged copper-based biocides: safety and efficacy against healthcare-associated organisms. *J. Antimicrob. Chemother.* **60**, 294-299 (2007).

10 Brunel, F., El Gueddari, N. E. & Moerschbacher, B. M. Complexation of copper(II) with chitosan nanogels: Toward control of microbial growth. *Carbohydr. Polym.* **92**, 1348-1356 (2013).

11 Borkow, G. & Gabbay, J. Putting copper into action: copper-impregnated products with potent biocidal activities. *Faseb Journal* **18**, 1728-+ (2004).

12 Sun, X. *et al*. Putative copper- and zinc-binding motifs in Streptococcus pneumoniae identified by immobilized metal affinity chromatography and mass spectrometry. *Proteomics* **11**, 3288-3298 (2011).

13 Koch, K. A., Pena, M. M. O. & Thiele, D. J. Copper-binding motifs in catalysis, transport, detoxification and signaling. *Chem. Biol.* **4**, 549-560 (1997).

14 Katz, A. K. *et al*. Copper-binding motifs: Structural and theoretical aspects. *Helv. Chim. Acta* **86**, 1320-1338 (2003).

15 Giner-Lamia, J., Lopez-Maury, L. & Florencio, F. J. CopM is a novel copper-binding protein involved in copper resistance in Synechocystis sp PCC 6803. *Microbiologyopen* **4**, 167-185 (2015).

16 Djoko, K. Y., Ong, C. Y., Walker, M. J. & McEwan, A. G. The Role of Copper and Zinc Toxicity in Innate Immune Defense against Bacterial Pathogens. *J. Biol. Chem.* **290**, 18954-18961 (2015).

17 Moore, M. D., Goulter, R. M. & Jaykus, L. Human Norovirus as a Foodborne Pathogen: Challenges and Developments. *Ann. Rev. Food Sci. Technol.* **6**, 411-433 (2015).

18 Lindesmith, L. C., Donaldson, E. F. & Baric, R. S. Norovirus GII.4 Strain Antigenic Variation. *J. Virol.* **85**, 231-242 (2011).

19 Hutson, A., Atmar, R. & Estes, M. Norovirus disease: changing epidemiology and host susceptibility factors. *Trends Microbiol.* **12**, 279-287 (2004).

20 Zheng, D. *et al*. Norovirus classification and proposed strain nomenclature. *Virology* **346**, 312-323 (2006).

21 Ettayebi, K. *et al*. Replication of human noroviruses in stem cell–derived human enteroids. *Science* (2016).

22 Lindesmith, L. *et al*. Human susceptibility and resistance to Norwalk virus infection. *Nat. Med.* **9**, 548-553 (2003).

23 Hutson, A., Atmar, R., Graham, D. & Estes, M. Norwalk virus infection and disease is associated with ABO histo-blood group type. *J. Infect. Dis.* **185**, 1335-1337 (2002).

24 Murakami, K. *et al*. Norovirus Binding to Intestinal Epithelial Cells Is Independent of Histo-Blood Group Antigens. *PloS One* **8**, e66534 (2013).

25 Karst, S. M. & Wobus, C. E. A Working Model of How Noroviruses Infect the Intestine. *PloS Pathog.* **11**, UNSP e1004626 (2015).

26 Huang, P. W. *et al*. Norovirus and histo-blood group antigens: Demonstration of a wide spectrum of strain specificities and classification of two major binding groups among multiple binding patterns. *J. Virol.* **79**, 6714-6722 (2005).

27 Tan, M. & Jiang, X. Norovirus and its histo-blood group antigen receptors: an answer to a historical puzzle. *Trends Microbiol.* **13**, 285-293 (2005).

28 Donaldson, E. F., Lindesmith, L. C., Lobue, A. D. & Baric, R. S. Viral shape-shifting: norovirus evasion of the human immune system. *Nature Rev. Microbiol.* **8**, 231-241 (2010).

29 Shanker, S. *et al*. Structural Analysis of Histo-Blood Group Antigen Binding Specificity in a Norovirus GII.4 Epidemic Variant: Implications for Epochal Evolution. *J. Virol.* **85**, 8635-8645 (2011).

30 Samandoulgou, I., Fliss, I. & Jean, J. Zeta Potential and Aggregation of Virus-Like Particle of Human Norovirus and Feline Calicivirus Under Different Physicochemical Conditions. *Food Environ. Virol.* **7**, 249-260 (2015).

31 Mertens, B. S. & Velev, O. D. Characterization and control of surfactant-mediated Norovirus interactions. *Soft Matter* **11**, 8621-8631 (2015).

32 Thurman, R. B. & Gerba, C. P. The Molecular Mechanisms of Copper and Silver Ion Disinfection of Bacteria and Viruses. *Crit. Rev. Env. Contr*. **18**, 295-315 (1988).

33 Pasquet, J. *et al*. The contribution of zinc ions to the antimicrobial activity of zinc oxide. *Colloids Surf. A Physicochem. Eng. Asp.* **457**, 263-274 (2014).

CHAPTER 4

Efficacy and Mechanisms of Copper Ion-catalyzed Inactivation of Human Norovirus

4.1 Introduction

We seek to find the mechanisms behind the remarkable efficacy of copper bromide and sodium ascorbate mixtures in inactivating human norovirus. Noroviruses are particularly difficult to disinfect owing to their highly stable protein capsids, which are resistant to heat, pH, and drying.[1] Commonly used disinfection agents such as ethanol, quaternary ammonium compounds, and peroxides have little or debated effects on the virus,[2] so viruses may still persist in the environment and spread after typical cleaning protocols. Bleach remains the most widely accepted inactivation agent against norovirus,[2] but it is also too corrosive and aggressive for many applications.[3]

Cu(I) ions have been identified as contributors to the innate immune response against bacterial pathogens. Upon phagocytosis of a pathogen by a macrophage, the phagolysosome develops a myriad of antimicrobial conditions, including increased uptake of Cu(I) ions that can cause oxidative damage to proteins, lipids, and DNA via Fenton chemistry.[4] Many bacterial pathogens have developed resistance to the toxic effects of copper ions using ion-specific pumps to remove elevated ion levels,[5,6] but viruses do not have the ability to acquire this kind of defense mechanism. Copper iodide nanoparticles that release Cu(I) ions have demonstrated high efficacy against feline calicivirus (FCV), a surrogate for the human norovirus.[7]

The biocidal effects of Cu(I) ions appear to be a result of the oxidative effects from copper's redox activity.[8] Copper is a redox-active transition metal that can be present in its monovalent or divalent form in solution. Cu(I) ions are unstable and either react with dissolved oxygen to form Cu(II) or disproportionate into Cu(s) and Cu(II).[9] The required concentration of Cu(I) ions in solution can be attained by addition of a reducing agent to solutions of Cu(II). Many reactions, such as those carried out in Click chemistry,[10] commonly use the ascorbate ion as a reducing agent for copper. Solid iron surfaces have also been used as reducing agents for copper ions to generate a biocidal environment.[11]

Some literature sources point out that human norovirus disinfection by a variety of methods is strain-dependent. Specifically, GI strains have been found more susceptible than GII strains to inactivation by alcohols[12,13] and heat treatment.[14] GII generally represents the more resistant genogroup, and GII.4 is the most prevalent genotype of this group.[15] Therefore many disinfection studies use GII.4 strains of human norovirus in addition to a surrogate virus. The amino acids involved in receptor binding in GII.4 strains are highly conserved amidst genetic mutations,[16] so demonstration of loss of receptor binding is useful in evaluating disinfection. We compare the effects of copper-mediated oxidative damage on GI.7 and GII.4 VLPs to further elucidate differences in susceptibility to disinfectant treatments between human norovirus strains.

Different disinfection methods target non-enveloped viruses in distinct ways. For example, in disinfection of MS2 bacteriophage, free chlorine causes capsid protein cleavage that inhibits genome injection in addition to direct genome damage that inhibits replication, while singlet oxygen mainly targets genome replication.[17] Multiple mechanisms by which

microorganisms are killed by contact with metallic copper have been suggested, including damage to nucleic acid; damage to the plasma membrane of cells; obstruction of enzyme activity; and indirect oxidation of proteins, lipids, and nucleic acids by the formation of reactive oxygen species (ROS).[18] Because of their lack of a membrane and enzymes, non-enveloped viruses are only susceptible to the effects of nucleic acid damage and oxidative damage by generation of ROS. Both of these mechanisms have been implicated in the contact killing of human norovirus and its surrogates on copper alloys.[19-21] In copper ion-mediated disinfection, copper ions in multiple oxidation states, reduction products of dissolved oxygen,[22] and reducing agents could all be present and active. Oxidative nucleic acid damage has been recognized and studied extensively due to its implications in carcinogenesis and other age-related diseases.[23-25] The generation of ROS during copper ion redox produces more potent oxidative conditions than in vivo metabolism because of the absence of as many antioxidants,[26] so nucleic acid damage is expected to be a significant contributor to loss of virus infectivity in copper ion-mediated virucides. Indeed, Manuel *et al.* demonstrate a 4-log reduction in human norovirus RNA copy number after incubation on copper alloy surfaces.[21]

Although work has been done on the effects of copper surfaces and nanoparticles, the efficacy and effects on human noroviruses of ionic copper in solution in conjunction with a reducing agent, as well as their underlying mechanisms have not been thoroughly investigated. We report the mechanisms of action of alternative copper-ion based disinfectants on human norovirus while investigating differences in strain susceptibilities. Tulane virus has been described as the most representative surrogate for the human norovirus due to its pH, heat, ethanol, and chlorine resistance compared with other surrogate candidates.[27,28] After treatment,

we estimate loss of human norovirus infectivity and capsid integrity using Tulane virus (TV) plaque assays, histo-blood group antigen (HBGA) binding assays of virus-like particles (VLPs), sodium dodecyl sulfate-polyacrylamide gel electrophoresis (SDS-PAGE) of VLPs, and reverse transcriptase-quantitative polymerase chain reaction (RT-qPCR) of infectious virus from stool.

4.2 Results and Discussion

4.2.1 Effects of Copper Concentration and Treatment Time on Human Norovirus Surrogate Inactivation

We used plaque assays of a human norovirus surrogate, Tulane virus (TV), in combination with binding assays of human norovirus VLPs, to approximate the effects of different copper ion formulations on human norovirus infectivity. We selected copper bromide as a source of divalent copper ions and added sodium ascorbate in at least 10-fold excess to reduce Cu(II) and create a redox active environment. For plaque assay experiments, we treated TV stocks with $CuBr_2$ in concentrations ranging from 0.01 mM to 1 mM for 30 minutes to evaluate the effects of Cu(II) ions alone. We also treated TV stocks with $CuBr_2$ in concentrations ranging from 0.001 mM to 1 mM in combination with 100x excess ascorbate for 30 minutes. After determining a formulation that induces greater than 4-log reduction in TV infectivity using a 30 minute incubation, we treated the virus stocks for shorter times to find out the minimum time it takes to achieve substantial inactivation.

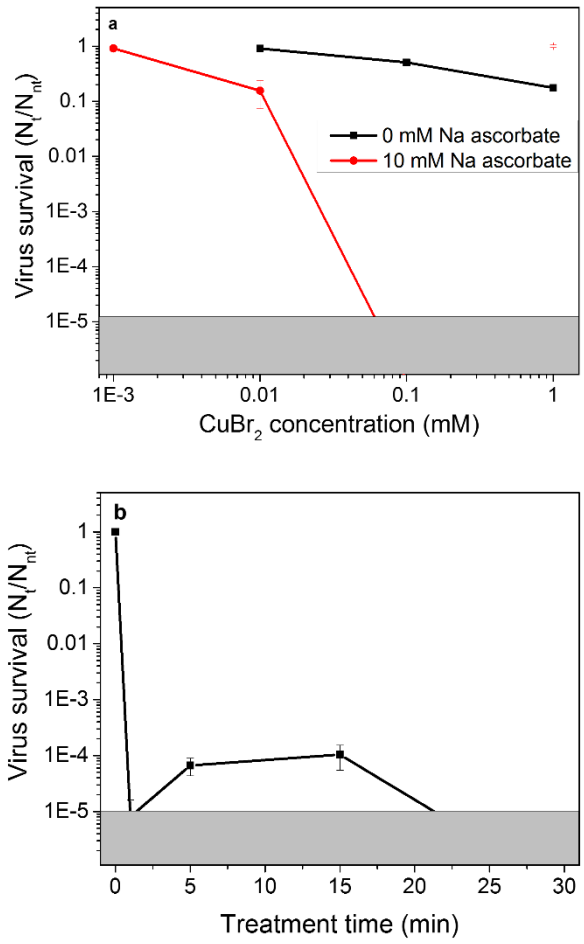

Figure 4.1 Results of TV plaque assay after treatment with a) varying concentrations of $CuBr_2$ with and without 10 mM sodium ascorbate as reducing agent and b) 0.1 mM $CuBr_2$ with 10 mM sodium ascorbate at varying time points. Virus survival is the number of pfu after each treatment (N_t) normalized to the number of pfu without treatment (N_{nt}) determined during the same set of experiments. The areas outside the limit of detection of the assay are marked in gray. Error bars represent the average of three replicates at each condition.

The virus reduction data are plotted in Figure 4.1. $CuBr_2$ alone at 1 mM induces only 1-log reduction in virus titer and even lower reduction at lower concentration (Figure 4.1a). The addition of ascorbate significantly amplifies inactivation, causing greater than 4-log reduction in virus titer with as low as 0.1 mM copper concentration and approximately 1-log reduction at 0.01 mM copper. Based on these results, we evaluated the efficacy of a solution comprising 0.1 mM $CuBr_2$ and 10 mM ascorbate at different treatment times. As seen in Figure 4.1b, 4-log reduction of virus titer was observed in as little as one minute, indicating rapid and effective inactivation at these solution conditions.

For binding assays, we evaluated the ability of the virus capsid to bind histo-blood group antigens (HBGA), a carbohydrate cell marker and putative viral receptor,[29,30] using VLPs of the GI.7 and GII.4 Sydney strains of human norovirus. The degree of VLP binding to HBGA is an indication of capsid integrity, as loss in binding is generally correlated with a loss of infectivity. These assays are colorimetric, and we normalized each absorbance data point to a positive VLP control that was not treated. GI.7 VLPs were treated for 30 minutes with solutions of $CuBr_2$ ranging in concentration from 0.001 to 100 mM both with and without ascorbate. 1 mM ascorbate was used because higher concentrations interfered with assay results. Concentrations of $CuBr_2$ ranging from 0.0001 to 0.1 mM $CuBr_2$ in combination with ascorbate were applied to the VLPs at shorter times to determine the time required for loss of capsid integrity at each concentration.

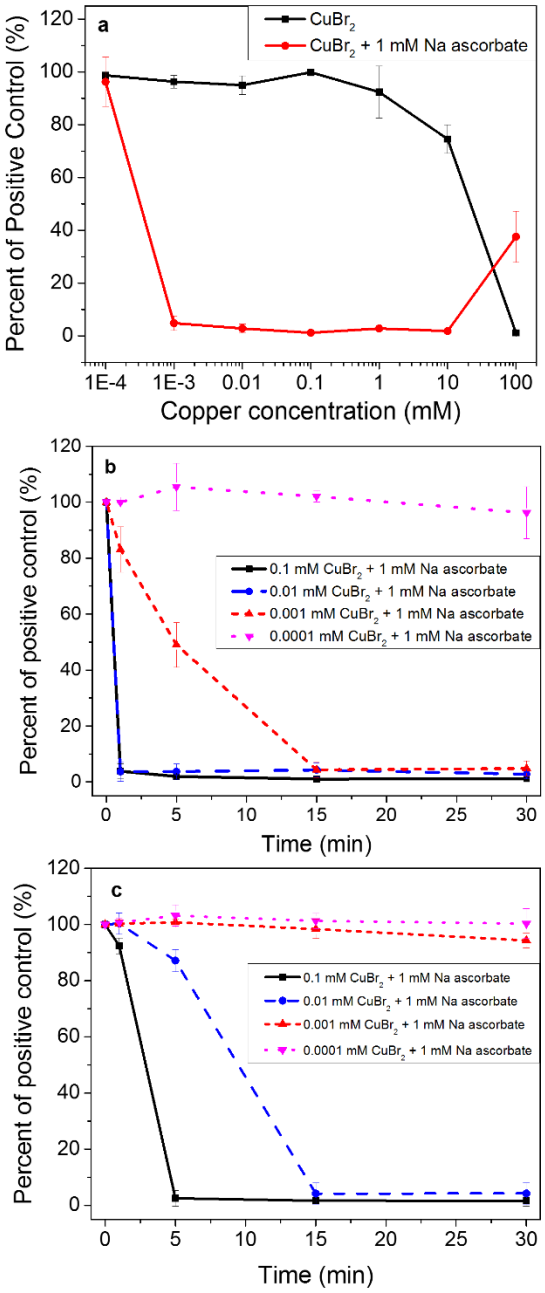

Figure 4.2 Results of VLP binding assay with HBGA after a) GI.7 VLP exposure to $CuBr_2$ at varying concentrations for 30 minutes with and without sodium ascorbate and b) GI.7 VLP and c) GII.4 Sydney VLP exposure to $CuBr_2$ at varying concentrations with 1 mM sodium ascorbate over time. Error bars represent the standard error of three replicate samples.

As seen in Figure 4.2a, $CuBr_2$ alone only slightly reduces GI.7 VLP binding to HBGA at 10 mM copper, while complete reduction required 100 mM copper. Complete reduction in binding occurred after treatment with $CuBr_2$ at 10^5-fold lower concentration in combination with ascorbate. At 100 mM Cu(II) + ascorbate, higher VLP-HBGA binding was observed than with Cu(II) alone. Ascorbate is only in excess of Cu(II) ions below 1 mM $CuBr_2$, so we used only copper concentrations below 1 mM to evaluate the efficacy of $CuBr_2$/ascorbate mixtures to reduce VLP-HBGA binding at shorter treatment times.

As seen in Figure 4.2b we observed very strong antiviral action at low Cu ion concentrations. Only one minute was required to damage capsid integrity with as low as 0.01 mM $CuBr_2$ combined with ascorbate. Even 0.001 mM $CuBr_2$ with ascorbate can eliminate VLP-HBGA binding in 15 minutes. We observed significant differences between the susceptibility of GI.7 and GII.4 VLPs to inactivation by Cu(I) solutions. GII.4 Sydney VLPs appeared to be much more resistant to copper, requiring about an order of magnitude higher concentration to induce the same reduction in HBGA binding. As seen in Figure 4.2c, even 0.1 mM $CuBr_2$ combined with ascorbate took 5 minutes to reduce GII.4 Sydney VLP binding to HBGA, and 0.01 mM $CuBr_2$ with ascorbate took 15 minutes for complete binding reduction. No reduction in binding was observed for treatments of 0.001 and 0.0001 mM $CuBr_2$ with ascorbate. The difference in susceptibility to Cu(I) solution treatment between GI.7 and GII.4 Sydney VLPs indicates that sequence and morphological changes in human norovirus capsids that come with adaptive mutations influence virus resistance to disinfection methods. Therefore, it cannot be assumed that new emerging strains will be inactivated by the same treatments that have been effective against previous strains. This higher susceptibility of GI

compared to GII is also reported for different alcohols[12] and for copper surfaces (Manuel *et al. unpublished data*).

4.2.2 Loss of Capsid Structure and Inactivation of Intact Human Noroviruses

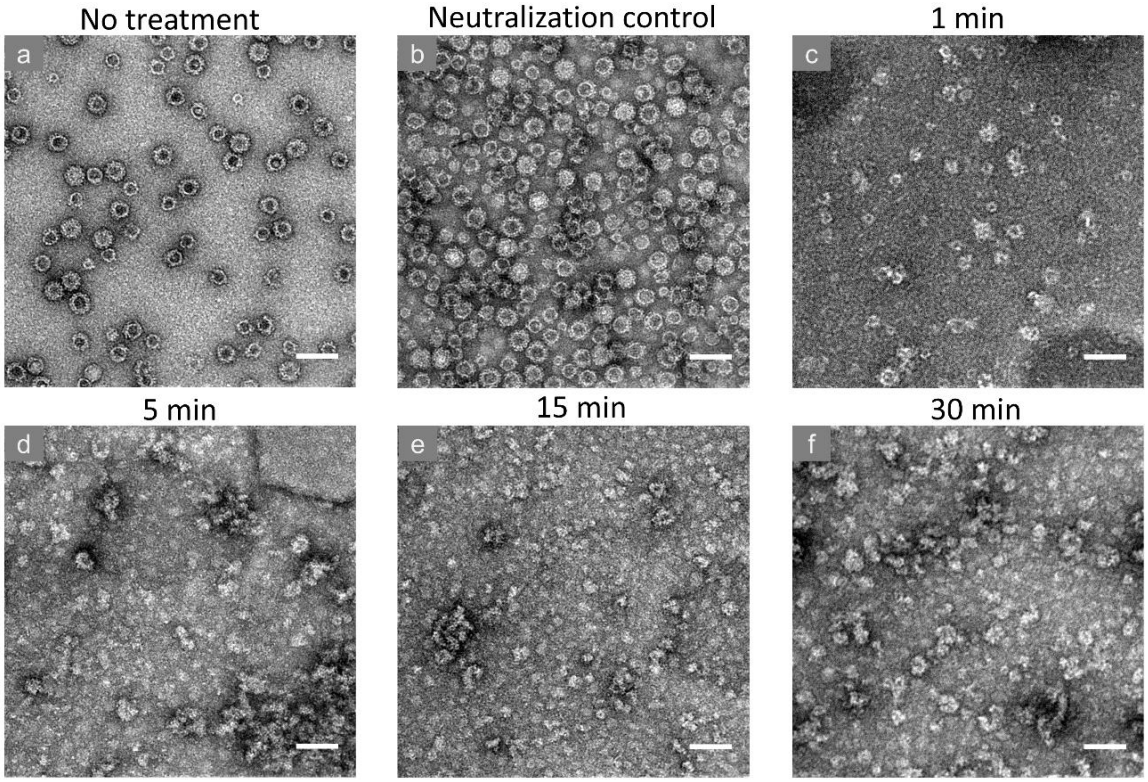

Figure 4.3 Representative TEM images of GI.7 VLPs a) without treatment, b) after treatment with 0.1 mM $CuBr_2$ and 10 mM sodium ascorbate in the presence of 10 mM EDTA (to bind copper ions), and after treatment with 0.1 mM $CuBr_2$ and 10 mM sodium ascorbate for c) 1 minute, d) 5 minutes, e) 15 minutes, and f) 30 minutes. Significant capsid degradation is seen within minutes, leaving mostly capsid protein aggregates and a few recognizable capsid structures. Scale bars represent 100 nm.

Both TV plaque assays and VLP-HBGA binding assays indicate that Cu(II) ions alone are relatively ineffective in causing norovirus inactivation except at very high concentration. The addition of a reducing agent such as ascorbate is required to generate Cu(I) ions and introduce an oxidative environment that damages the viruses enough to reduce infectivity. The resultant inactivation occurs at very short treatment time, making these solutions both rapid and highly effective. This is accompanied by loss of capsid integrity observed in TEM images of VLPs treated with $CuBr_2$/ascorbate mixtures for varying times. Intact VLPs that have not been treated with any copper solution can be seen in Figure 4.3a. VLPs treated with 0.1 mM $CuBr_2$ and 10 mM ascorbate for as short as 1 minute have lost most of their structure, with only capsid protein aggregates and a few damaged capsids remaining, as seen in Figure 4.3c-f. These images correlate with the disinfection data obtained from TV plaque assays and VLP-HBGA binding assays, which indicate loss of infectivity and binding at the same copper concentration in combination with ascorbate.

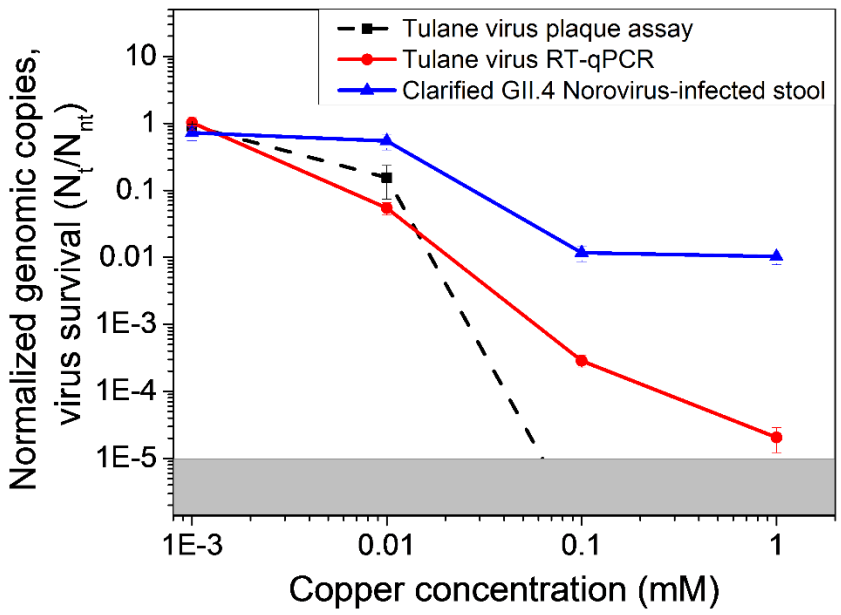

Figure 4.4 Loss of genomic copy number of Tulane virus and clarified stool containing GII.4 norovirus after treatment with 100 mM sodium ascorbate and various copper concentrations. After copper treatments, samples were digested with RNase. Error bars represent the standard error of three replicate samples. TV plaque assay data are also included for comparison.

In the absence of access to one of the recently reported human norovirus cell culture systems[31,32] to measure loss of human norovirus infectivity directly, we used RT-qPCR of GII.4 norovirus-infected stool to evaluate loss of genomic copy numbers. This method allowed us to determine the effects of Cu(I) solutions on human norovirus RNA. Because we have plaque assay data for TV, we also measured loss of genomic copy number within TV samples after treatment with Cu(I) solutions. The comparison of TV plaque assay and RT-qPCR data allowed us to determine whether genome damage was an important mechanism in virus inactivation. As shown in Figure 4.4, only 2-log reduction in GII.4 norovirus genomic copy

number occurs after treatment with 0.1 mM $CuBr_2$ in combination with 10 mM sodium ascorbate. At this copper concentration, we observed about 4-log reduction in TV genomic copy number. Similarly, at 1 mM $CuBr_2$ with 10 mM sodium ascorbate, a 3-log difference exists in the loss in genomic copy numbers between TV and GII.4 norovirus. This 3-log difference in inactivation between GII.4 norovirus and TV may potentially reveal fundamental differences in the nature of susceptibility to copper between the two viruses. However, given the previously reported relative resilience of TV to other oxidative disinfectants,[27,28] this seems less likely. It may be possible that the presence of stool in the human norovirus samples had a more pronounced quenching effect on the copper than the cell culture buffer, as doping feline calicivirus into stool has been reported to increase its resistance to heat.[33] As has been observed in multiple previous studies and reviewed by Moore, et al.,[34] RNase treatment followed by RT-qPCR overestimated the number of infectious Tulane virus particles in solution at the various treatments (Figure 4.4), thus indicating lower reductions than were observed with plaque assay. This is likely due to inactivation of particles by more subtle damage to intact capsids' higher order protein structure, which is likely needed to bind receptor(s).[35]

4.2.3 Evidence of Covalent Capsid Damage

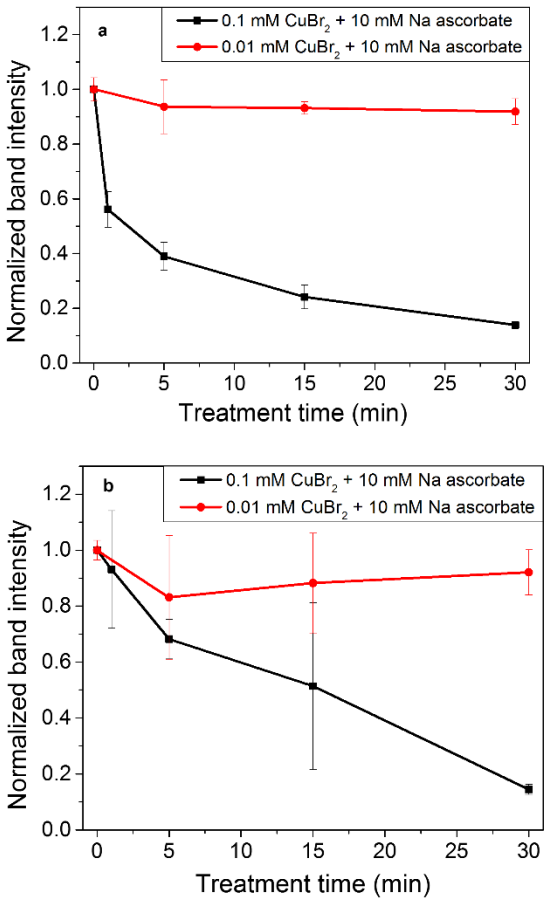

Figure 4.5 SDS-PAGE data demonstrating capsid protein cleavage of a) GI.7 VLPs and b) GII.4 Sydney VLPs after treatment with 1 mM sodium ascorbate and 0.1 mM or 0.01 mM copper bromide. Normalized intensity represents the intensity of the major capsid protein band adjusted to the background of the gel and normalized to a control sample that was not treated. The GI.7 capsid protein is degraded more rapidly by copper ion treatment than GII.4 Sydney VLPs at 0.1 mM ion concentration. Error bars represent the standard error of three replicate samples.

HBGA-VLP binding assays demonstrated that GII.4 VLPs completely lost their ability to bind HBGA after treatment with 0.01 mM and 0.1 mM $CuBr_2$ with ascorbate for 30 minutes, whereas RT-qPCR data showed 1-log reduction or less in genomic copy number at these conditions. These data indicate that Cu(I) solutions may inactivate human norovirus by disrupting binding to host cells instead of destroying the virus particle completely. We therefore investigated the effects of Cu(I) solution treatments on human norovirus capsid proteins using SDS-PAGE of GI.7 and GII.4 Sydney VLPs. As seen in Figure 4.5a, the major capsid protein band of GI.7 VLPs was reduced to less than 40% of the value of an untreated control after only 5 minutes of treatment and was reduced to less than 20% of the control after 30 minutes of treatment with 0.1 mM $CuBr_2$ and ascorbate. This loss of band intensity indicates that significant capsid protein cleavage occurred during the treatment. Thus, redox activity involving ascorbate as a reducing agent and copper as a catalyst to generate damaging ROS is the likely mechanism behind the substantial covalent destruction of the major capsid protein.

Minimal protein cleavage occurred after treatment with 0.01 mM $CuBr_2$ and ascorbate, with less than 10% loss of band intensity regardless of treatment time. As seen in Figure 4.5b, the major capsid band of GII.4 Sydney VLPs was reduced to about 15% of the untreated control after 30 minutes of treatment with 0.1 mM $CuBr_2$ and ascorbate. Minimal loss of capsid protein band intensity was observed after treatment with 0.01 mM copper and ascorbate, regardless of treatment time. These would be expected given the lower reduction observed in RT-qPCR results, as capsid degradation was not severe for GII.4 at this concentration. At time points shorter than 30 minutes, the loss in band intensity after copper treatment was about 20-30% less for GII.4 Sydney VLPs than for GI.7 VLPs, indicating that the GII.4 major capsid protein

has greater stability and resistance to oxidative treatments. Representative gels for GI.7 and GII.4 VLPs are presented in Figure C.1.

For both GI.7 and GII.4 Sydney VLPs, there is a distinct difference between the effects of copper at 0.01 mM and 0.1 mM concentrations as evaluated by SDS-PAGE. These data correlate well with TV plaque assay data, which showed a decrease of 4-log in virus survival after increasing the copper concentration from 0.01 mM to 0.1 mM. This increase in copper concentration could be a threshold for raising ROS to a level where free radical initiation and propagation reactions significantly exceed termination reactions and therefore cause widespread protein damage. HBGA-VLP assay data showed loss of binding after treatments below 0.01 mM, but loss of binding could occur with capsid conformational changes induced by less potent oxidizing conditions. Both HBGA-VLP binding assays and SDS-PAGE data indicated that GII.4 Sydney VLPs are less susceptible to damage by Cu(I) solutions than GI.7 VLPs.

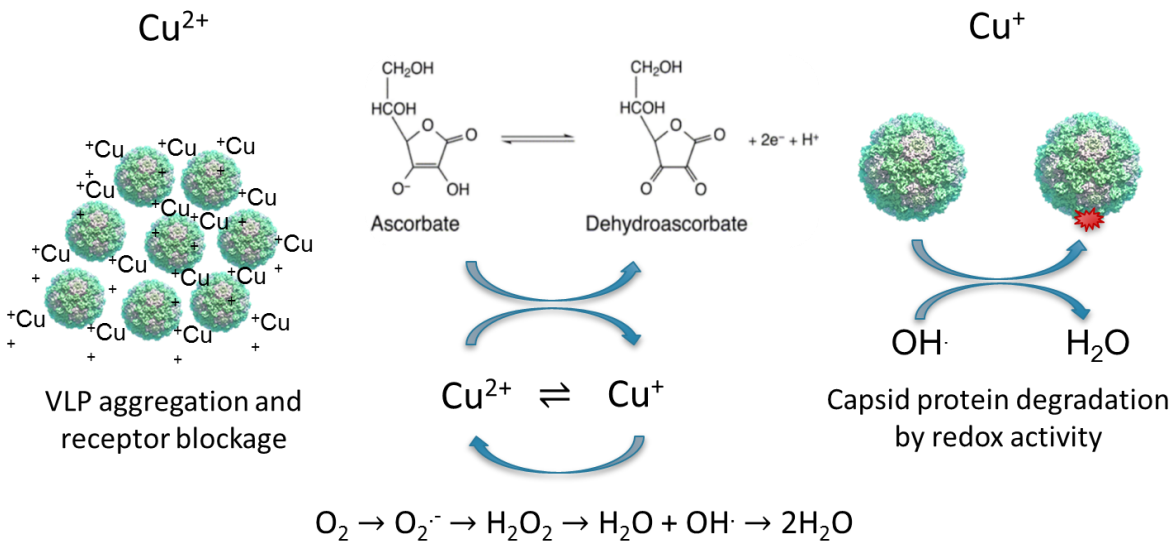

Figure 4.6 Schematic showing a summary of the effects of Cu(II) ions and Cu-ion catalyzed ROS generation on virus particle stability and integrity. Cu(II) ions aggregate viruses and cause some inactivation at high concentration. With an added reducing agent such as ascorbate, Cu(II) acts as a catalyst to generate ROS that, in addition to the unstable Cu(I) ion, cause covalent damage to the virus capsid.

The effects of copper solutions containing ions in the +2 or +1 oxidation states on human norovirus and its surrogates are summarized in Figure 4.6. Stable Cu(II) ions in the absence of a reducing agent bind onto the surface of the virus capsid and cause VLP aggregation. At high concentrations, the bound ions may have the potential to block HBGA receptor binding, as demonstrated by HBGA-VLP binding assays, and cause 1-log loss of virus titer, as demonstrated by TV plaque assay. In the presence of ascorbate as a reducing agent, copper ions cycle between the +2 and +1 oxidation state. Ascorbate oxidizes to dehydroascorbate as it reduces Cu(II) to Cu(I), and Cu(I) oxidizes back to Cu(II) by either

dissolved oxygen and its reduction products or by reacting directly with the protein capsid. Cu(I) may reduce disulfide bonds within the major capsid protein and cause protein unfolding that inhibits VLP binding to HBGAs, which has been reported in binding assays to rely heavily on maintenance of higher order capsid protein structure.[35] ROS are generated as oxygen is sequentially reduced to water, and these species cause covalent damage to the viral capsids, as demonstrated by SDS-PAGE. This ascorbate and copper system relies on a fresh supply of ascorbate and treatment of virus or VLPs immediately after mixing. Ascorbate is rapidly depleted in the presence of copper and dissolved oxygen. Thus, we have a system of coupled redox reactions that is very efficient in inactivating the virus, but requires a precise balance of the components in order to operate efficiently.

4.3 Conclusions

Human noroviruses can persist in the environment and are generally resistant to most disinfection techniques, so novel disinfectant formulations are needed. We have demonstrated that mixtures of copper bromide and sodium ascorbate rapidly and efficiently inactivate human norovirus surrogates, with some evidence suggesting that these mixtures show promise against the human pathogen. TV plaque assays and HBGA-VLP binding assays proved that solutions of Cu(I) are substantially more effective than Cu(II) at virus inactivation. Virus inactivation with Cu(I) solutions occurs at low concentration and short treatment time. As little as 0.1 mM copper ions had high efficacy with little risk to environmental harm, as the EPA limit on safe drinking water is 0.02 mM.[36] TEM images and SDS-PAGE data confirmed that Cu(I) solutions cause significant damage to viral capsids, even at short treatment times and low concentrations.

HBGA-VLP binding assays and SDS-PAGE of treated major capsid protein indicate that GII.4 Sydney VLPs are much less susceptible to damage by Cu(I) solutions than GI.7 VLPs. It is therefore important to evaluate the effectiveness of current inactivation strategies on new emerging strains to confirm that they remain effective on evolved and possibly more stable virus strains. The results suggest that TV may be more susceptible than human norovirus to copper based on RT-qPCR, however, further study on the effects of the stool matrix on copper effectiveness should be conducted. Copper and ascorbate systems have promise for being the active ingredients in novel safe, rapid, and effective antiviral mixtures. Future research can be directed at increasing the stability and robustness of these ionic-redox systems for use in practical applications.

4.4 Materials and Methods

4.4.1 Tulane Virus Plaque Assays

Rhesus monkey kidney cells (LLC-MK2, ATCC CCL-7) were passaged in M199 media (Corning/Cellgro) containing 10% fetal bovine serum (Gibco/Life Technologies) and 1% Penicillin/Streptomycin (Gibco). For the assay, cells were grown to about 90% confluence on 60mm cell culture plates (Corning). To infect the cells, 450 µl of TV sample dilutions were applied to each plate following aspiration of spent media. The plates were infected for 60 minutes, during which they were rotated every 15 minutes to ensure effective delivery of viruses to the cells. After infection, 3 ml of M199 media with 1.5% low melting temperature agarose (SeaKem) was added as overlay. Plates were then incubated at 37°C and under 5% CO_2 for 3 days to facilitate plaque formation. After 3 days, 2 ml of 3.7% formaldehyde (Sigma-

Aldrich) in PBS was poured over each plate to fix the cells. After fixing for 3-4 hours the agarose overlay was removed, and 1.5 ml of 0.1% crystal violet in PBS was added to the plates for 15 minutes to stain. The crystal violet solution was then poured off, and the plates were rinsed twice with tap water to remove excess stain before counting plaques.

Before performing the plaque assay, TV stocks were subjected to various treatments with copper in suspension. 100 µl of TV stock was added to 900 µl of each copper solution for a 1 ml total sample volume. Copper solutions containing ascorbate were prepared using 100 µl of 10× sodium ascorbate (Sigma Aldrich) stock, 10 µl of 100× $CuBr_2$ (Sigma-Aldrich) stock, and the balance PBS. Unless otherwise specified, all incubation times were 30 minutes. Copper ions were quenched by addition of EDTA (Sigma-Aldrich) in 10× excess. After quenching, TV samples were subjected to 10× series dilutions in PBS prior to application to culture plates.

4.4.2 Histo-blood Group Antigen Binding Assays

Receptor binding assays to infer the effects different copper treatments have on the norovirus capsid were conducted as done previously with slight modification.[35,37] Purified VLPs containing the assembled major capsid protein (VP1) of human norovirus GI.7 and GII.4 Sydney were obtained courtesy R. Atmar (Baylor College of Medicine, Houston, TX) and kept at 4^{o}C in concentrated form until use. VLPs were diluted to 3 µg/ml in 1x phosphate-buffered saline (PBS) and 100 µl/well of the VLP solution applied to 96-well medium-binding EIA plates (Costar 3591). Additionally, negative control wells with no VLP were seeded. Plates were incubated at 4^{o}C overnight with gentle shaking, and then blocked for 2 h at room temperature with 5% skim milk solids (w/v) in PBS + 0.05% (v/v) Tween 20 (PBST) and

gentle shaking. The wells were then washed thrice with 200 µl/well PBST, and 100 µl/well of selected dilutions of $CuBr_2$ with or without 1 mM sodium ascorbate in 0.15 M NaCl were applied at both different time points or for 30 minutes with different copper solution concentrations. After selected treatment time, wells were quenched with 100 µl/well 10 mM bathocuproinedisulfonic acid (BCSA). The quenched solutions were then removed and plates washed twice with 200 µl/well PBST. Next, 100 µl/well of a solution containing 1 µg biotinylated HBGA type A (Glycotech, #01-017, Gaithersburg, MD) in 0.25% skim milk-PBST was applied for 1 h at room temperature with shaking. The plates were then washed thrice with PBST, and 100 µl/well of 0.2 µg/ml streptavidin-horseradish peroxidase conjugate (Invitrogen, Carlsbad, CA) in PBS applied to plates for 15 min at room temperature. Plates were washed thrice with PBST and 100 µl/well room temperature 3,3',5,5'-Tetramethylbenzidine (TMB) substrate (KPL, Gaithersburg, MD) applied for 5-10 minutes. The reaction was then stopped with 100 µl/well TMB Stop Solution (KPL) and plate read at 450 nm in a Tecan Infinite m200Pro microplate reader.

Negative control wells were seeded with only PBS and no VLPs, while positive control wells included untreated VLPs and neutralization control (BCSA and highest copper solution premixed and applied to wells for 30 minutes). At least two wells per treatment per plate and three separate plate replicates were performed. For each treatment, the average absorbance of the no VLP wells was subtracted from the average absorbance of each VLP well. These adjusted absorbances were then use to calculate the value of the signal of a treatment well taken as a percentage of the neutralization (positive) control.

4.4.3 Transmission Electron Microscopy

For viewing under TEM, 100 mg ml^{-1} human norovirus GI.7 VLPs were treated with 0.1 mM copper bromide and 10 mM sodium ascorbate for varying periods of time and then quenched with 10 mM EDTA. 10 µl droplets of each treated VLP solution were adsorbed onto nickel grids with carbon support films (Ladd Research, Williston, VT) for 2 minutes. Excess liquid was then removed, followed by 5–10 seconds of negative staining with 2% uranyl acetate. The grids were imaged by conventional TEM using a 2000FX S/TEM (JEOL, Tokyo, Japan) at 200 kV.

4.4.4 RT-qPCR

Samples with GII.4 Sydney infected stool kindly provided courtesy of S.R. Green (North Carolina Department of Health and Human Services, Raleigh, NC) and suspended 20% in PBS were clarified by centrifugation for 10 minutes at 10,000×g followed by 1:1 dilution in PBS. Additionally, clarified Tulane virus cell culture lysates diluted 1:10 were also evaluated in suspension assay. The clarified stool or Tulane cell culture stock was added 1:10 into 0.15 M sodium chloride (NaCl) solutions containing 100 mM sodium ascorbate and varying copper concentration for a final volume of 100 µL. After 30 minutes of treatment at room temperature, EDTA was added to a final concentration of 0.1 M to quench the copper ions.

Sample preparation and PCR reactions closely followed the protocol used by Manuel *et al*.[37] and are summarized briefly here. Before RNA extraction, samples were pretreated with 1 µL RNase ONE (Promega, Madison, WI) enzyme in 12 µL 10x reaction buffer and 7 µL nuclease-free H_2O for 15 minutes at 37°C. The RNase reaction was stopped by placing the

samples on ice for 5 minutes and adding 80 µL cold PBS. The NucliSENS easyMAG system (bioMérieux, St. Louis, MO) was used for RNA extraction, and final extracted nucleic acid was collected in 40 µL of provided buffer. A CFX96 Touch real-time PCR system (Bio-rad, Hercules, CA) was used to carry out the reaction with the following protocol: 1) reverse transcription for 15 min at 50°C, 2) denaturation for 2 min at 95°C, and 3) 45 cycles of 15 s at 95°C, 30 s at 54°C, and 30 s at 72°C (for fluorescence reading). Primers JJV2F (5′-CAAGAGTCAATGTTTAGGTGGATGAG-3′) and COG2R (5′-TCGACGCCATCTTCATTCACA-3′) and probe RING2-P (5′-FAM [6-carboxyfluorescein]-TGGGAGGGCGATCGCAATCT-BHQ [black hole quencher]-3′) were used for GII.4 Sydney;[38] and Tulane primers FW (5'-GAGATTGGTGTCAAAACACTCTTTG-3'), RV (5'-ATCCAGTGGCACACACAATTT-3'), and probe (5'-6-FAM-AGTTGATTGACCTGCTGTGTCA-BHQ-3') were used. Tulane reaction cycling was 2 min at 50°C, 10 min at 95°C, and 45 cycles of 95°C for 15 s followed by 60°C for 1 min.[39] The baseline threshold was set to 30 during analysis.

Serial dilutions of GII.4 Sydney infected stool were used to create the standard curve shown in Figure B.1. The slope of the linear regression result was used to calculate log reductions in number of genomic copies based on Ct value for all subsequent experiments.

4.4.5 SDS-PAGE

GI.7 and GII.4 Sydney VLP stocks were diluted into 0.15 M NaCl solutions containing 10 mM sodium ascorbate and varying concentrations of copper bromide for a final volume of 10 µL. Each sample contained 1 µg of VLPs. After varying treatment times at room temperature,

EDTA was added to a final concentration of 0.01 M to quench the copper ions. 10 µL of Laemmli buffer (Bio-rad, Hercules, CA) containing β-mercaptoethanol (Sigma-Aldrich) according to the manufacturer's instructions was added to each sample, bringing the total volume to 20 µL. Samples were then held at 95°C for 5 minutes for protein denaturation. 20 µL of each sample as well as 10 µL of a Spectra multicolor broad range protein ladder (Thermo Scientific) were loaded into separate lanes of a precast 4-15% agarose gel (Bio-rad, Hercules, CA). Gels were subjected to 200 V for 30 minutes, until the loading dye travelled across the entire gel. Gels were placed in PBS until staining with Acquagel (Bulldog Biolabs) for 1 hour. The gels were then rinsed 3 times with PBS and destained in PBS overnight before imaging with a scanner (Epson, Long Beach, CA).

The lasso tool within Photoshop software (Adobe, San Jose, CA) was used to outline each major capsid protein band as identified by size comparison with the standard protein ladder. The histogram analysis tool was then used to determine the average intensity of each band. Each band was outlined and analyzed three separate times to determine error associated with this method. Each treatment condition was repeated on three separate gels. The gel images in Figure C.1a and b are representative of GI.7 and GII.4 Sydney VLPs, respectively. Normalized intensity was calculated by first normalizing the intensity to the background intensity of the image to obtain an optical density ratio (ODR),

$$ODR = \frac{(I_{band} - I_{background})}{I_{background}} \tag{4.1}$$

where I_{band} represents the average intensity of a protein band and $I_{background}$ represents the average intensity of the image background. Then the ODR of each sample was divided by the ODR of an untreated sample to obtain normalized intensity (I_n)

$$I_n = \frac{ODR_{treated}}{ODR_{untreated}} \tag{4.2}$$

here $ODR_{treated}$ represents the ODR of a treated sample and $ODR_{untreated}$ represents the ODR of an untreated control.

4.5 Acknowledgments

Funding for this work was provided by the USDA-NIFA Food Virology Collaborative (NoroCORE), supported by the National Institute of Food and Agriculture, U.S. Department of Agriculture, under award number 2011-68003-30395. We also acknowledge funding from the Molecular Biotechnology Training Program (MBTP) sponsored by the National Institutes of Health and the Graduate School at North Carolina State University (5 T32 GM008776-15). TEM work was completed at the Analytical Instrumentation Facility (AIF) at North Carolina State University, which is supported by the State of North Carolina and the NSF.

4.6 References

1 Barclay, L. *et al*. Infection control for norovirus. *Clin. Microbiol. Infect.* **20**, 731-740 (2014).

2 Ronnqvist, M. & Maunula, L. Noroviruses on surfaces: detection, persistence, disinfection and role in environmental transmission. *Future Virol.* **11**, 207-217 (2016).

3 Hoelzer, K., Fanaselle, W., Pouillot, R., Van Doren, J. M. & Dennis, S. Virus Inactivation on Hard Surfaces or in Suspension by Chemical Disinfectants: Systematic Review and Meta-Analysis of Norovirus Surrogates. *J. Food Prot.* **76**, 1006-1016 (2013).

4 Hood, M. I. & Skaar, E. P. Nutritional immunity: transition metals at the pathogen-host interface. *Nature Rev. Microbiol.* **10**, 525-537 (2012).

5 Samanovic, M. I., Ding, C., Thiele, D. J. & Darwin, K. H. Copper in Microbial Pathogenesis: Meddling with the Metal. *Cell Host & Microbe* **11**, 106-115 (2012).

6 Festa, R. A. & Thiele, D. J. Copper at the Front Line of the Host-Pathogen Battle. *PloS Pathog.* **8**, e1002887 (2012).

7 Shionoiri, N. *et al*. Investigation of the antiviral properties of copper iodide nanoparticles against feline calicivirus. *J. Biosci. Bioeng.* **113**, 580-586 (2012).

8 Cross, J. B. *et al*. Killing of Bacillus spores by aqueous dissolved oxygen, ascorbic acid, and copper ions. *Appl. Environ. Microbiol.* **69**, 2245-2252 (2003).

9 Miller, D., Buettner, G. & Aust, S. Transition-Metals as Catalysts of Autoxidation Reactions. *Free Radic. Biol. Med.* **8**, 95-108 (1990).

10 Hein, J. E. & Fokin, V. V. Copper-catalyzed azide-alkyne cycloaddition (CuAAC) and beyond: new reactivity of copper(I) acetylides. *Chem. Soc. Rev.* **39**, 1302-1315 (2010).

11 Mathews, S., Kumar, R. & Solioz, M. Copper Reduction and Contact Killing of Bacteria by Iron Surfaces. *Appl. Environ. Microbiol.* **81**, 6399-403 (2015).

12 Park, G. W. *et al*. Strain-Specific Virolysis Patterns of Human Noroviruses in Response to Alcohols. *PloS One* **11**, e0157787 (2016).

13 Liu, P. *et al*. Comparison of the Activity of Alcohol-Based Handrubs Against Human Noroviruses Using the Fingerpad Method and Quantitative Real-Time PCR. *Food Environ. Virol.* 3, 35-42 (2011).

14 Li, D. *et al*. Evaluation of methods measuring the capsid integrity and/or functions of noroviruses by heat inactivation. *J. Virol. Methods* **181**, 1-5 (2012).

15 Kroneman, A. *et al*. Analysis of integrated virological and epidemiological reports of norovirus outbreaks collected within the Foodborne Viruses in Europe Network from 1 July 2001 to 30 June 2006. *J. Clin. Microbiol.* **46**, 2959-2965 (2008).

16 Dai, Y. *et al*. Antigenic Relatedness of Norovirus GII.4 Variants Determined by Human Challenge Sera. *PloS One* **10**, e0124945 (2015).

17 Wigginton, K. R., Pecson, B. M., Sigstam, T., Bosshard, F. & Kohn, T. Virus Inactivation Mechanisms: Impact of Disinfectants on Virus Function and Structural Integrity. *Environ. Sci. Technol.* **46**, 12069-12078 (2012).

18 Hans, M., Mathews, S., Muecklich, F. & Solioz, M. Physicochemical properties of copper important for its antibacterial activity and development of a unified model. *Biointerphases* **11**, 018902 (2016).

19 Warnes, S. L. & Keevil, C. W. Inactivation of Norovirus on Dry Copper Alloy Surfaces. *PloS One* **8**, e75017 (2013).

20 Warnes, S. L., Summersgill, E. N. & Keevil, C. W. Inactivation of Murine Norovirus on a Range of Copper Alloy Surfaces Is Accompanied by Loss of Capsid Integrity. *Appl. Environ. Microbiol.* **81**, 1085-1091 (2015).

21 Manuel, C. S., Moore, M. D. & Jaykus, L. A. Destruction of the Capsid and Genome of GII.4 Human Norovirus Occurs during Exposure to Metal Alloys Containing Copper. *Appl. Environ. Microbiol.* **81**, 4940-4946 (2015).

22 Wood, P. The Potential Diagram for Oxygen at Ph-7. *Biochem. J.* **253**, 287-289 (1988).

23 Lindahl, T. Instability and Decay of the Primary Structure of Dna. *Nature* **362**, 709-715 (1993).

24 Ames, B., Shigenaga, M. & Hagen, T. Oxidants, Antioxidants, and the Degenerative Diseases of Aging. *Proc. Natl. Acad. Sci. U. S. A.* **90**, 7915-7922 (1993).

25 Berlett, B. & Stadtman, E. Protein oxidation in aging, disease, and oxidative stress. *J. Biol. Chem.* **272**, 20313-20316 (1997).

26 Gaetke, L. & Chow, C. Copper toxicity, oxidative stress, and antioxidant nutrients. *Toxicology* **189**, 147-163 (2003).

27 Arthur, S. E. & Gibson, K. E. Physicochemical stability profile of Tulane virus: a human norovirus surrogate. *J. Appl. Microbiol.* **119**, 868-75 (2015).

28 Cromeans, T. *et al*. Comprehensive Comparison of Cultivable Norovirus Surrogates in Response to Different Inactivation and Disinfection Treatments. *Appl. Environ. Microbiol.* **80**, 5743-5751 (2014).

29 Hutson, A., Atmar, R. & Estes, M. Norovirus disease: changing epidemiology and host susceptibility factors. *Trends Microbiol*. **12**, 279-287 (2004).

30 Tan, M. & Jiang, X. Norovirus and its histo-blood group antigen receptors: an answer to a historical puzzle. *Trends Microbiol.* **13**, 285-293 (2005).

31 Ettayebi, K. *et al*. Replication of human noroviruses in stem cell–derived human enteroids. *Science* (2016).

32 Jones, M. K. *et al*. Enteric bacteria promote human and mouse norovirus infection of B cells. *Science* **346**, 755-759 (2014).

33 Topping, J. R. *et al*. Temperature inactivation of Feline calicivirus vaccine strain FCV F-9 in comparison with human noroviruses using an RNA exposure assay and reverse transcribed quantitative real-time polymerase chain reaction-A novel method for predicting virus infectivity. *J. Virol. Methods* **156**, 89-95 (2009).

34 Moore, M. D., Goulter, R. M. & Jaykus, L. Human Norovirus as a Foodborne Pathogen: Challenges and Developments. *Ann. Rev. Food Sci. Technol.* **6**, 411-433 (2015).

35 Moore, M. D., Bobay, B. G., Mertens, B. & Jaykus, L. A. Human Norovirus Aptamer Exhibits High Degree of Target Conformation-Dependent Binding Similar to That of Receptors and Discriminates Particle Functionality. *mSphere* (2016).

36 56 FR 26548 §141.80.2, June 7, 1991.

37 Manuel, C. S., Moore, M. D. & Jaykus, L. A. Destruction of the Capsid and Genome of GII.4 Human Norovirus Occurs during Exposure to Metal Alloys Containing Copper. *Appl. Environ. Microbiol.* **81**, 4940-4946 (2015).

38 Jothikumar, N. *et al*. Rapid and sensitive detection of noroviruses by using TaqMan-based one-step reverse transcription-PCR assays and application to naturally contaminated shellfish samples. *Appl. Environ. Microbiol.* **71**, 1870-1875 (2005).

39 Sestak, K. *et al*. Experimental Inoculation of Juvenile Rhesus Macaques with Primate Enteric Caliciviruses. *PloS One* **7**, e37973 (2012).

CHAPTER 5

Synergistic Effects of Copper Ions and (+)-Catechin on Human Norovirus Survival

5.1 Introduction

We seek to introduce new efficient and stable antiviral formulations based on ionic-reductor compositions as described in the previous chapter. The biocidal effects of Cu(I) ions appear to be a result of the oxidative effects from copper's redox activity.[1] Copper is a redox-active transition metal that can be present in its monovalent or divalent form in solution. Cu(I) ions are unstable and either react with dissolved oxygen to form Cu(II) or disproportionate into Cu(s) and Cu(II).[2] The required concentration of Cu(I) ions in solution can be generated by the addition of a reducing agent to solutions of Cu(II). Many reactions, such as those carried out in Click chemistry,[3] commonly use the ascorbate ion as a reducing agent for copper. Solid iron surfaces have also been used as reducing agents for copper ions to generate a biocidal environment.[4]

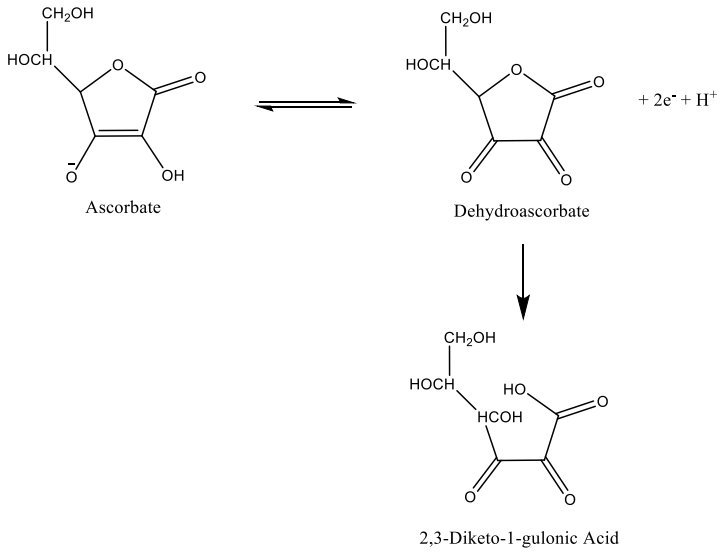

Scheme 5.1 Reversible and irreversible oxidation pathways of ascorbate.[7]

In the presence of copper ions or other redox-active transition metal ions, ascorbate behaves as an antioxidant at high concentration and as a pro-oxidant at low concentration relative to the metal ions.[5] The ions of iron and other transition metals have been reported as less efficient in catalyzing ascorbate oxidation than Cu(II) ions.[6] Ascorbate undergoes reversible oxidation to dehydroascorbate (DHA)[7] according to Scheme 5.1, so continuous redox cycling of ascorbate and a redox-active metal ion can be achieved with an element such as copper. It has been hypothesized that the redox cycling of copper ions and ascorbate demonstrate "Fenton-like" chemistry because they generate reactive oxygen species in a similar fashion to hydrogen peroxide and iron ions in the well-described Fenton reaction.[1,8] As shown in Scheme 5.2, dissolved oxygen is reduced down to water through a series of intermediates, including hydrogen peroxide and two highly reactive species, superoxide and hydroxyl radical.[9] Molecular oxygen and hydrogen peroxide are reduced by transition metal,

and the oxygen radical species can be reduced by either transition metal or biomolecules, causing oxidative damage.[10] In the case of copper present in the systems, the Cu(I) ion acts as a reductant for the oxygen species.

$$O_2 \rightarrow O_2^{\cdot -} \rightarrow H_2O_2 \rightarrow H_2O + OH^{\cdot} \rightarrow 2H_2O$$

Scheme 5.2 Reduction pathway of dissolved oxygen species.[9]

Despite its reversible oxidation to DHA, ascorbate disappears over time as DHA also irreversibly oxidizes to diketogulonic acid,[7] as seen in Scheme 5.1. Therefore efforts have been made to stabilize ascorbate or present an alternative pro-oxidant compound for generation of Cu(I) ions. Redox chemistry dictates that the net reduction potential of a redox reaction must be positive for the reaction to take place spontaneously.[11] Thus the reduction potential of a reducing agent for the Cu(II) to Cu(I) half reaction must be less than the reduction potential of the copper half reaction, which is 0.158 V.[12] The oxidation of ascorbate to DHA involves the loss of two electrons, and multiple steps are involved. The standard reduction potential of ascorbate/DHA is generally reported as -0.06 V, but the redox reaction of Cu(II) with ascorbate is complex and pH-dependent because ascorbate, DHA, and reaction intermediates all have acid-base equilibria.[13]

Due to the low stability of the ascorbate ion in the presence of dissolved oxygen from the air, we have investigated the use of alternate reducing agents to generate the same redox environment using Cu(II) as a catalyst. Because of their phenolic groups and thiol reducing

groups, we selected lignin in the form of nanoparticles, tannic acid, and (+)-catechin as possible candidates. Lignin is a widely available biomaterial that has been used as a reducing agent to generate metal nanoparticles.[14] Lignin-based nanoparticles can chelate metals and have been used to deliver antimicrobial silver ions as an environmentally-benign alternative to solid silver nanoparticles.[15] We hypothesized that the high molecular weight of the lignin and tannic acid structures may contribute to high stability and enhanced redox buffering capacity. The smaller polyphenols, catechins, have demonstrated high pH-dependent stability relative to other antioxidant compounds,[16, 17] especially if encapsulated in a protective colloidal structure such as a surfactant micelle or liposome.[18]

Catechins, classified as flavanols, are a group of natural compounds with strong antioxidant properties that are obtained from tea extracts and other plants.[19] (+)-Catechin and epigallocatechin gallate (EGCG) are members of this group of chemicals that have antimicrobial, antiviral, antifungal, and antitoxin properties.[20] Specifically, EGCG has significant antiviral activity against Herpes Simplex Virus (HSV),[21] Hepatitis B,[22] and Hepatitis C,[23] all enveloped viruses. EGCG binding to membrane-bound receptors is regarded as its main antiviral mechanism. In combination with Cu(II) and in some cases Fe(II) ions, (+)-catechin has significant antimicrobial activity caused by oxidative effects.[24] (+)-Catechin behaves as a reducing agent and participates in redox cycling with the transition metal, introducing reactive oxygen species into the system.[25-27] Similar to ascorbate, (+)-catechin reduces copper more readily than iron.[28] Studies have shown that heat treatment prior to (+)-catechin use and adding ascorbate may increase its antimicrobial properties.[24,29] Because of their potency in combination with copper, catechin complexes are also used as part of cancer

treatments. Cancer cells contain a higher level of copper than normal cells, resulting in targeted cell death upon the introduction of a catechin.[30] We selected (+)-catechin as a result of its availability in larger quantities and lower cost in comparison to other catechins.

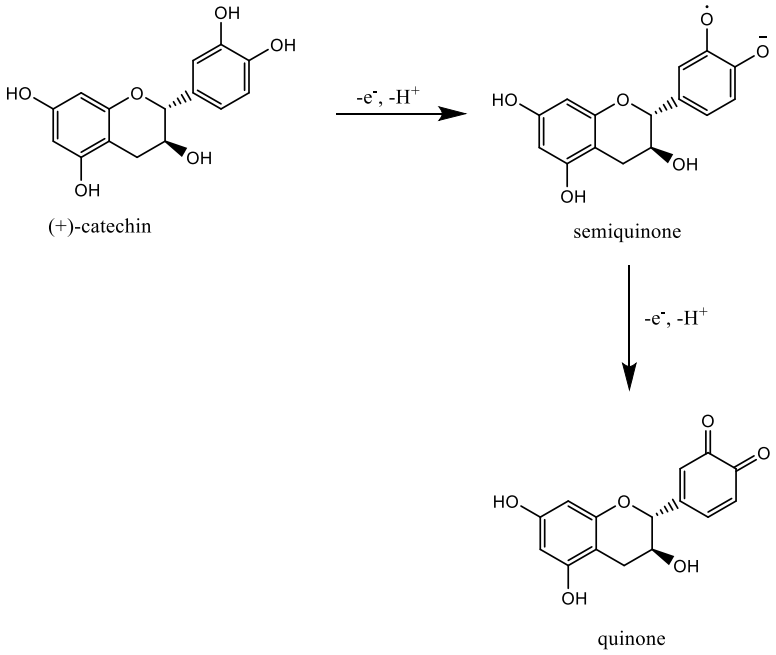

Scheme 5.3 Oxidation pathway of (+)-catechin to quinone.[31]

Similar to ascorbate, (+)-catechin loses two electrons in its oxidation in multiple pH-dependent steps, according to Scheme 5.3. The final oxidation product of the reaction is quinone.[31] The standard reduction potential of (+)-catechin has been measured between 0.16 and 0.278 V[32] depending on the method used, so it lowers the solution's reduction capacity to a greater extent than ascorbate. We evaluate the long-term stability of ascorbate, lignin, tannic acid, and (+)-catechin for their use as reducing agents in generating an oxidative environment using $CuBr_2$ as a catalyst.

5.2 Results and Discussion

The instability of ascorbate when stored over time hinders the use of copper ion-based disinfectants in practical formulations. We have thus compared the stability and efficacy of ascorbate with other reducing agents to evaluate their potential as viable alternatives for ascorbate. We determined the stability of each reducing agent by testing their ability to generate Cu(I) ions from Cu(II) ions. We selected copper bromide as a source of divalent copper ions and added sodium ascorbate in at least 10-fold excess to reduce Cu(II) and create a redox active environment. The presence of Cu(I) ions was measured using the absorbance of copper/reducing agent solutions in the presence of a spectrophotometric chelator for Cu(I), bathocuproinedisulfonic acid (BCSA). BCSA changes conformation when it binds Cu(I) ions and produces a color change detectable at 483 nm. The Cu(I) concentration was calculated based on solution absorbance using a standard curve of different initial $CuBr_2$ concentrations, as seen in Figure A.1. We then calculated Cu conversion using Equation 5.1,

$$\text{Cu conversion} = \frac{[\text{Cu(I)}]}{[\text{CuBr}_2]} \tag{5.1}$$

where [Cu(I)] represents the concentration of Cu(I) ions calculated from the measured absorbance and [$CuBr_2$] represents the initial concentration of copper bromide in the sample. We tested the ability of ascorbate, lignin nanoparticles, tannic acid, and (+)-catechin to reduce copper ions after storage for periods of up to a month. We used plaque assays of Tulane virus (TV), a human norovirus surrogate, to approximate the effects of different copper ion formulations on human norovirus infectivity.

5.2.1 Comparison of Alternative Reducing Agents

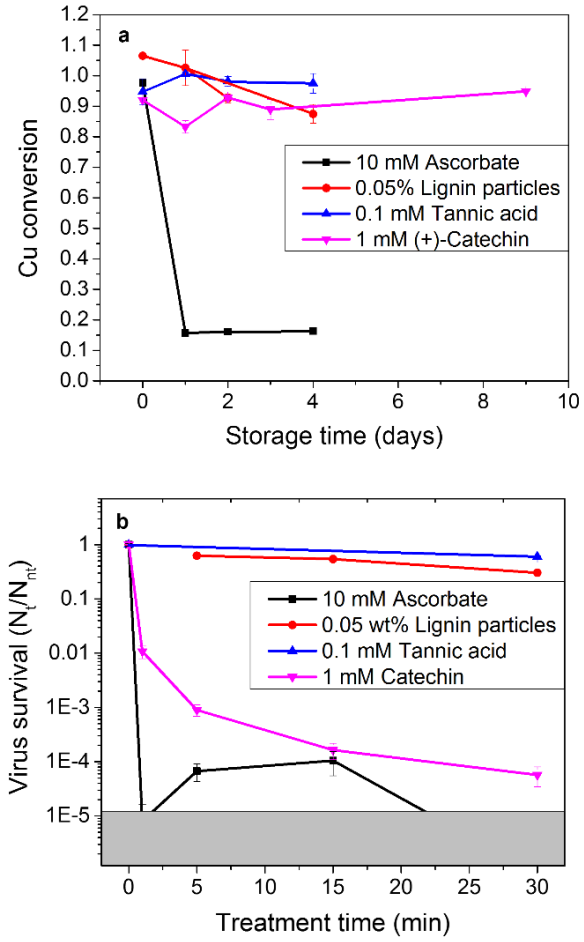

Figure 5.1 Comparison of four reducing agents for $CuBr_2$ in their ability to a) convert Cu(II) to Cu(I) after storage for different time periods and b) inactivate TV in combination with $CuBr_2$ at varying treatment times when prepared fresh. Virus survival is the number of pfu after each treatment (N_t) normalized to the number of pfu without treatment (N_{nt}) determined during the same set of experiments. Copper conversion (a) is the Cu(I) concentration normalized by the original $CuBr_2$ concentration. Reducing agents in (b) were in combination with 0.1 mM $CuBr_2$ except for (+)-catechin, which was in with 1 mM $CuBr_2$. Error bars represent the standard error of three replicate samples.

Initially, all four reducing agents almost completely converted Cu(II) to Cu(I), as seen in Figure 5.1a. Within one day, ascorbate lost its ability to reduce Cu(II) to Cu(I) completely, while lignin particles, tannic acid, and catechin all retained their reducing capabilities for weeks. However, the reducing agents were not all effective in inactivating Tulane virus in combination with Cu(II). Using fresh solutions of each reducing agent, we tested their virucidal effects in combination with $CuBr_2$ after different exposure times using TV plaque assays. Ascorbate caused greater than 4-log reduction in virus titer within five minutes of treatment, and (+)-catechin induced 3-log and 4-log reductions after 5 and 15 minutes, respectively. Lignin nanoparticles and tannic acid caused less than 1-log reduction in virus titer even after 30 minutes of treatment. This discrepancy is most likely due to strong binding of the copper ions to the large lignin and tannic acid structures. Cu(I) is classified as a soft Lewis acid and will bind strongly to soft Lewis bases, including sulfur groups.[33] After Cu(I) generation, the reduced ions remain tightly bound to the phenolic structures so that they are not re-oxidized to Cu(II) and thus do not catalyze the formation of damaging oxygen and hydroxy radicals. Catechin binds copper ions more loosely and can thus facilitate redox cycling and oxygen radical generation.

Lignin nanoparticles and tannic acid solutions can reduce Cu(II) to Cu(I), but their strong chelating properties prevent Cu(I) from being re-oxidized to Cu(II).[34] Because the oxidation of Cu(I) to Cu(II) generates damaging oxygen radicals, no virus inactivation is observed in the absence of this half reaction. We also note that the *ortho*-dihydroxyl groups on polyphenols, which are present on the (+)-catechin structure but not on the tannic acid structure, exhibit the greatest pro-oxidant tendencies.[35] Unlike lignin nanoparticles and tannic

acid, both ascorbate and (+)-catechin allow for the regeneration of Cu(II) from Cu(I) and therefore significant virus inactivation. (+)-Catechin has high affinity for Cu(II) and low affinity for Cu(I), so redox-cycling of the metal is possible as it is captured and released by the hydroxyl groups.[36]

5.2.2 (+)-Catechin/Cu Mixture Efficacy and Stability

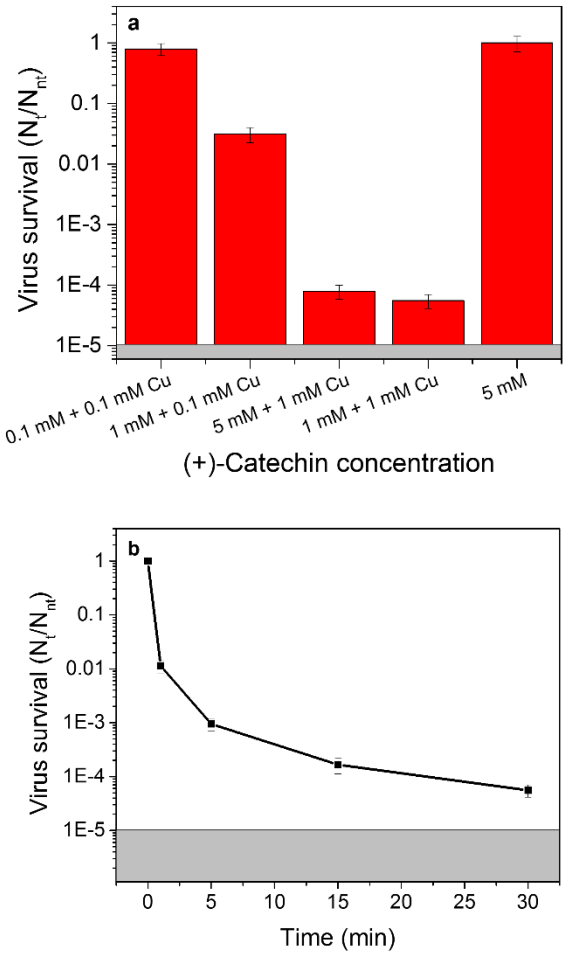

Figure 5.2 Results of TV plaque assay after treatment with a) varying combinations of $CuBr_2$ and (+)-catechin for 30 minutes and b) 1 mM $CuBr_2$ with 1 mM (+)-catechin at varying time points. Virus survival is the number of pfu after each treatment (N_t) normalized to the number of pfu without treatment (N_{nt}) determined during the same set of experiments. The areas outside the limit of detection of the assay are marked in gray. Error bars represent the average of two plates for each of three samples at each condition.

As seen in Figure 5.2a, a mixture of 1 mM or 5 mM (+)-catechin and 1 mM $CuBr_2$ induced greater than 4-log reduction in TV infectivity after 30 minutes of treatment. Other concentrations and ratios of copper and (+)-catechin produced less than 2-log inactivation, indicating that both the absolute concentration and the ratio of (+)-catechin to copper are important in an effective formulation. When combined with ionic copper, (+)-catechin solutions operate slightly slower than ascorbate solutions in reducing TV infectivity, requiring 5 minutes and 15 minutes to cause 3-log and 4-log inactivation, respectively. Although slower acting, (+)-catechin is still the best alternative to ascorbate of the reducing agents tested here.

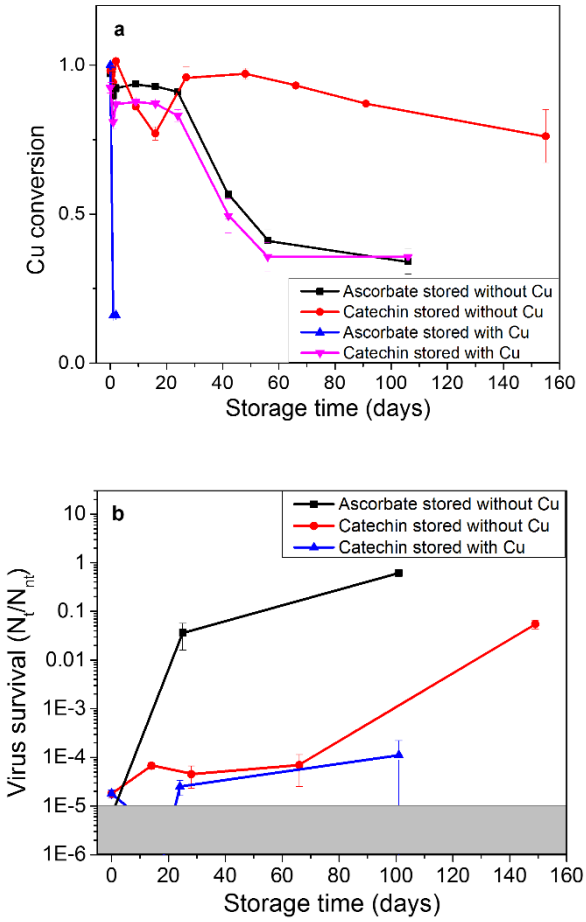

Figure 5.3 Comparison of ascorbate and (+)-catechin stored with and without $CuBr_2$ in their ability to a) convert Cu(II) to Cu(I) after storage for different time periods and b) inactivate TV in combination with $CuBr_2$ at varying treatment times. Copper conversion (a) is the Cu(I) concentration normalized by the original $CuBr_2$ concentration. 10 mM Ascorbate in (b) was in combination with 0.1 mM $CuBr_2$, and 1 mM (+)-catechin was in combination with 1 mM $CuBr_2$. Error bars represent the standard error of three replicate samples.

After demonstrating that (+)-catechin is the most viable replacement for ascorbate as a reducing agent for Cu(II), we compared the stability of these compounds under different conditions. Initially, ascorbate and (+)-catechin stored both with and without $CuBr_2$ converted Cu(II) to Cu(I) to an extent of almost 100%, as seen in Figure 5.3a. Within one day, ascorbate stored with copper lost its ability to reduce Cu(II) to Cu(I) completely, while (+)-catechin retained its reducing capabilities for weeks. Ascorbate stored without copper behaved similarly to (+)-catechin stored with copper and only lost reducing capacity after over 40 days. (+)-Catechin stored without copper slowly begins to lose reducing capacity in solution after about 2 months of storage.

The loss of ascorbate's reducing capacity correlates with its loss of efficacy in inactivating TV. As seen in Figure 5.3b, ascorbate stored without copper loses its potency against TV in less than a month. (+)-Catechin stored without copper loses some ability to inactivate TV when combined with fresh copper as it transitions from causing almost 5-log reduction in TV titer to less than 2-log reduction in TV titer after about 5 months of storage. This loss of TV inactivation corresponds with the slow loss of reducing capacity after 2 months of storage seen in Figure 5.3a. Conversely, (+)-catechin stored with copper retains its ability to reduce TV titer by more than 4 logs even after losing its ability to reduce copper after storage for 2 months. These data suggest that the redox activity involved in Cu(II) reduction to Cu(I) is not the only mechanism involved in the inactivation of TV by copper ions and (+)-catechin. During storage of ascorbate and (+)-catechin mixtures, the solution color darkens as loss of Cu conversion occurs. In solutions of (+)-catechin stored with copper, dark precipitates form over time. Particles of (+)-catechin with bound copper may form over time, and the copper may

help bind virus particles. The captured virus particles may then be unable to infect host cells. Alternatively, (+)-catechin and copper may form some synergistic complex over time that is able to bind and inactivate viruses but not release detectable Cu(I) ions.

In summary, as ascorbate loses its capacity to reduce Cu(II) rapidly over time, while (+)-catechin has the ability to both retain reducing capacity after storage for long periods and effectively inactivate TV in the presence of Cu(II) ions. (+)-Catechin is therefore a promising alternative to ascorbate for use in a stable disinfectant effective against human norovirus. Still, several differences exist in the application of ascorbate and (+)-catechin as reducing agents. First, virus inactivation by copper ions using ascorbate is more rapid than with (+)-catechin. The formation of nanoparticle complexes as done by Li *et al.*[37] to bind viruses and facilitate the local release of Cu(I) ions from the particles may help in shortening the required treatment time. Also, the ratio of $CuBr_2$ to reducing agent is different for ascorbate and (+)-catechin. We used ascorbate in at least 10-fold excess of Cu(II) to induce loss of virus titer, whereas a 1:1 ratio of (+)-catechin to Cu(II) was most effective. Indeed, polyphenols typically behave as antioxidants at high concentration by complexing redox-active metals.[36] Low concentrations of (+)-catechin relative to Cu(II) may not generate enough redox potency for effective inactivation.

5.2.2 Formulation Considerations

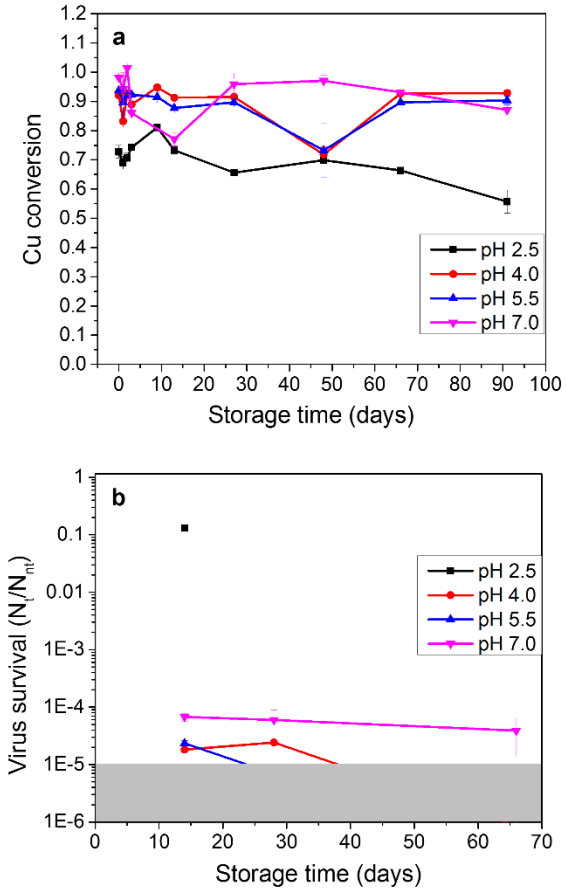

Figure 5.5 pH-dependence of (+)-catechin solution stability over time represented by a) Cu conversion and b) TV survival. 1 mM (+)-catechin solutions were prepared in pH-adjusted PBS and mixed with $CuBr_2$ immediately before assay. Error bars represent the standard error of three replicate samples.

The formulation of (+)-catechin and copper mixtures is very important in its practical use. The efficacy of (+)-catechin as a reducing agent is pH-dependent. As seen in Figure 5.5a,

(+)-catechin has the greatest reducing capacity and remains stable longest at acidic pH values greater than 2.5. (+)-Catechin at pH 4.0, 5.5, and 7.0 retains its ability to inactivate TV in the presence of copper for multiple months, as seen in Figure 5.5b. Fresh (+)-catechin at pH 2.5 does not have enough reducing capacity to inactivate TV by more than 1 log in the presence of copper ions. At certain pH values, (+)-catechin binds copper ions loosely and can thus facilitate redox cycling and oxygen radical generation. (+)-Catechin has the ability to effectively inactivate TV in the presence of Cu(II) ions even after storage for long periods. It is therefore a viable alternative to ascorbate for use in a stable disinfectant effective against human norovirus.

5.2.3 Mechanism of (+)-Catechin/Cu Mixture-induced Inactivation

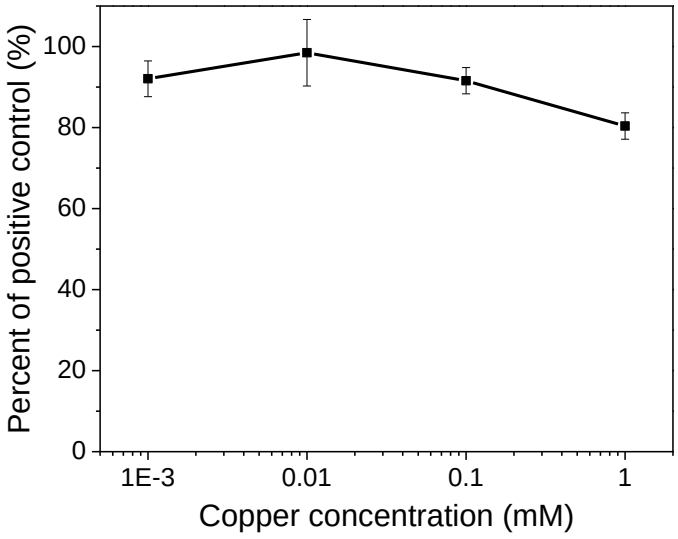

Figure 5.4 Results of VLP binding assay with HBGA after GII.4 VLP exposure to $CuBr_2$ at varying concentrations for 30 minutes with 1 mM (+)-catechin. Error bars represent the standard error of two replicate samples.

HBGA binding assays were carried out to further elucidate the difference in mechanism between ascorbate/Cu mixtures and (+)-catechin/Cu mixtures. GI.7 and GII.4 VLP treatment with ascorbate/Cu mixtures resulted in complete loss of HBGA binding even using concentrations as low as 0.01 mM and treatment times as short as 1 minute (Figure 4.2). GII.4 VLP treatment for 30 minutes with 1 mM (+)-catechin in combination with copper bromide ranging from 0.001 to 1 mM resulted in less than 20% loss of HBGA binding at each copper concentration (Figure 5.4). These data suggest that the VLP major capsid protein retains sufficient structure and integrity after treatment with (+)-catechin/Cu mixtures to bind to HBGA receptors and that virus inactivation must be caused by some other mode of action. (+)-Catechin/Cu mixtures may disrupt interactions between capsid proteins, causing the virus particle to lose its structure and therefore infectivity without significant loss of individual protein folding or conformation. The major capsid protein of human norovirus VLPs may also be significantly more stable than the Tulane virus capsid proteins, resulting in significant differences between the susceptibility of TV and HuNoV to inactivation by (+)-catechin/Cu mixtures. Additional research must be done to reveal the mechanism of (+)-catechin/Cu mixture-induced TV inactivation and whether such a substantial difference exists between TV and HuNoV inactivation under these conditions.

5.3 Conclusions

The instability of ascorbate in aqueous solution precludes its use in practical disinfectant formulations. We evaluated lignin nanoparticles, tannic acid, and (+)-catechin as natural and stable alternatives to ascorbate. (+)-Catechin proved to have greater stability than ascorbate

while retaining potency against a human norovirus surrogate when combined with copper bromide. Further research can optimize the use of (+)-catechin and copper formulations as virucidals. Other compounds in the flavan-3-ol group may be even more effective than (+)-catechin, and introducing colloidal techniques may reduce the treatment time necessary for sufficient deactivation. Copper and (+)-catechin mixtures can likely be used to disinfect many other pathogens, extending the implications of this research.

Copper sulfate, another source of Cu(II) ions, is generally recognized as safe (GRAS) by the Food and Drug Administration (FDA).[40] (+)-Catechin is found naturally in green tea extracts and used as part of FDA-approved products. Low concentrations of Cu(II) in combination with a reducing agent are needed for efficient inactivation of viruses, so the toxicity and environmental impacts of these mixtures are also likely to be rather low in comparison with commonly used disinfectants such as bleach.

5.4 Materials and Methods

5.4.1 Tulane Virus Plaque Assays

Cell culture and TV plaque assays were performed as described in Section 4.4.1. Before performing the plaque assay, TV stocks were subjected to various treatments with copper in suspension. 100 µl of TV stock was added to 900 µl of each copper solution for a 1 ml total sample volume. Copper solutions containing ascorbate were prepared using 100 µl of 10× sodium ascorbate (Sigma Aldrich) stock, 10 µl of 100× $CuBr_2$ (Sigma Aldrich) stock, and the balance PBS. Copper solutions containing (+)-catechin or tannic acid were prepared using the desired concentration of (+)-catechin or tannic acid in pH-adjusted PBS and 10 µl of 100×

$CuBr_2$. 0.05% lignin nanoparticles were prepared by flash precipitation of IAT lignin as described by Richter et al[15] and infused with 0.1 mM $CuBr_2$ for at least 30 minutes. The particles were then coated with 0.04% poly(diallyldimethylammonium) (PDAC) for at least 30 minutes before use in the assay. PDAC is a cationic polyelectrolyte that facilitates electrostatic attraction of the particles to the negatively charged viruses. Unless otherwise specified, all incubation times were 30 minutes. Copper solutions were quenched by addition of EDTA in 10× excess. After quenching, TV samples were subjected to 10× series dilutions in PBS prior to application to culture plates.

5.4.2 Determination of Cu(I) Concentration

Cu(I) concentration was determined by measuring the absorbance of copper mixtures in the presence of bathocuproinedisulfonic acid (BCSA), a spectrophotometric chelator of Cu(I). 190 ul of reducing agent solution, 10 ul of 10 mM $CuBr_2$ stock, and 10 ul of 50 mM BCSA stock were added to wells of a 96-well plate, and the absorbance was measured at 483 nm. Control wells were also measured using 10 ul extra reducing agent solution in place of the $CuBr_2$ stock, and this reference absorbance was subtracted from the sample absorbance. Cu(I) concentration was calculated from the line of best fit obtained from a standard curve (Figure B.2) generated using 10 mM ascorbate with varying concentrations of $CuBr_2$.

5.5 Acknowledgments

Funding for this work was provided by the USDA-NIFA Food Virology Collaborative (NoroCORE), supported by the National Institute of Food and Agriculture, U.S. Department of Agriculture, under award number 2011-68003-30395.

5.6 References

1 Cross, J. B. *et al*. Killing of Bacillus spores by aqueous dissolved oxygen, ascorbic acid, and copper ions. *Appl. Environ. Microbiol.* **69**, 2245-2252 (2003).

2 Miller, D., Buettner, G. & Aust, S. Transition-Metals as Catalysts of Autoxidation Reactions. *Free Radic. Biol. Med.* **8**, 95-108 (1990).

3 Hein, J. E. & Fokin, V. V. Copper-catalyzed azide-alkyne cycloaddition (CuAAC) and beyond: new reactivity of copper(I) acetylides. *Chem. Soc. Rev.* **39**, 1302-1315 (2010).

4 Mathews, S., Kumar, R. & Solioz, M. Copper Reduction and Contact Killing of Bacteria by Iron Surfaces. *Appl. Environ. Microbiol.* **81**, 6399-403 (2015).

5 Buettner, G. & Jurkiewicz, B. Catalytic metals, ascorbate and free radicals: Combinations to avoid. *Radiat. Res.* **145**, 532-541 (1996).

6 Davies, M. B. Reactions of L-ascorbic acid with transition metal complexes. *Polyhedron* **11**, 285-321 (1992).

7 Borsook, H., Davenport, H., Jeffreys, C. & Warner, R. The oxidation of ascorbic acid and its reduction in vitro and in vivo. *J. Biol. Chem.* **117**, 237-279 (1937).

8 Burkitt, M. & Gilbert, B. Model Studies of the Iron-Catalyzed Haber-Weiss Cycle and the Ascorbate-Driven Fenton Reaction. *Free Radic. Res. Commun.* **10**, 265-280 (1990).

9 Wood, P. The Potential Diagram for Oxygen at Ph-7. *Biochem. J.* **253**, 287-289 (1988).

10 Pisoschi, A. M. & Pop, A. The role of antioxidants in the chemistry of oxidative stress: A review. *Eur. J. Med. Chem.* **97**, 55-74 (2015).

11 Ball, D. in *Physical Chemistry, Second Edition* **230** Cengage Learning, Stamford, CT (2015).

12 Atkins, P. & de Paula, J. in *Elements of Physical Chemistry* **592** Oxford University Press, Oxford, UK (2013).

13 Davies, M. B. The International Journal for Inorganic and Organometallic Chemistry Reactions of L-ascorbic acid with transition metal complexes. *Polyhedron* **11**, 285-321 (1992).

14 Rak, M. J., Friscic, T. & Moores, A. Mechanochemical synthesis of Au, Pd, Ru and Re nanoparticles with lignin as a bio-based reducing agent and stabilizing matrix. *Faraday Discuss.* **170**, 155-167 (2014).

15 Richter, A. P. *et al*. An environmentally benign antimicrobial nanoparticle based on a silver-infused lignin core. *Nat. Nanotech.* **10**, 817- (2015).

16 Zhu, Q. Y., Zhang, A. Q., Tsang, D., Huang, Y. & Chen, Z. Y. Stability of green tea catechins. *J. Agric. Food Chem.* **45**, 4624-4628 (1997).

17 Li, N., Taylor, L. S., Ferruzzi, M. G. & Mauer, L. J. Kinetic Study of Catechin Stability: Effects of pH, Concentration, and Temperature. *J. Agric. Food Chem.* **60**, 12531-12539 (2012).

18 Lin, Q., Åkesson, B. & Bergenståhl, B. Effect of colloidal structures on the stability of five flavonoids with different hydrophilicity. *Food Hydrocoll.* **22**, 700-705 (2008).

19 Gadkari, P. V. & Balaraman, M. Catechins: Sources, extraction and encapsulation: A review. *Food Bioprod. Process.* **93**, 122-138 (2015).

20 Friedman, M. Overview of antibacterial, antitoxin, antiviral, and antifungal activities of tea flavonoids and teas. *Mol. Nutr. Food Res.* **51**, 116-134 (2007).

21 Isaacs, C. E. *et al*. Epigallocatechin gallate inactivates clinical isolates of herpes simplex virus. *Antimicrob. Agents Chemother.* **52**, 962-970 (2008).

22 Huang, H. *et al*. (-)-Epigallocatechin-3-gallate inhibits entry of hepatitis B virus into hepatocytes. *Antiviral Res.* **111**, 100-111 (2014).

23 Calland, N. *et al*. Polyphenols Inhibit Hepatitis C Virus Entry by a New Mechanism of Action. *J. Virol.* **89**, 10053-10063 (2015).

24 Holloway, A. C. *et al*. The effect of copper(II), iron(II) sulphate, and vitamin C combinations on the weak antimicrobial activity of (+)-catechin against Staphylococcus aureus and other microbes. *Metallomics* **4**, 1280-1286 (2012).

25 Hoshino, N., Kimura, T., Yamaji, A. & Ando, T. Damage to the cytoplasmic membrane of Escherichia coli by catechin-copper (II) complexes. *Free Radic. Biol. Med.* **27**, 1245-1250 (1999).

26 Nakagawa, K. *et al*. Copper(II) ions convert catechins from antioxidants to prooxidants in protein carbonyl formation. *J. Health Sci.* **53**, 591-595 (2007).

27 Hayakawa, F. *et al*. Prooxidative activities of tea catechins in the presence of Cu2+. *Biosci. Biotechnol. Biochem.* **68**, 1825-1830 (2004).

28 Mira, L. *et al*. Interactions of flavonoids with iron and copper ions: A mechanism for their antioxidant activity. *Free Radic. Res.* **36**, 1199-1208 (2002).

29 Holloway, A. C. *et al*. Heat treatment enhances the antimicrobial activity of (+)-Catechin when combined with copper sulphate. *Lett. Appl. Microbiol.* **61**, 381-389 (2015).

30 Farhan, M. *et al*. Cancer Therapy by Catechins Involves Redox Cycling of Copper Ions and Generation of Reactive Oxygen Species. *Toxins* **8**, 37 (2016).

31 Janeiro, P. & Brett, A. Catechin electrochemical oxidation mechanisms. *Anal. Chim. Acta* **518**, 109-115 (2004).

32 Medvidovic-Kosanovic, M., Seruga, M., Jakobek, L. & Novak, I. Electrochemical and Antioxidant Properties of (+)-Catechin, Quercetin and Rutin. *Croat. Chem. Acta* **83**, 197-207 (2010).

33 Pearson, R. Hard and Soft Acids and Bases. *J. Am. Chem. Soc.* **85**, 3533-& (1963).

34 Andrade, R. *et al*. The antioxidant effect of tannic acid on the in vitro copper-mediated formation of free radicals. *Arch. Biochem. Biophys.* **437**, 1-9 (2005).

35 Iwasaki, Y. *et al*. Effect of interaction between phenolic compounds and copper ion on antioxidant and pro-oxidant activities. *Toxicology in Vitro* **25**, 1320-1327 (2011).

36 Perron, N. R. & Brumaghim, J. L. A Review of the Antioxidant Mechanisms of Polyphenol Compounds Related to Iron Binding. *Cell Biochem. Biophys.* **53**, 75-100 (2009).

37 Li, H., Chen, Q., Zhao, J. & Urmila, K. Enhancing the antimicrobial activity of natural extraction using the synthetic ultrasmall metal nanoparticles. *Sci. Rep.* **5**, 11033 (2015).

38 Manuel, C. S., Moore, M. D. & Jaykus, L. A. Destruction of the Capsid and Genome of GII.4 Human Norovirus Occurs during Exposure to Metal Alloys Containing Copper. *Appl. Environ. Microbiol.* **81**, 4940-4946 (2015).

39 Moore, M. D., Bobay, B. G., Mertens, B. & Jaykus, L. A. Human Norovirus Aptamer Exhibits High Degree of Target Conformation-Dependent Binding Similar to That of Receptors and Discriminates Particle Functionality. *mSphere* (2016).

40 Listing of Specific Substances Affirmed as GRAS, 21CFR §184.1261. (2016).

CHAPTER 6

Conclusions and Future Directions

6.1 Summary

The aim of this body of work was to find ways to reduce the spread of human norovirus by characterizing and modifying particle interactions and by developing an inactivation strategy that permanently damages the particles. We used colloidal techniques to characterize VLP interactions and controlled those interactions using different types of surfactants. Solid copper surfaces had previously been shown to inactivate adsorbed human noroviruses, but the effects of solvated copper ions on virus survival was not well understood. We used copper ions with a reducing agent to generate oxide radicals and cause covalent damage to human noroviruses and surrogate viruses. The formulation of these reducing agent/copper ion mixtures will result in an environmentally-benign disinfectant strong enough to inactivate human noroviruses.

In the research described in Chapter 2, we focused on characterizing VLP interactions in the presence of anionic, cationic, and nonionic surfactants and as a function of pH. At neutral pH, VLPs have a net negative surface charge, so adsorption of cationic surfactant at low concentration resulted in particle aggregation due to reduced electrostatic repulsion. Increasing the surfactant concentration above CMC resulted in breakdown of aggregates and particles into individual capsid proteins or dimers. Similar behavior occurred at high concentrations of anionic surfactant above CMC. At low concentration of anionic surfactant, VLPs were dispersed due to increased electrostatic repulsion between particles. VLPs were dispersed at

all concentrations of nonionic surfactant studied. We used zeta potential measurements to characterize the particles at varying pH and charged surfactant concentration. The isoelectric point of the VLPs was found to be about pH 4.5, and particles were aggregated around this pH due to minimized electrostatic repulsion. Above the pI particles had negative charge, and below the pI particles had positive charge. Cationic and anionic surfactant adsorption onto VLP surface was effectively modeled using simple adsorption models. These particle interactions in the presence of surfactant can help determine optimal formulations for cleaning products and antimicrobials that contain surfactants and aim to clear pathogens from a contaminated surface.

Chapter 3 presents studies focused on describing the behavior of VLPs in the presence of divalent copper ions. VLPs were aggregated in the presence of divalent copper ions at low concentration. Concentrations ranging from micromolar to millimolar were necessary to aggregate VLPs depending on the strain of human norovirus used. Based on the lack of significant variations between the capsid charge of the varying VLP strains studied, we hypothesized that specific copper-binding motifs exist on the surface of VLPs that are responsible for strain-specific susceptibility to aggregation by divalent copper ions. Copper ion-induced VLP aggregation was eliminated below the capsid isoelectric point, and higher ionic strength increased the amount of copper ions required to induce aggregation. Other transition metals also caused VLP aggregation at low concentration with the following efficiency: silver > zinc > copper > iron.

Chapter 4 describes the inactivation of human noroviruses by solutions with monovalent copper ions. Cu(I) ions were generated by the addition of sodium ascorbate as a reducing agent to solutions of copper bromide. TV titer was reduced by greater than 4 logs within 1 minute at 0.1 mM copper concentration with ascorbate. Without ascorbate, TV titer was reduced by insignificant levels even after treatment for 30 minutes at 1 mM copper bromide. RT-qPCR of human norovirus-infected stool indicated a decrease in the number of genomic copies of 2 logs after treatment with 0.1 and 1 mM copper with ascorbate. HBGA-VLP binding assays using both GI.7 and GII.4 Sydney VLPs showed complete loss of binding within minutes of treatment with copper concentrations as low as 0.01 mM in the presence of ascorbate. The efficacy of ascorbate/Cu mixtures shown using TV plaque assays, RT-qPCR of infected stool, and HBGA-VLP binding assays indicate that viable human noroviruses are likely also inactivated using this strategy. Significant loss of band intensity in SDS-PAGE gels run with ascorbate/Cu-treated VLPs indicated that particle damage was covalent in nature and included protein cleavage. TEM also confirmed loss of capsid integrity after VLP treatment with ascorbate/Cu mixtures for as little as 1 minute. The research presented in this chapter proved that divalent copper ions in the presence of an effective reducing agent induce effective and rapid inactivation of human norovirus and surrogates.

Finally, the work described in Chapter 5 provided means for a practical formulation of copper ions with a reducing agent that would be stable over time. Ascorbate readily oxidizes in solution and so would have a short shelf-life in an antiviral formulation. Tannic acid, lignin nanoparticles, and (+)-catechin were all tested as alternatives to ascorbate for use as reducing agents for copper ions. All three polyphenolic compounds were able to reduce Cu(II) to Cu(I)

after storage with copper, while ascorbate lost this ability within a day. Tannic acid and lignin nanoparticles in the presence of copper ions were not effective in reducing TV titer likely due to strong binding of copper that prevented copper redox chemistry from occurring. (+)-Catechin was selected as the most viable alternative to ascorbate as a reducing agent for copper ions based on its ability to retain efficacy against TV even after storage for months. In the presence of copper ions, (+)-catechin retained its efficacy against TV even after losing its ability to reduce Cu(II) to Cu(I). We therefore concluded that (+)-catechin/Cu mixtures have a different mechanism of human norovirus inactivation than ascorbate/Cu mixtures. (+)-Catechin/Cu mixtures were also unable to reduce HBGA-VLP binding, indicating another deviation from ascorbate/Cu mixture effects on virus particles. The precise, data-driven formulation of these (+)-catechin/Cu mixtures is very important as their efficacy was found to be strongly dependent on pH.

6.2 Future Outlook

The results presented in this dissertation could have a real impact on the spread of human noroviruses in the environment. As we develop a better understanding of the pathogen's interactions in the presence of commonly used cleaners and disinfectants, more advanced and effective formulations become possible. The introduction of metal-based disinfectants that possess high efficacy against human norovirus will make virus cleaning and inactivation achievable in more settings and with more mild conditions than current antiviral agents such as bleach. The (+)-catechin/Cu mixtures have been submitted as part of an invention disclosure with promise for commercial licensing. Additional development work will focus on testing

these formulations on surfaces and continuing the optimization of their stability during storage and efficiency during application.

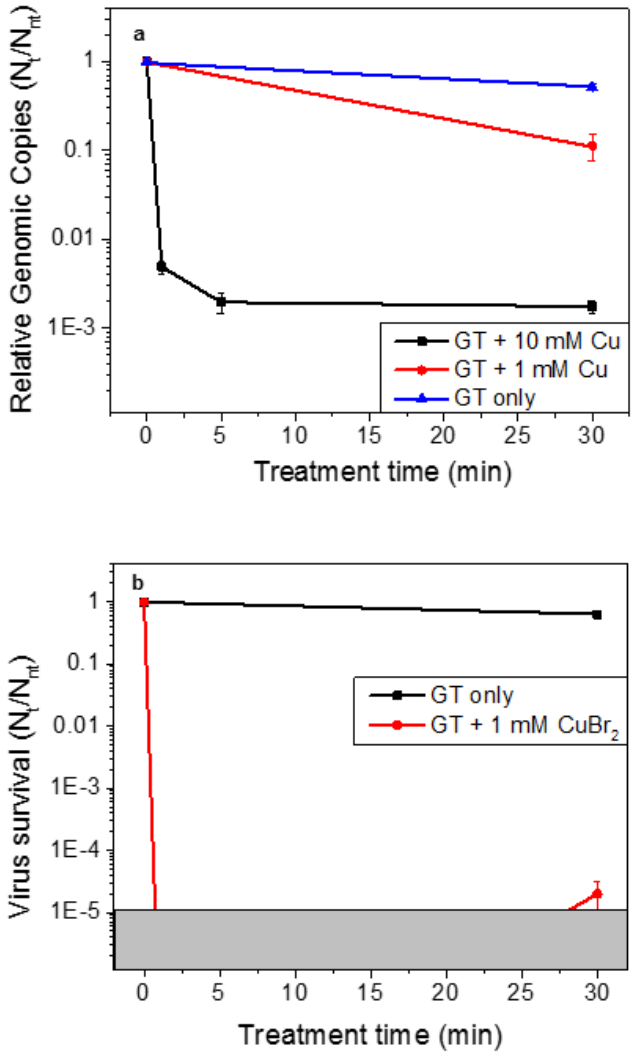

Figure 6.1 Preliminary results showing inactivation of human norovirus by green tea combined with copper bromide at various treatment times evaluated using a) RT-qPCR of GII.4 Sydney-infected stool and b) Tulane virus plaque assays.

Based on the efficacy of (+)-catechin/Cu mixtures in TV inactivation and the prevalence of catechins in green tea, we also evaluated human norovirus inactivation by natural green tea in combination with copper bromide using RT-qPCR of human norovirus-contaminated stool and TV plaque assays. Treatment with green tea and 10 mM copper caused about 3-log reduction in the number of genomic copies in GII.4 Sydney-infected stool (Figure 6.1a). Treatment with green tea and 1 mM copper caused more than 5-log reduction in TV titer after only 1 minute (Figure 6.1b). These preliminary results indicate that green tea/Cu mixtures are even more effective than (+)-catechin/Cu mixtures in causing human norovirus inactivation. The increased efficacy using green tea in place of (+)-catechin is likely a result of the diverse catechins at high concentrations found in green tea.[1] Other types of catechins have been shown to possess even higher anti-oxidant capacity than (+)-catechin.[2,3]

One final message derived from this thesis is that colloidal interactions should be taken into account when formulating cleaners and disinfectants. Copper-based antivirals have the potential to provide rapid and effective human norovirus inactivation in products and human activity. Future research can focus on elucidating the mechanisms of a new generation of more efficient disinfectants composed of copper ions and catechins. Such formulations can then be optimized using the most environmentally-benign and cost effective catechin or mixture of catechins. The analysis of various green tea components may help in determining these formulations. Additional studies comparing differences in susceptibility to copper treatments between human norovirus strains would also benefit disinfectant development. This work can also be expanded to other viral and bacterial pathogens to generate multiple types of broadly effective surface disinfectants.

6.3 References

1 Henning, S.M., *et al*. Catechin Content of 18 Teas and a Green Tea Extract Supplement Correlates With the Antioxidant Capacity. *Nutr*. *Cancer* **45**, 226-235 (2003).

2 Aron, P.M. and Kennedy, J.A. Flavan-3-ols: Nature, Occurrence and Biological Activity. *Molec. Nut. & Food Res.* **52**, 79-104 (2008).

3 Hayakawa, F., *et al.* Prooxidative Activities of Tea Catechins in the Presence of Cu^{2+}. *Biosci. Biotechnol. Biochem.* **68**, 1825-30 (2004).

APPENDIX A

Additional Light Scattering Data

Appendix A provides additional information and raw light scattering data. Figure A.1 includes the correlation data for representative conditions of the data shown in Figures 2.1-2.4. These curves demonstrate the quality of DLS data included in this thesis. Figures A.2 and A.3 show VLP behavior in solutions of varying concentrations of CTAB and SDS at pH 7.4 as well as pH values near and below the isoelectric point. In each of these measurements, pH adjustments were made after the addition of surfactant. For further analysis of the combined effects of pH and surfactant type and concentration on VLP behavior, the order of pH adjustment, surfactant addition, and VLP addition are very important. Also, the CMC of each surfactant and micelle size and shape at varying pH values need careful consideration.

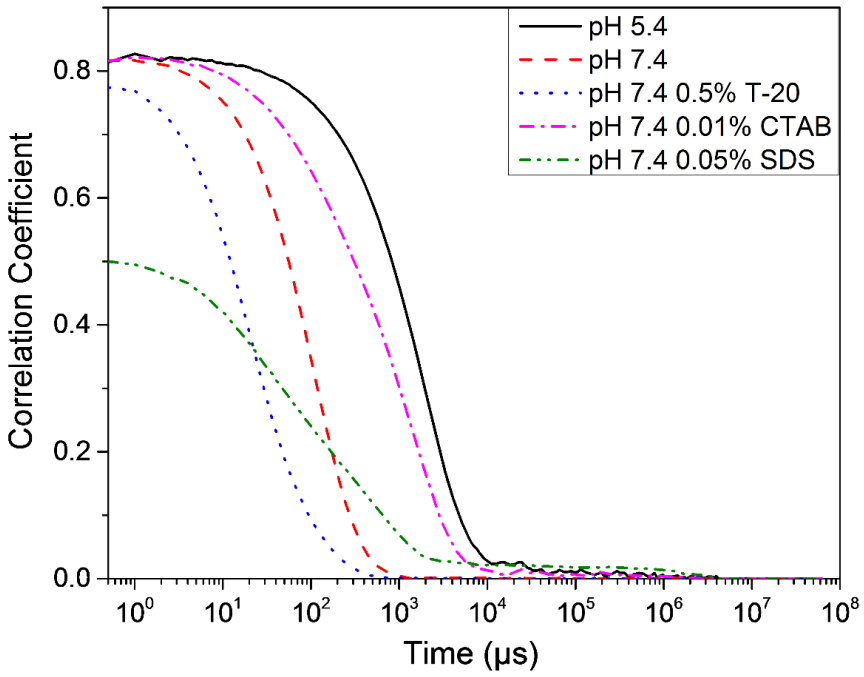

Figure A.1 Raw correlation data used in fitting the DLS size data for VLPs at selected conditions shown in Figures 2.1-2.4. DLS data show a single peak for VLPs in buffer at pH 5.4, pH 7.4, and pH 7.4 with 0.01% CTAB. The correlation data for these conditions show a sharp decline in correlation coefficient at different times, indicating a good fit for a monomodal distribution. DLS data have multiple peaks for VLPs in buffer at pH 7.4 with 0.05% SDS and 0.5% Tween 20. The correlation data for the SDS condition shows a gradual decline in correlation coefficient over time, indicating the presence of a broad distribution of particle size. The correlation data for 0.5% Tween 20 show a sharp decline followed by gradual leveling in correlation coefficient over time, indicating the presence of multiple particle size peaks.

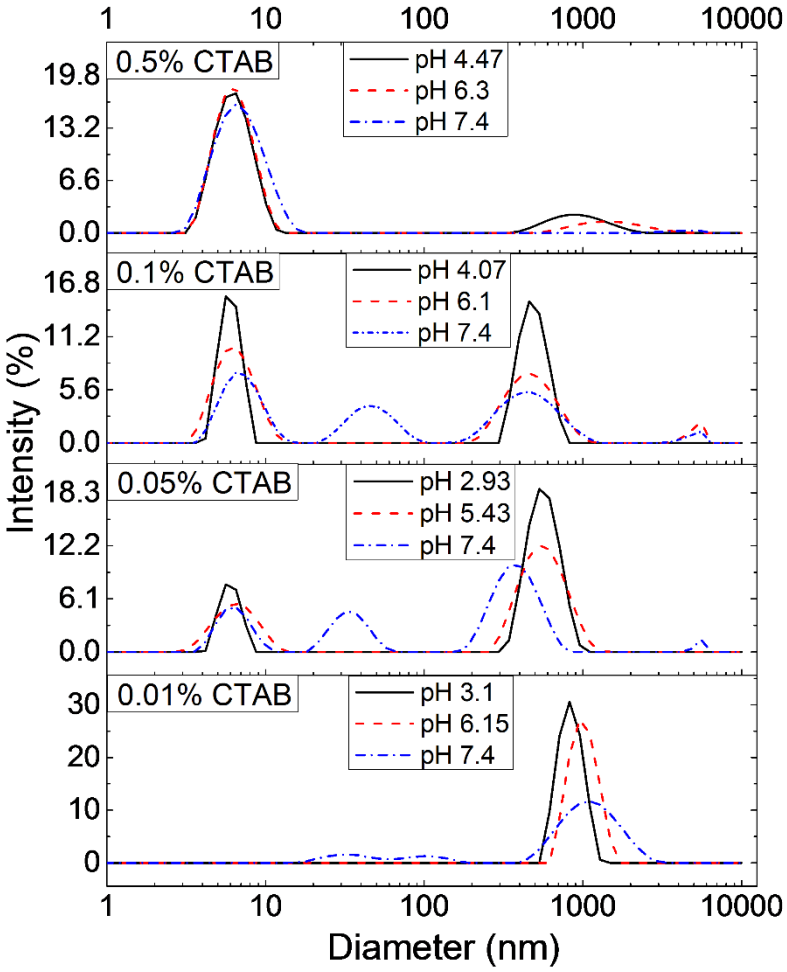

Figure A.2 Intensity distributions from DLS experiment of norovirus VLPs in PBS at varying pH containing 0.01%, 0.05%, 0.1%, and 0.5% CTAB. pH adjustments were made after surfactant addition to VLPs. Differences in VLP behavior at low pH from VLP behavior at pH 7.4 exist mainly at 0.05% and 0.1% CTAB. VLPs at low pH are less likely to be dispersed at these CTAB concentrations probably due to approaching or passing through the isoelectric point after surfactant addition. At pH values below the isoelectric point, peaks appear less broad probably due to pH-induced aggregation after passing through the isoelectric point.

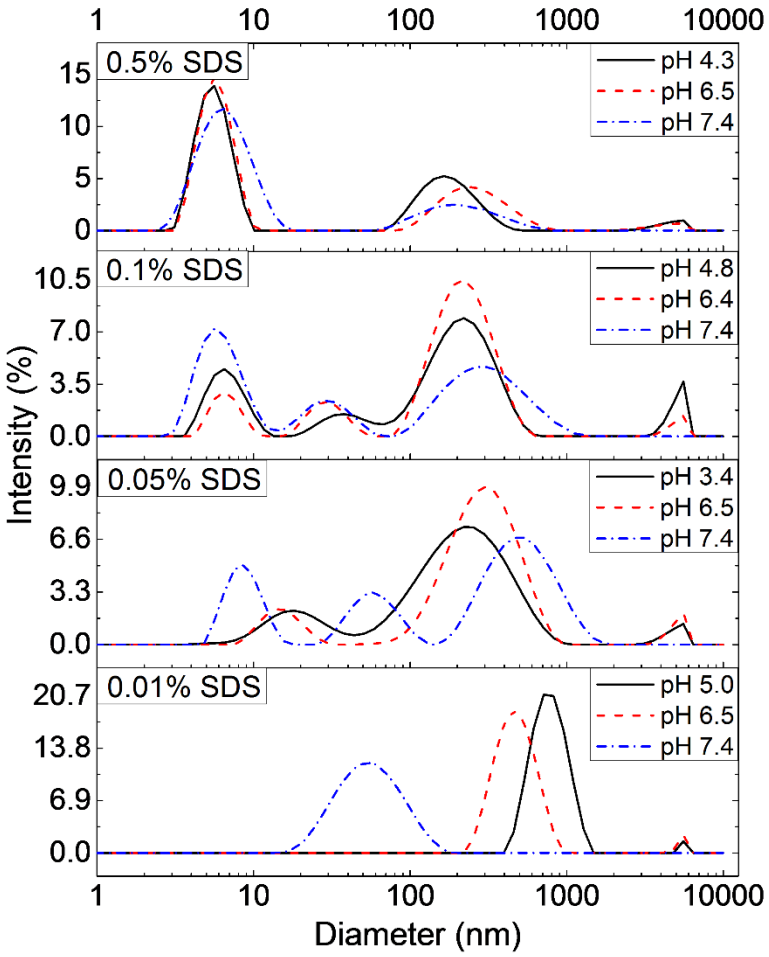

Figure A.3 Intensity distributions from DLS experiment of norovirus VLPs in PBS at varying pH containing 0.01%, 0.05%, 0.1%, and 0.5% SDS. pH adjustments were made after surfactant addition to VLPs. Major differences in VLP behavior at low pH and VLP behavior at pH 7.4 exist at 0.01% and 0.05% SDS. VLPs are more aggregated at these concentrations, probably due to approaching or passing through the isoelectric point after surfactant addition. At 0.05% SDS, the smallest diameter peak at low pH is larger than in other conditions possibly due to larger portions of the capsid or different sized micelles.

APPENDIX B

Standard Curves

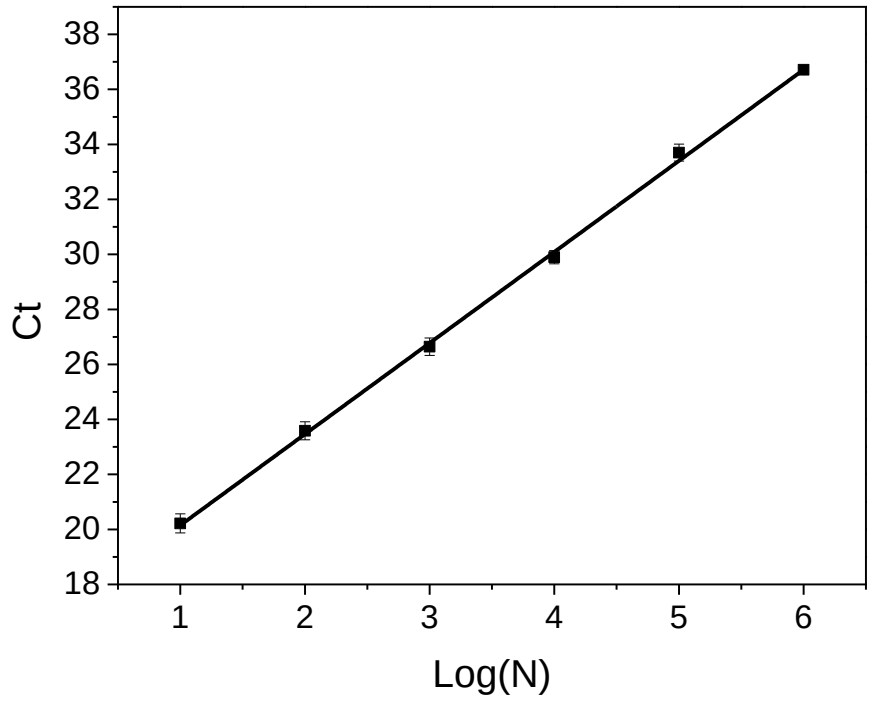

Figure B.1 Standard curve for RT-qPCR experiments with GII.4 Sydney-infected stool relating cutoff value, Ct, to log changes in genomic copies. The standard curve was generated by measuring the Ct values of a 1:10 dilution series of HuNoV infected stool. Linear regression yielded Ct = 3.32*log(N) + 16.85 with R^2 = 0.9992. Error bars represent the standard error of three replicate samples at each concentration.

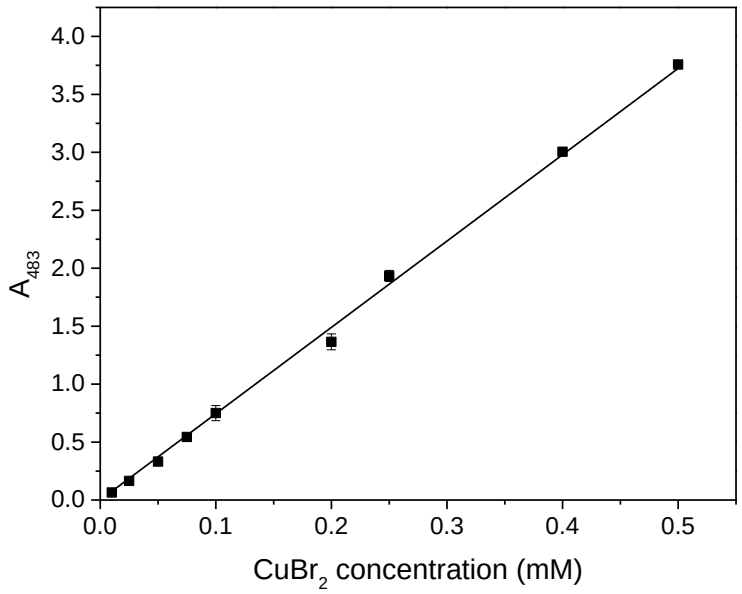

Figure B.2 Standard curve of absorbance at 483 nm of solutions with varying $CuBr_2$ concentration in the presence of excess sodium ascorbate and Cu(I) spectrophotometric chelator, BCSA. The line shown has equation $A_{483} = 7.48[CuBr_2]$, and $R^2 = 0.998$. After addition of excess fresh ascorbate, we assume $[CuBr_2] \sim [Cu(I)]$.

APPENDIX C

Sample SDS-PAGE Images

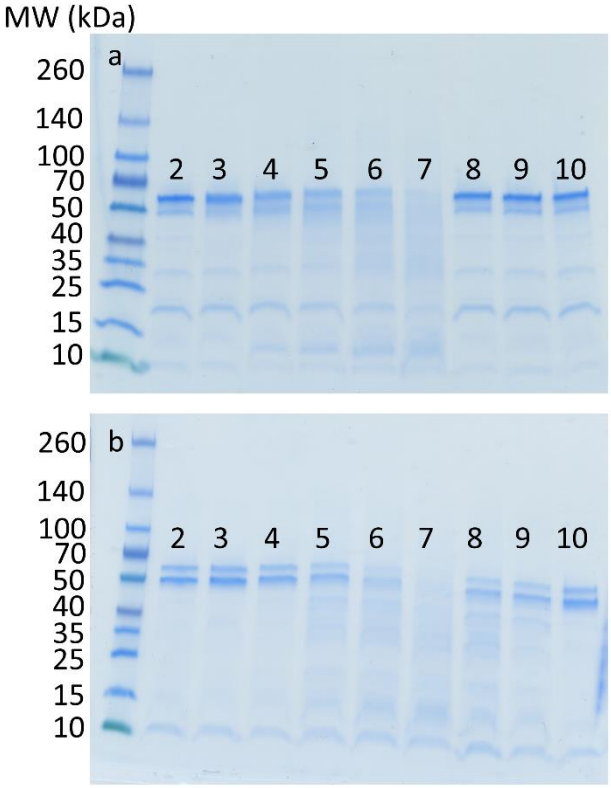

Figure C.1 Images of representative SDS-PAGE gels of a) GI.7 and b) GII.4 Sydney VLPs used for band intensity analysis. Lanes contain 1) standard protein ladder; 2) VLPs in 0.15 M NaCl; 3) VLPs treated with 1 mM EDTA, 0.1 mM $CuBr_2$, and 10 mM sodium ascorbate for 30 minutes (neutralization control); VLPs treated with 0.1 mM $CuBr_2$ and 10 mM sodium ascorbate for 4) 1 minute, 5) 5 minutes, 6) 15 minutes, and 7) 30 minutes; and VLPs treated with 0.01 mM $CuBr_2$ and 10 mM sodium ascorbate for 8) 5 minutes, 9) 15 minutes, and 10) 30 minutes.